University of Kentucky
UKnowledge

Theses and Dissertations--Chemistry | Chemistry

2022

SYNTHESIS OF 6,6- AND 7,7-DIFLUORO-1-ACETAMIDOPYRROLIZIDINES AND THEIR OXIDATION CATALYZED BY THE NONHEME Fe OXYGENASE LolO

Nabin Panth
University of Kentucky, nabinpanth@ymail.com
Author ORCID Identifier:
https://orcid.org/0000-0002-9868-3289
Digital Object Identifier: https://doi.org/10.13023/etd.2022.008

Right click to open a feedback form in a new tab to let us know how this document benefits you.

Recommended Citation
Panth, Nabin, "SYNTHESIS OF 6,6- AND 7,7-DIFLUORO-1-ACETAMIDOPYRROLIZIDINES AND THEIR OXIDATION CATALYZED BY THE NONHEME Fe OXYGENASE LolO" (2022). *Theses and Dissertations--Chemistry*. 152.
https://uknowledge.uky.edu/chemistry_etds/152

This Doctoral Dissertation is brought to you for free and open access by the Chemistry at UKnowledge. It has been accepted for inclusion in Theses and Dissertations--Chemistry by an authorized administrator of UKnowledge. For more information, please contact UKnowledge@lsv.uky.edu.

STUDENT AGREEMENT:

I represent that my thesis or dissertation and abstract are my original work. Proper attribution has been given to all outside sources. I understand that I am solely responsible for obtaining any needed copyright permissions. I have obtained needed written permission statement(s) from the owner(s) of each third-party copyrighted matter to be included in my work, allowing electronic distribution (if such use is not permitted by the fair use doctrine) which will be submitted to UKnowledge as Additional File.

I hereby grant to The University of Kentucky and its agents the irrevocable, non-exclusive, and royalty-free license to archive and make accessible my work in whole or in part in all forms of media, now or hereafter known. I agree that the document mentioned above may be made available immediately for worldwide access unless an embargo applies.

I retain all other ownership rights to the copyright of my work. I also retain the right to use in future works (such as articles or books) all or part of my work. I understand that I am free to register the copyright to my work.

REVIEW, APPROVAL AND ACCEPTANCE

The document mentioned above has been reviewed and accepted by the student's advisor, on behalf of the advisory committee, and by the Director of Graduate Studies (DGS), on behalf of the program; we verify that this is the final, approved version of the student's thesis including all changes required by the advisory committee. The undersigned agree to abide by the statements above.

Nabin Panth, Student

Dr. Robert B. Grossman, Major Professor

Dr. Yinan Wei, Director of Graduate Studies

SYNTHESIS OF 6,6- AND 7,7-DIFLUORO-1-ACETAMIDOPYRROLIZIDINES AND THEIR OXIDATION CATALYZED BY THE NONHEME Fe OXYGENASE LolO

DISSERTATION

A dissertation submitted in partial fulfillment of the
requirements for the degree of Doctor of Philosophy in the
College of Arts and Sciences
at the University of Kentucky

By
Nabin Panth
Lexington, Kentucky
Director: Dr. Robert B. Grossman, Professor of Chemistry
Lexington, Kentucky
2021

Copyright © Nabin Panth 2021
https://orcid.org/0000-0002-9868-3289

ABSTRACT OF DISSERTATION

SYNTHESIS OF 6,6- AND 7,7-DIFLUORO-1-ACETAMIDOPYRROLIZIDINES AND THEIR OXIDATION CATALYZED BY THE NONHEME Fe OXYGENASE LolO

One of the remarkable steps in loline alkaloid biosynthesis is the installation of an ether bridge between two unactivated C atoms in 1-*exo*-acetamidopyrrolizidine (AcAP). LolO, a 2-oxoglutarate-dependent nonheme Fe oxygenase, catalyzes both the hydroxylation of AcAP and the resulting alcohol's cycloetherification to give *N*-acetylnornoline (NANL). The mechanism of hydroxylation is well understood, but the mechanism of the oxacyclization is not. I synthesized difluorinated analogs of AcAP in an attempt to further understand the mechanism of the unusual cycloetherification step.

I prepared 6,6-F_2-AcAP in eight steps from *N*,*O*-protected 4-oxoproline. The key step was a Dieckmann condensation that annulated the A ring onto the B ring. When I subjected 6,6-F_2-AcAP to LolO, the enzyme was able to catalyze both the hydroxylation and the cycloetherification to make 6,6-F_2-NANL, suggesting that the LolO has a flexible active site, as it did not differentiate between the natural substrate (AcAP) and this difluorinated analog of AcAP. Also, it suggested that the cycloetherification mechanism most likely involves a C(7) radical as opposed to a C(7) carbocation. Then, I prepared 7,7-F_2-AcAP from 3-oxoproline in 17 steps where the key step was radical cyclization to make the pyrrolizidine ring in 5-*exo*-*dig* fashion. By contrast, when I subjected the difluorinated analog 7,7-F_2-AcAP to LolO, the cycloetherification step was shut down completely, giving 2-OH-7,7-F_2-AcAP as the sole product. Because 7,7-F_2-AcAP completely blocks the cycloetherification step, it may be used in the future to further understand the cycloetherification of 2-hydroxy-AcAP by accumulating and characterizing the LolO intermediates responsible for cycloetherification.

KEYWORDS: biosynthesis, loline alkaloids, cycloetherification, difluorinated compound

Nabin Panth

(Name of Student)

12/10/2021

Date

SYNTHESIS OF 6,6- AND 7,7-DIFLUORO-1-ACETAMIDOPYRROLIZIDINES AND THEIR OXIDATION CATALYZED BY THE NONHEME Fe OXYGENASE LolO

By
Nabin Panth

Dr. Robert B. Grossman
Director of Dissertation

Dr. Yinan Wei
Director of Graduate Studies

12/10/2021
Date

DEDICATION

To my parents Nanda Ram Panth and Sita Devi Panth

ACKNOWLEDGMENTS

I am very grateful to Dr. Robert B. Grossman for his constant support, encouragement, and constructive criticism during the course of my PhD. I would like to thank him for having patience with me, and training me from a novice chemist to a proud synthetic organic chemist. It has been such a pleasure to work in his group and I have enjoyed every bit of my PhD journey.

I would like to thank my committee members (Dr. Arthur Cammers, Dr. Christopher L. Schardl, and Dr. Yinan Wei) for their guidance and helpful feedback to complete the project. I would like to thank Dr. Padmaja Nagabhyru from Dr. Schardl's lab for teaching me some biology during fungal feeding studies. I would like to thank my external examiner Dr. Craig William van der Koi for helpful feedback in my dissertation and for his time during my final defense.

I would like to acknowledge our collaborators at Pennsylvania State University, Dr. J. Martin Bollinger, Jr. and Dr. Carsten Krebs. I would like to specifically thank two members of their joint research group: Dr. Juan Pan, for her help with initial biological assays of 6,6-F_2-AcAP with LolO, and Eliott S. Wenger for his tremendous help and guidance while doing the biological assays during my visit to Penn State. It was hard to teach biochemistry to a synthetic organic chemist, but he made it so easy.

I would like to thank Dr. Mark Watson for his continuous guidance, support and helpful tips during my PhD as well as during the job search process. I learned a lot from him when I got the chance to become his Teaching Assistant in CHE 533. He not only helped in repairing the various instruments (chiral GC, departmental GC-MS) but also taught me how to fix them. I am forever grateful to him for always making me believe that what I am doing in the lab will be helpful in jobs later on.

I would like to thank Dr. Sean R. Parkin for the beautiful crystal structures and teaching me how the X-ray crystallography works. I would like to acknowledge Mr. Jeff Babbit for making and repairing various glassware for me. I am very grateful to Mr. Art Sebesta for fixing almost every piece of equipment in the lab and teaching me how to fix them. I would like to thank Dr. Manjiri Patwardhan for giving me leadership roles while being the Teaching Assistant in her organic chemistry labs. This has certainly helped me in my personal and professional development.

I would like to thank my lab member Setareh Saryazdi for teaching me all the synthetic skills. It was not an easy task for her to teach all the synthetic organic skills to someone who had just ventured into a synthetic field. However, she made the process so easy. I am grateful to our undergrad Amanda Medina for making a cheerful environment in the lab.

I would like to acknowledge my wife Samiksha Kandel Panth for her constant support and care during my Ph.D. I am very grateful to her for taking care of our son (Nirvan Panth) without any complaints as there was very limited time I could give to my family during my PhD. I would like to acknowledge my sisters Mina Panth Banjade and Durga Panth Poudel for all the love and care.

I would like to acknowledge my friends; Ankit Pandeya, Surya Aryal, Priya Karna, and Khaga Raj Neupane for making Lexington, KY as a home away from home. I would like to thank Dr. Dhruba Poudel, Dr. Rishi Sapkota, and Binod Nepal for their support during the process. I am very grateful to have all of them in my life.

Last but not the least, I am forever grateful to my parents (Nanda Ram Panth and Sitadevi Panth) for all the pain they have endured so that I can get a proper education. It would not have been possible at all if my father had not prioritized my education with utmost importance. Even though he could not get the proper education he wanted due to financial hardships, he always made sure that I could get all the degrees that I want. I am very happy that I am able to fulfill his dream and with due respect, I am dedicating this degree to my parents.

TABLE OF CONTENTS

LIST OF TABLES

LIST OF FIGURES

LIST OF SCHEMES

CHAPTER 1. INTRODUCTION

1.1 Aim and Scope of this study

One of the most remarkable steps in loline alkaloid biosynthesis is the introduction of an ether bridge connecting two unactivated C atoms. As part of understanding the mechanism of ether bond formation, in this report, I describe the synthesis of 6,6-difluoro-1-*exo*-acetamidopyrrolizidine (6,6-F_2-AcAP) and 7,7-difluoro-1-*exo*-acetamidopyrrolizidine (7,7-F_2-AcAP) and their oxidation catalyzed by LolO, the enzyme responsible for catalyzing the cycloetherification reaction in loline alkaloid biosynthesis.

1.2 Loline alkaloids

Lolines are a group of natural products that have a saturated pyrrolizidine ring and an unusual ether bridge between C(2) and C(7) which causes the pyrrolizidine ring to be strained (Figure 1.1).[1] Various substituents on amino groups define different lolines (Figure 1.2).

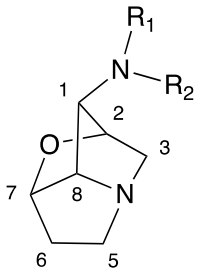

Figure 1.1 Loline alkaloids; a heterotricyclic core including ether bridge between C(2) and C(7).

The first loline alkaloid to be discovered was reported by Hofmeister (1892) and named temuline. Yunusov and Akramov in 1955 isolated an alkaloid from darnel seeds and named it loline. Besides loline, they isolated another alkaloid, *N*-acetylloline, which they called

lolinine.[2] Later on, Dannhardt and Steindl in 1985 demonstrated that norloline (loline without the *N*-methyl group) and temuline had the same structure.[3]

In a further investigation of loline alkaloids, Yunusov and Akramov in 1960 demonstrated that the two rings of the pyrrolizidine are bridged by an oxygen atom.[4] They proposed that lolines had an exocyclic amino group and an oxygen atom attached to the same ring carbon. The suggestion was later corrected by the same researchers in 1966 when they suggested the *N*-methyl-1-*endo*-aminopyrrolizidine structure with an ether bridge between C(2) and C(7) (Figure 1.3).

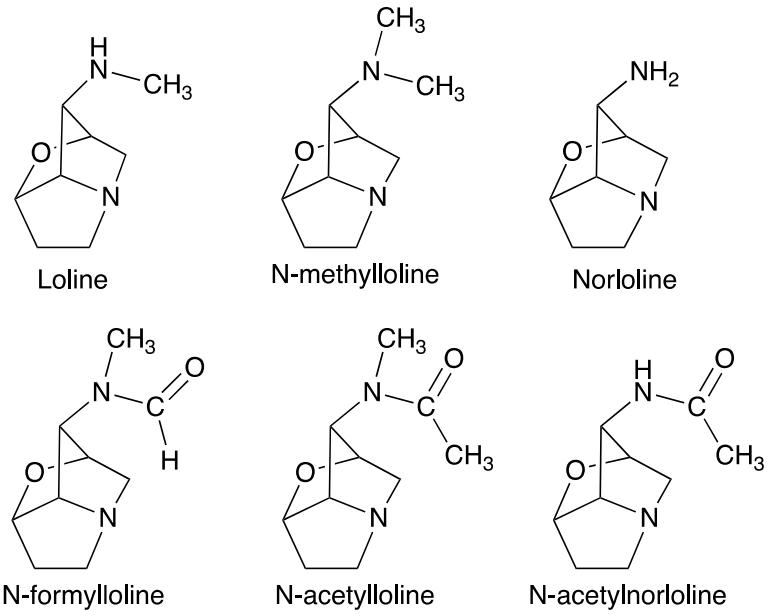

Figure 1.2 Various naturally occuring loline alkaloids

In 1965, Yates and Tookey isolated an alkaloid from *Lolium arundinaceum* which they called festucine. The proposed structure of festucine was similar to loline except that the $NHCH_3$ substituent was on the exo face of the pyrrolizidine. The structure of festucine was confirmed by Aasen and Culvenor in 1969 by using various spectroscopic techniques and

melting point studies. With these studies, they showed that the structure of loline was in fact identical to festucine.[5] Bates and Morehead in 1972 finally confirmed the absolute configuration of loline by using dispersion X-ray diffraction analysis.[6]

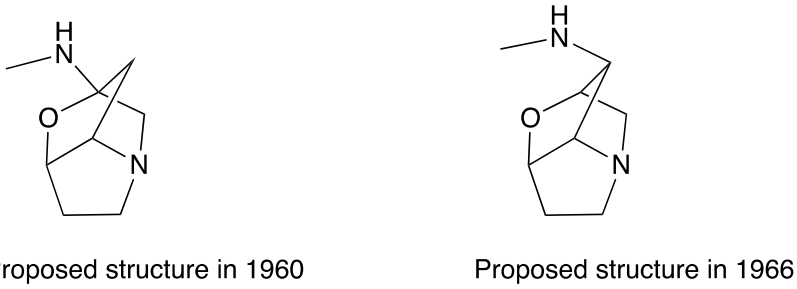

Proposed structure in 1960 Proposed structure in 1966

Figure 1.3 Loline structures proposed by Yunusov and Akramov.

With the structure of loline established, research was directed towards the other derivatives of loline alkaloids with different substituents at 1-amine. Among them, *N*-methylloline (NML), *N*-formylloline (NFL) and *N*-oxide of *N*-acetylloline (NAL) were isolated from *L. temulentum*, whereas *N*-acetylloline (NAL), *N*-formylloline and *N*-acetylnorloline (NANL) were reported from *L. arundinaceum.*[7] Batirov et al., in 1977, reported the unusual structure of lolidine, a loline alkaloid connected to another saturated pyrrolizidine that instead of the C(2)-O-C(7) bond, has a chlorine atom at C(7) and is hydroxylated at C(2).[8]

The biogenic source of loline was uncertain for a long time until Blankenship *et al* in 2001 demonstrated that the endophytic fungus *Epichloe uncinata* is fully capable of *de novo* synthesis of loline alkaloids in defined-medium fermentation cultures.[9]

1.3 Biological activities of loline alkaloids

Lolines are insect-deterrent compounds which are produced in cool season grasses infected by endophytic fungi of the genus *Epichloe*. These endophytic symbiotic fungi grant their host chemoprotection from insects.[10] The insecticidal effect of loline alkaloids were reported for large milkweed bug, green bug aphid and bird-cherry oat aphid.[7] Loline alkaloids have been shown to be feeding deterrents against Japanese beetles and larvae of large milkweed bug.[7] Furthermore, *in vitro* tests of *N*-formylloline, *N*-methylloline and *N*-acetylloline showed feeding deterrence against fall armyworm and European corn borer larvae.[11] Lolines increase the resistance of endophytic infected grass to insect herbivores but have been found to be nontoxic to mammals.[10] These broad spectrum insecticidal effects and feeding deterrent effects of loline alkaloids could be useful as a potential alternative of insecticides.[12]

1.4 Overview of loline alkaloid biosynthesis

The lolines are structurally similar to necines, pyrrolizidine alkaloids produced by many plants (Figure 1.4), which led to the early hypothesis that biosynthesis of loline alkaloids might be similar to plant pyrrolizidines.[13]

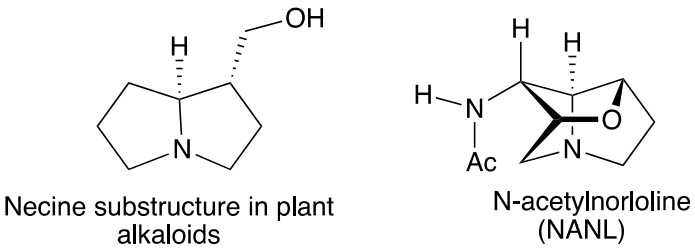

Figure 1.4 Comparison of lolines with plant alkaloids

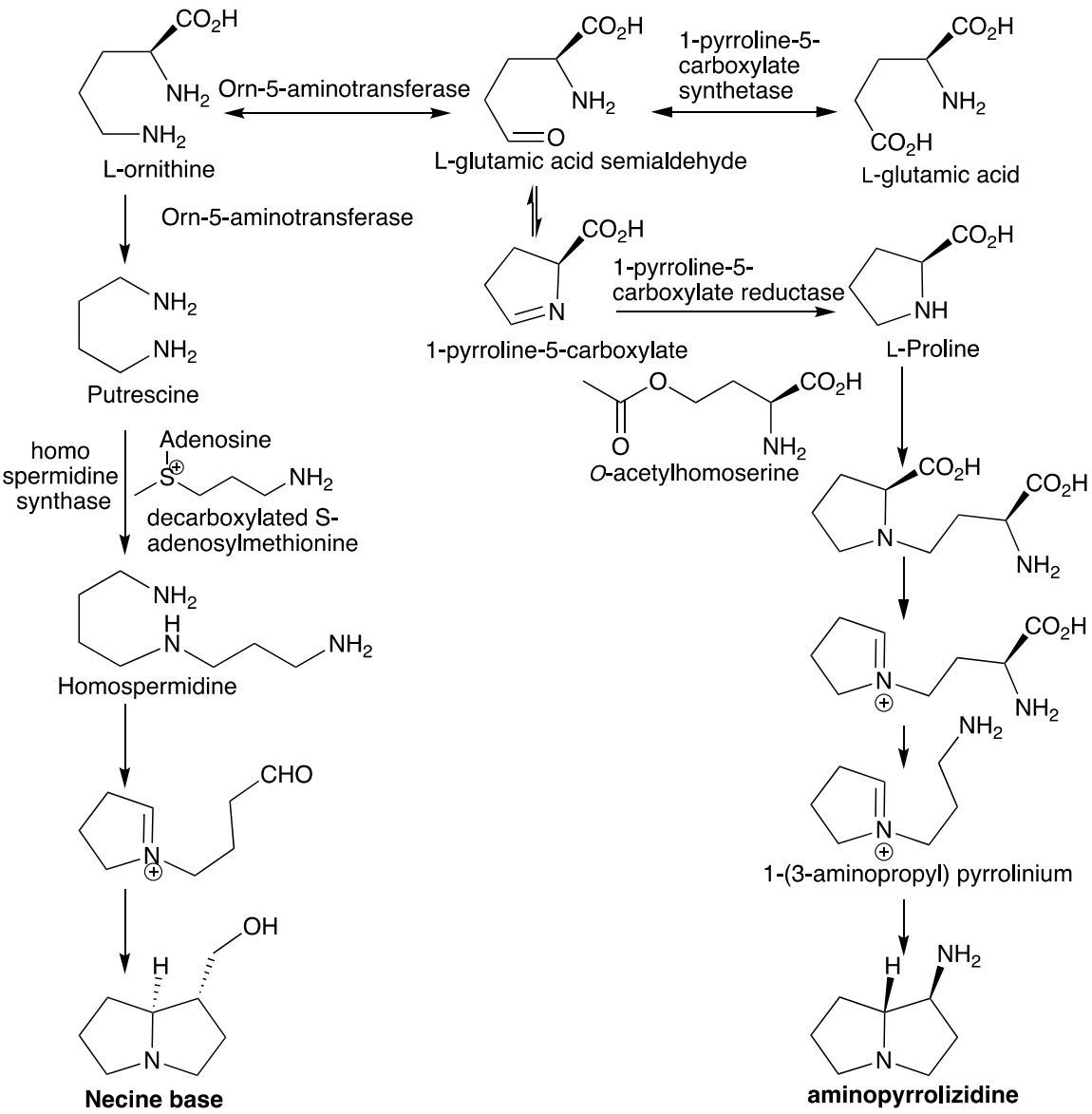

Scheme 1.1 Biosynthesis of necine-type pyrrolizidine alkaloids in plants (left) and early steps in proposed loline pathway (right).[14, 15]

However, feeding studies with ^{15}N-, ^{13}C-, and ^{2}H-labelled amino acids demonstrated that the biosynthesis of loline alkaloids is different from plant pyrrolizidines.[16] A cluster of 11 genes designated as *LOL* encodes enzymes that are associated with loline alkaloid biosynthesis. The putative gene products include three pyridoxal-5´-phosphate (PLP) containing enzymes (LolC, LolD, LolT), four oxidation enzymes (LolE, LolF, LolO, LolP),

an *N*-acetamidase (LolN), two *N*-methyltransferase (LolM, LolU), and an amino acid binding protein (LolA).[16]

By using deuterium-labelled putative intermediates in feeding studies, Blankenship *et al*. demonstrated that the first step in loline alkaloid biosynthesis (Scheme 1.2) is condensation of L-proline and homoserine (probably *O*-acetylated) to make the diamino diacid, NACPP.[17] This finding led to the suggestion that this condensation is catalyzed by LolC, a γ-type pyridoxal-5'-phosphate (PLP) dependent enzyme.[17, 18] Cyclization, decarboxylation, and acetylation of NACPP produces 1-*exo*-acetamidopyrrolizidine (AcAP).[16] Pan *et al*. observed that mutations in LolO in natural fungal variants resulted in the accumulation of AcAP as the end product, and the inhibition of LolO expression by RNAi resulted in accumulation of AcAP.[16] These experiments suggest that LolO catalyzed the introduction of an ether bridge into AcAP to give the tricyclic loline NANL, the first loline alkaloid along the biosynthetic pathway. Purified LolO, in the presence of Fe(II) and an excess of 2-OG in air, catalyzed conversion of AcAP to NANL, showing that LolO alone is fully capable of catalyzing both hydroxylation and oxacyclization to introduce the strained ether bridge.[10] Manipulation of the acetamido group of NANL by various modification enzymes LolM, LolN, LolP then converted it into other loline alkaloids (Table 1.1).[1, 19]

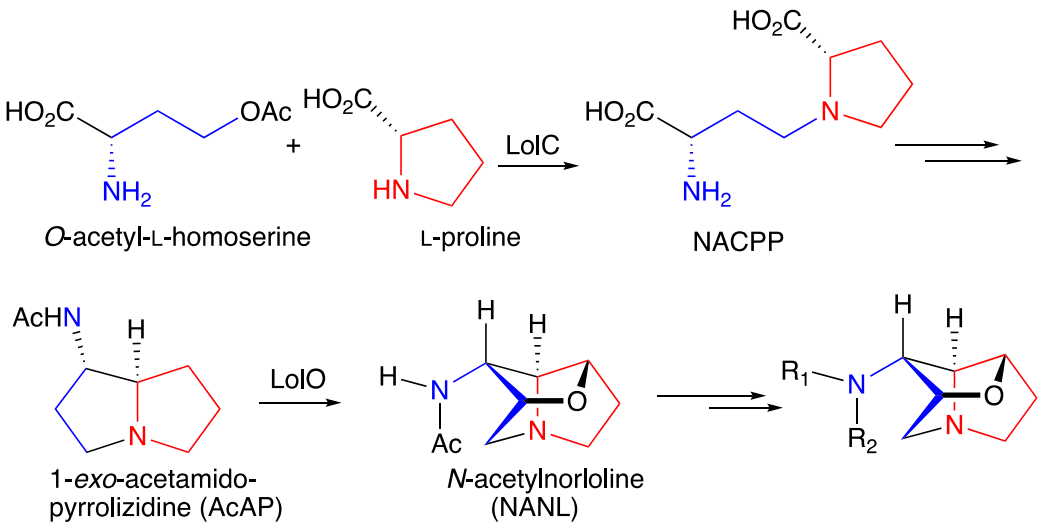

Scheme 1.2 Overview of loline alkaloid biosynthetic pathway.[1]

Table 1.1 Formation of various loline alkaloids and respective enzymes.

R_1	**R_2**	**Other lolines**	**Enzymes**
H	H	norloline	LolN
H	Me	loline	LolM
Me	Me	*N*-methylloline	LolM
Me	CHO	*N*-formylloline	LolP
Me	Ac	*N*-acetylloline	

1.5 Study of LolO catalysis and investigation of oxacyclization mechanism

Activation of two C–H bonds by a single Fe/2-OG oxygenase to make an ether bridge is rare but precedented. Only a handful of enzymes, such as hyoscyamine 6β-hydroxylase (H6H), clavulanic acid synthase (CAS), and AurH, a cytochrome P450 monooxygenase, are known to catalyze two C–H bond activations and to install an ether bridge.[20-23]

Hyoscyamine and scopolamine are tropane alkaloids produced by a perennial herbaceous plant *Atropa belladonna*. Scopolamine is reported to potentially have various pharmacological uses like analgesia, treatment of Parkinson's disease, motion sickness,

and also as anesthesia before surgery.[24] To combat the limited supply of scopolamine available naturally, studies have been conducted to make transgenic plants by overexpressing certain enzymes.[24] H6H, an Fe/2-OG dependent enzyme, was found to have an indispensable role during biosynthesis of scopolamine as it catalyzes the final epoxidation of hyoscyamine through two C–H bond activations (Scheme 1.3).[20]

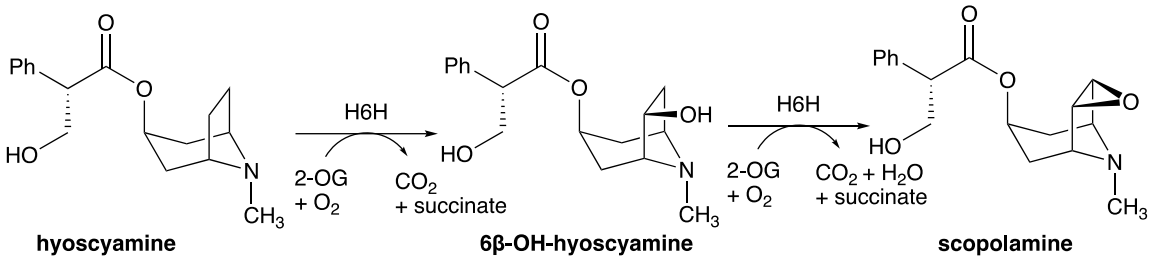

Scheme 1.3 C–H bond activations in scopolamine biosynthesis.

Clavulanic acid is a widely used inhibitor of serine β-lactamases (a group of bacterial enzymes that inactivate antibiotics) in the fight against antibiotic resistance.[25, 26] CAS is another Fe/2-OG dependent enzyme that catalyzes three key steps — hydroxylation, cyclization and desaturation — in the biosynthesis of clavulanic acid. It is very unusual for an enzyme to catalyze three different reactions in a biosynthetic pathway (Scheme 1.4).[23]

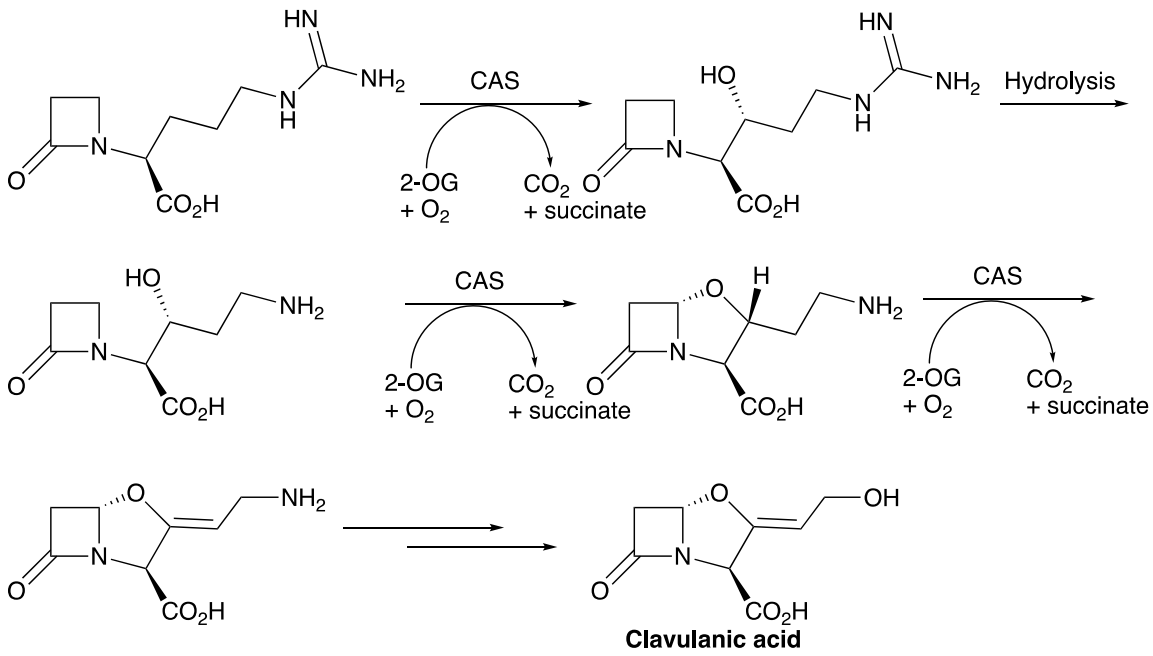

Scheme 1.4 C–H bond activation in clavulanic acid biosynthesis.

AurH, a cytochrome P450 monooxygenase found in *Streptomyces thioluteus*, is capable of activating two allylic carbon atoms to make a chiral substituted tetrahydrofuran ring as a single enantiomer.[21] This *O*-heterocycle is an important part of the antibiotic aureothin as it provides rigidity to the carbon backbone and contributes significantly to the antifungal activity of the antibiotic.[22, 27] In the first step, AurH catalyzes the asymmetric hydroxylation of deoxyaureothin to make 7-hydroxydeoxyaureothin, and in the second step, it mediates C–O bond formation which leads to oxacyclization.[27]

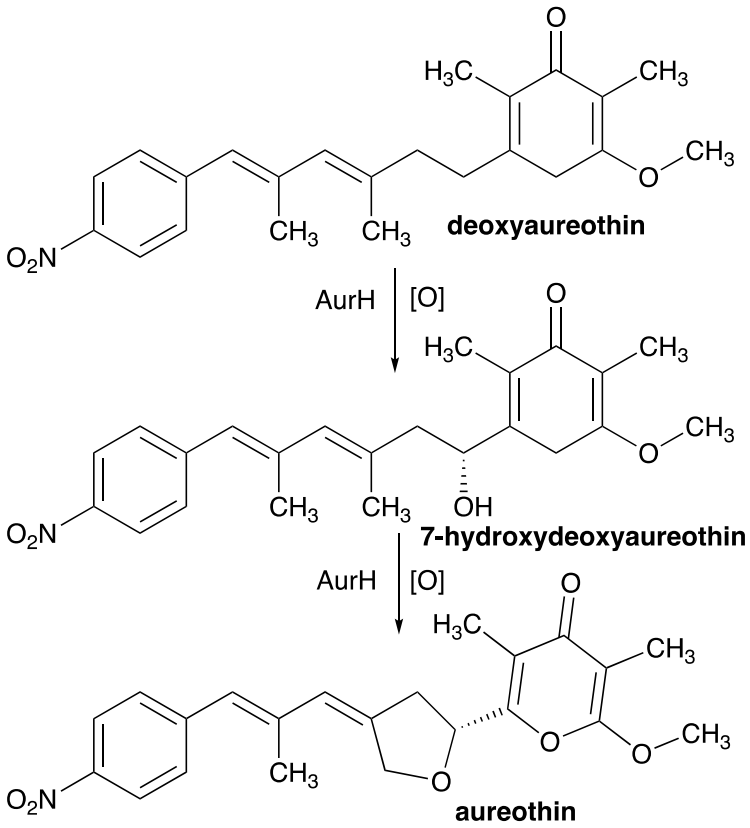

Scheme 1.5 C–H bond activation in aureothin biosynthesis.

Another example of an ether bridge can be found in the nargenicin family of antibiotic macrolides (Figure 1.5), which feature a rare ether-bridged *cis*-decalin moiety and show a narrow spectrum of antibiotic activity.[28]

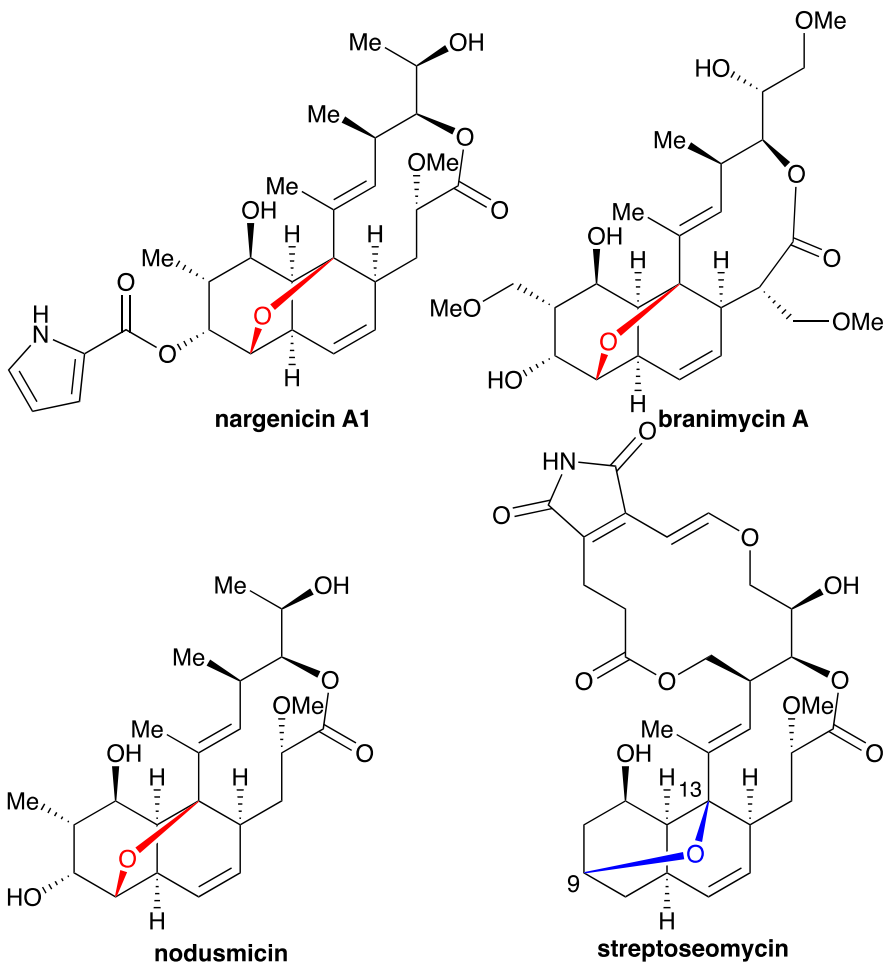

Figure 1.5 Representative nargenicin family antibiotics having ether bridge between C(8) and C(13); C(9) and C(13).

In an *in vitro* deoxynargenicin-conversion assay, NarN in presence of Fe and 2-OG was reported to catalyze installation of the ether bridge in 8,13-deoxynargenicin to make nargenicin A1, suggesting that the enzyme may be a useful tool in enzyme-assisted synthetic studies (Scheme 1.6).[28] Also, by using *narN* inactivated by homologous recombination, production of 8,13-deoxynargenicin was observed instead of nargenicin A1, further confirming the involvement of NarN in ether bridge installation. The resulting 8,13-deoxynargenicin, lacked the antibiotic activity of nargenicin A1, supporting the importance of the ether bridges in these antibiotics.[28]

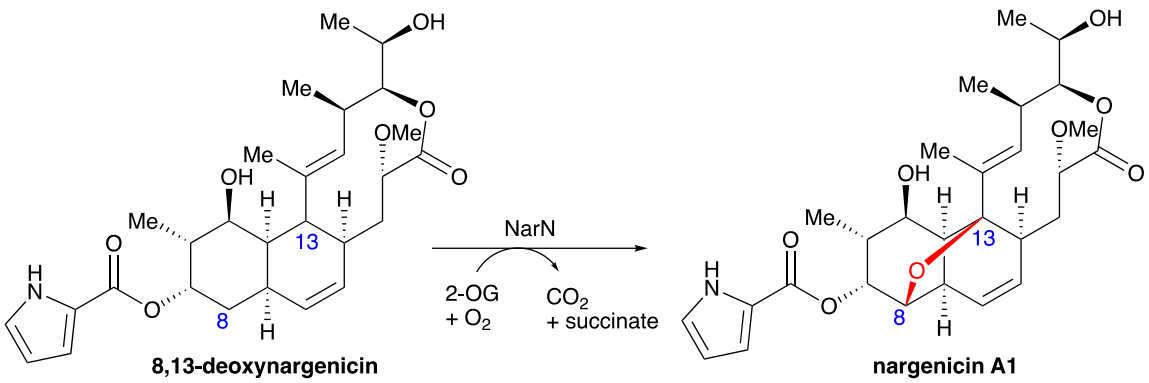

Scheme 1.6 Installation of the ether bridge in nargenicin biosynthesis.

LolO, an iron- and 2-oxoglutarate-dependent (Fe/2-OG) oxygenase, catalyzes the conversion of AcAP to NANL whereby the ether bridge is installed through the activation of two C–H bonds (Scheme 1.7).[10] Because conversion of AcAP to NANL is a four-electron oxidation step which requires removal of two hydrogen atoms from unactivated C atoms, each conversion requires one equivalent of 2-OG. When racemic AcAP was subjected to an excess of oxygen and the concentration of 2-OG was limited, 2-*endo*-OH-AcAP was detected through LC-MS analysis (Figure 1.6).[10] Production of 2-*endo*-OH-AcAP reached a maximum when the ratio of 2-OG:(1*S*)-AcAP was approximately 0.5. Upon further increasing the ratio, the amount of 2-*endo*-OH-AcAP decreased, and NANL was observed. When the ratio of 2-OG:(1*S*)-AcAP was 2 or higher, (1*S*)-AcAP was fully converted to NANL.

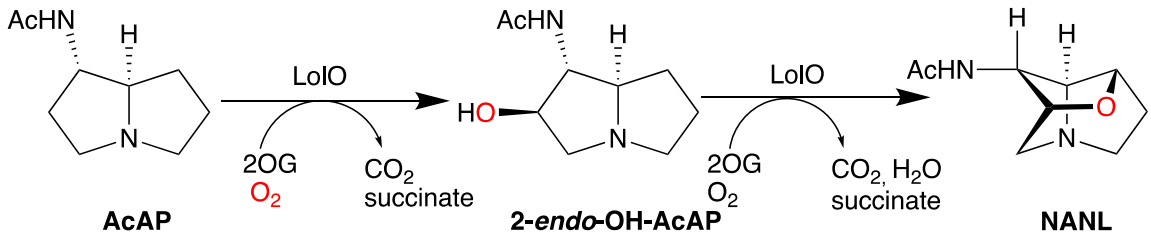

Scheme 1.7 Overall transformation catalyzed by LolO

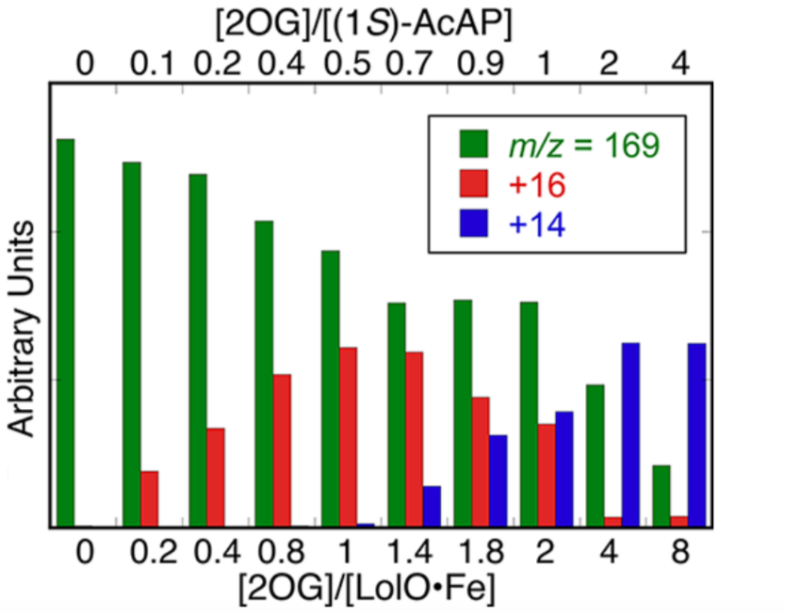

Figure 1.6 Analysis of LolO reaction with varying 2-OG levels. [10] (https://pubs.acs.org/doi/abs/10.1021/acs.biochem.8b00157) further permission should be directed to ACS

1.6 Investigation of the second step of ether bond formation (cycloetherification)

The mechanism of hydroxylation of a C–H bond has been thoroughly studied (Scheme 1.8)[29]. First, the 2-OG replaces two water molecules in the active site of LolO in binary complex I to form ternary complex II, which absorbs light at 530 nm. Then, the hydroxylation substrate displaces a water molecule from Fe and coordinates to the Fe(II) center in its place to form quaternary complex III, which absorbs light at 520 nm.

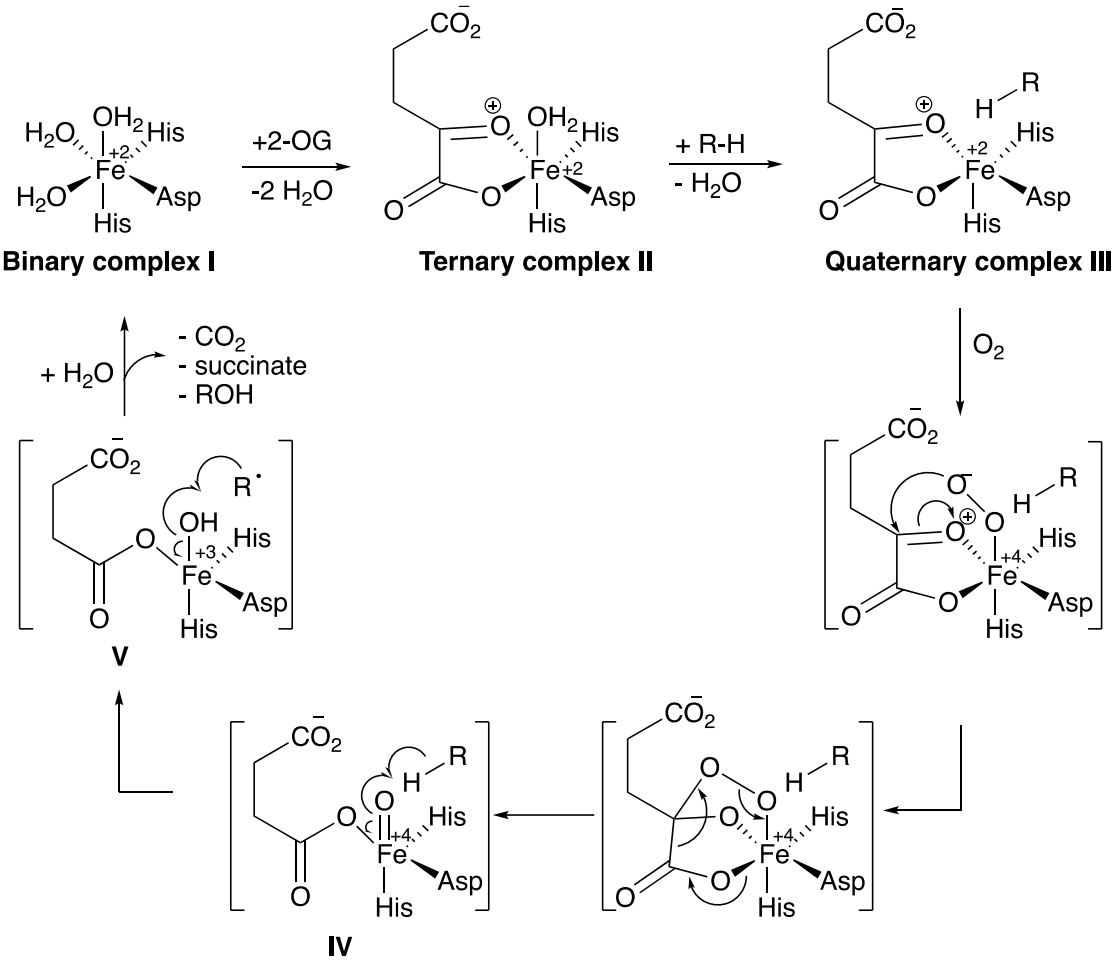

Scheme 1.8 General mechanism of hydroxylation by Fe/2-OG-dependent dioxygenase.[29]

In the next step, O_2 binds to the Fe(II) center in a linear fashion, and the terminal O atom attacks the carbonyl carbon of 2-OG to form intermediate complex IV having Fe(IV)=O and UV light absorption at 318 nm. The complex IV then uses the Fe-bound O atom to abstract an H atom from the substrate to form an alkyl radical Fe(III)–OH complex V. Finally, the radical abstracts the OH group from complex V to produce hydroxylated product and, after some ligand exchanges with water, to regenerate the binary complex I.[29]

We knew that LolO catalyzed both the hydroxylation and oxacyclization steps of ether bridge formation.[10] The hydroxylation step could occur either at C(2) or C(7) (Scheme 1.9).

Pan *et al.* used deuterium kinetic isotope effect and stop flow experiments to learn which carbon atom was hydroxylated first.[10] When an abstractable hydrogen is replaced with deuterium, the decay rate of the Fe(IV)=O complex decreases, leading to its accumulation, which can be observed through the stop-flow technique. Under low 2-OG conditions, under which only hydroxylation was expected to take place, the Fe(IV)=O complex absorbing at 318 nm accumulated to a much greater extent when LolO was subjected to 2,2,8-[$^2H_3$]AcAP as compared to 7,7-[$^2H_2$]AcAP, confirming that hydroxylation occurred at C(2) first, and then oxacyclization with C(7) occurred to make the ether bridge.[10]

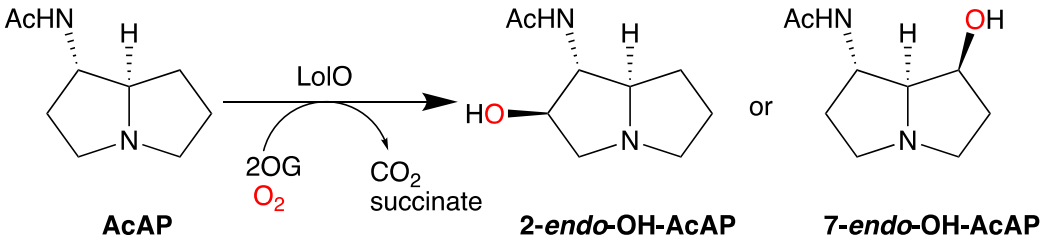

Scheme 1.9 Possibility of hydroxylation at C(2) and C(7).

The mechanism for oxacyclization catalyzed by CAS has been proposed based on isotope labelling studies and the crystal structure of the CAS-Fe(II)-2-2OG-PCA complex, as shown in Scheme 1.10.[30, 31] The Fe(IV)=O complex in (**a**) abstracts the H atom from substrate C(4)'*S* to form Fe(III)–OH complex along with C(4)'-centered radical substrate. In the next step, a C(3)-bound hydroxyl group attacks at C(4)' with transfer of a H atom to Fe(III)–OH to make DHCA along with Fe(III)-OH_2 (complex **d**).

In an alternative possible mechanism, an electron transfer may occur from the C(4)' radical to Fe(III)-OH making complex **c** with an iminium ion and a Fe(II)-OH complex. In the next step, C(3)-bound hydroxyl group attacks at C(4)' cation with transfer of H atom to Fe(II)-OH to make DHCA and Fe(II)-OH_2 complex (**d**).

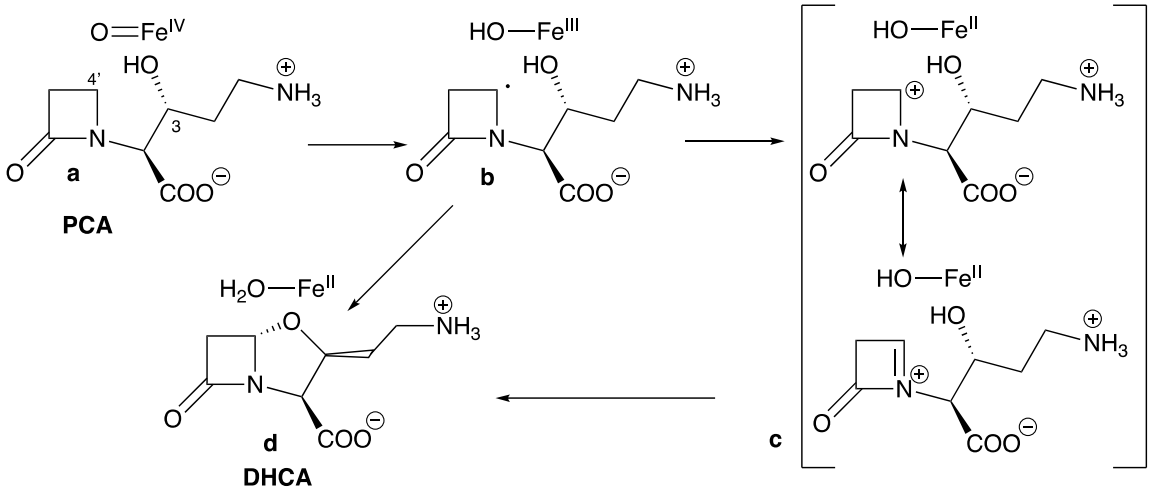

Scheme 1.10 Suggested mechanism for oxidative cyclization catalyzed by CAS.

We understand the mechanism of the first step of the ether bridge installation by LolO. However, we still know little about the oxacyclization step. It would be interesting to know how the same enzyme is capable of catalyzing two different reactions. Understanding the mechanism of this type of reaction might inform strategies for engineering the enzyme to carry out the oxacyclization reaction in other desired compounds.

Dr. Juan Pan at Penn State University observed that the 4.2-K/zero-field Mossbauer spectrum of the LolO-Fe^{II}-2-OH-7,7-[$^2H_2$]AcAP reactant complex showed the presence of two distinct quadrupole doublets characteristic of high spin ferrous ion (Figure 1.7 left). When reactant complex reacted with O_2 for varying times, she observed that the area of the minor quadrupole doublet remained constant while the major quadrupole doublet decreased in intensity, suggesting that the major quadruple doublet might be the O_2-reacting form. Additionally, two partially resolved lines at ~0.5 mm/s and ~1.0 mm/s in spectra of O_2-treated samples indicated the presence of two ferryl complexes in the LolO-catalyzed oxacyclization reaction (Figure 1.7 right).

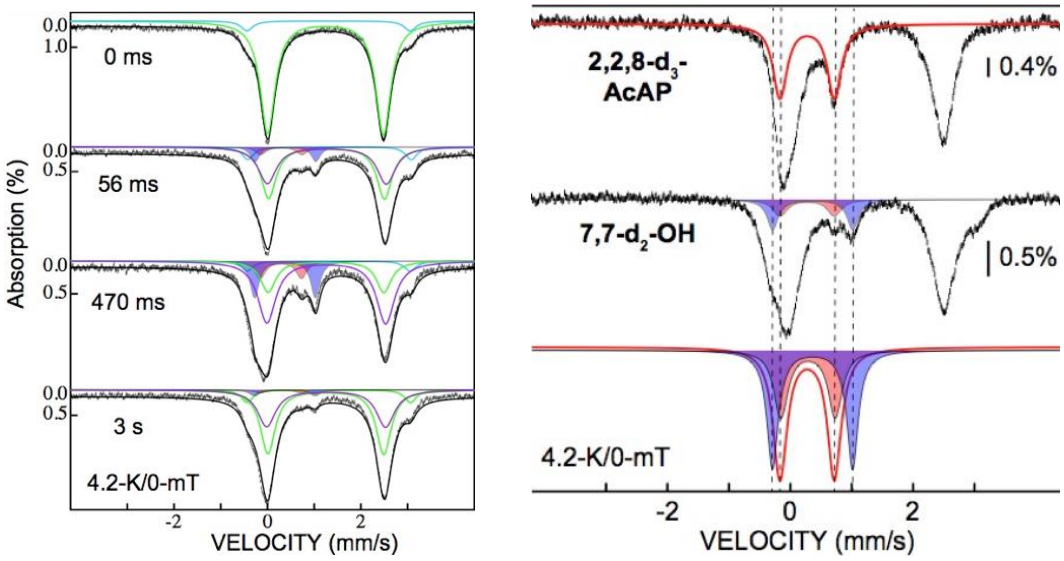

Figure 1.7 Mossbauer spectra of LolO in reaction with 7,7-[$^2H_2$]-2-OH-AcAP (left), Comparison of Mossbauer spectra of intermediates in LolO reactions (right). (Pan, J., unpublished data, permission granted by author)

The parameters of the first ferryl species (Fe^{IV} a) were identical to the ferryl intermediate observed in the hydroxylation reaction of LolO (Table 1.2), whereas the second ferryl species (Fe^{IV} b) showed a large isomer shift, indicating an unusual ligand arrangement at the Fe center. Also, by fitting the total and individual ferryl species in the cyclization reaction to a 3-step minimum reaction model, Dr. Pan showed that the two ferryl species had very similar kinetics (Figure 1.8). Based on these features of the two ferryl complexes, we hypothesized that either both of these ferryl species are oxidizing intermediates in the reaction, or, more likely, the two species are in rapid equilibrium, and only one actually abstracts the C(7)–H atom for cyclization. The fact that the Mossbauer parameters of one of the ferryl species were identical to ferryl species observed during the hydroxylation step suggests that the new ferryl species might be responsible for the C(7)–H hydrogen atom abstraction to initiate the cyclization.

Table 1.2 Parameters of ferryl complexes during hydroxylation and oxidative cyclization step.

Fe^{IV}	δ (mm/s)	$\lvert\Delta E_Q\rvert$ (mm/s)
Cyclization **a**	0.28	0.89
Cyclization **b**	0.37	1.30
Hydroxylation	0.28	0.89

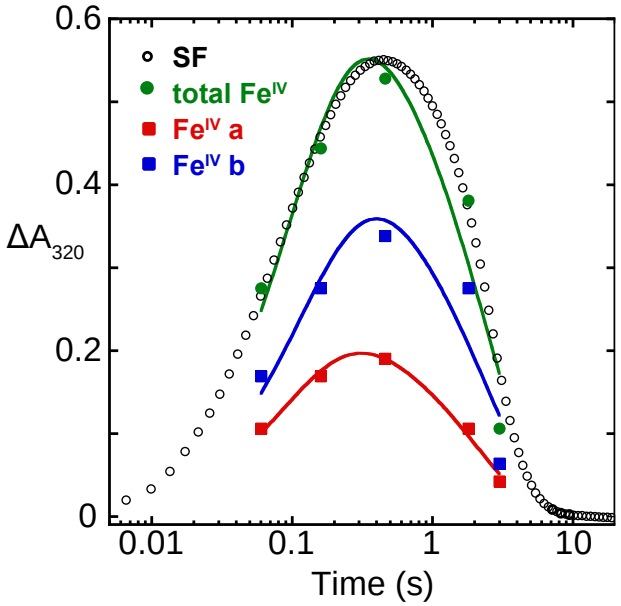

Figure 1.8 Comparison of FQ-Mossbauer experiment to SF-Abs in oxidative cyclization reaction. (Pan, J., unpublished data, permission granted by author)

We hypothesized that the hydroxylation and cyclization reactions may proceed in a similar manner until ferryl intermediate IV (Scheme 1.11). During the hydroxylation, the ferryl intermediate decays in the typical hydroxylation reaction manner. However, during the cyclization, the already installed C(2)–OH group, due to its close proximity, may coordinate to the Fe center, which could change the electronic structure at the Fe center enough to generate different Mossbauer spectra and to facilitate the cyclization. The hypothesis of direct association of C(2)–OH to Fe was consistent with the observation that

for some Fe/2OG-catalyzed hydroxylation reactions, the crystal structures of enzymes with product still bound show direct OH coordination to Fe.[32, 33]

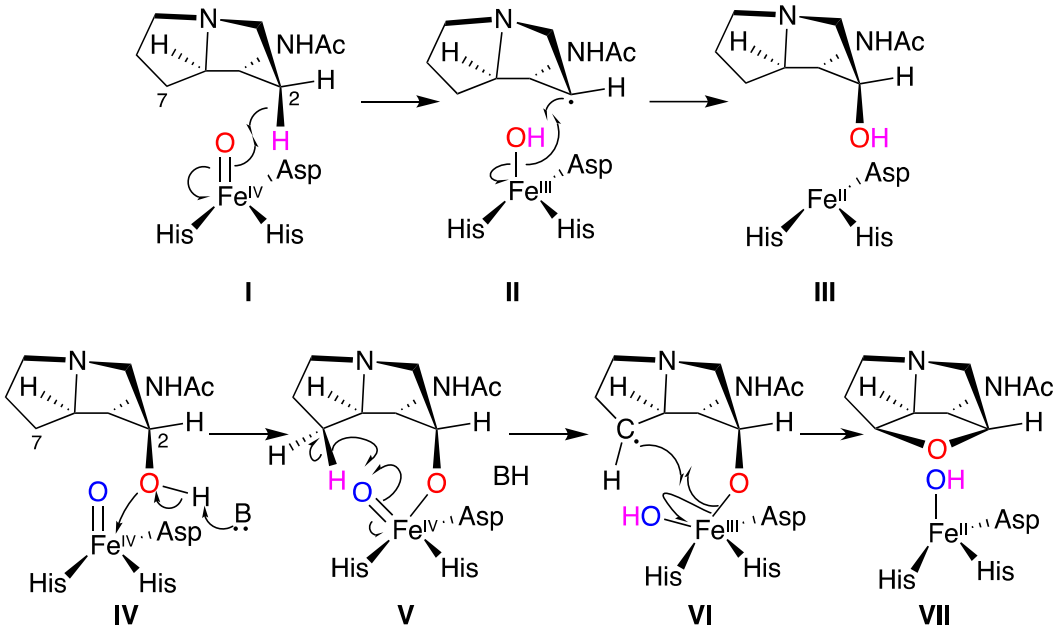

Scheme 1.11 Proposed mechanism for the presence of two equilibrating ferryls in oxacyclization; hydroxylation (top), cyclization (bottom) in LolO-catalyzed synthesis of *N*-acetylnorloline.

In an alternate mechanism (Scheme 1.12), the oxacyclization reaction may go through a polar coupling pathway in which single electron transfer (SET) from the C(7) radical to Fe in complex (**IX**) would lead to the formation of a C(7) carbocation. In the next step, a base could deprotonate the hydroxyl group, which could couple with C(7) carbocation to make the ether bridge between C(2) and C(7).

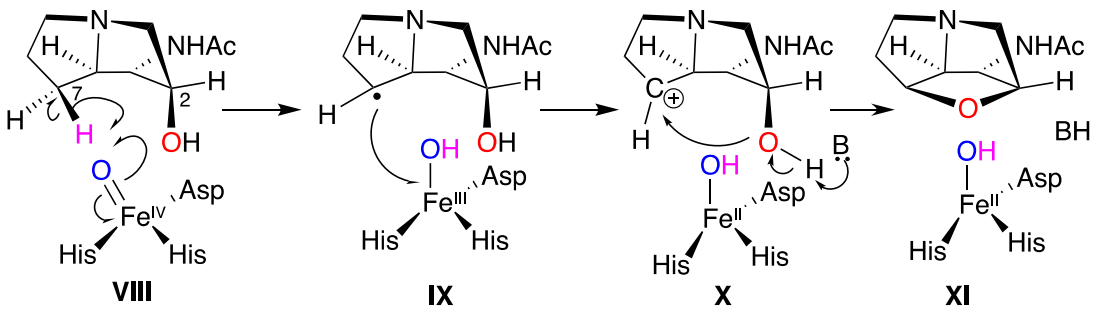

Scheme 1.12 Proposed alternative oxacyclization mechanism involving polar coupling pathway.

In order to test these hypotheses, we needed large amounts of the two ferryl oxo species. The information about coordination number on the Fe center and Fe–O bond length of these ferryl species can be obtained from EXAFS (Extended X-ray absorption fine structure). To generate the large amount of ferryl species, we needed a substrate that would bind to Fe in LolO like 2-OH-AcAP but would not undergo the second C(7)–H abstraction. In the next chapter, I will explain how we thought that this goal might be achieved through the use of 2-OH-6,6-F_2-AcAP, prepared by LolO-catalyzed hydroxylation of 6,6-F_2-AcAP, and how it came out to be not the proper substrate for the purpose. This finding led us to synthesize 2-OH-7,7-F_2-AcAP.

1.7 Why fluorinated analogs?

Fluorine is a favorite element for pharmacologists and enzymologists because of its small size and the short internuclear distance to carbon in the carbon–fluorine covalent bond. Fluorine is regarded as a bioisostere of hydrogen.[34] Fluorine has been introduced in many biological molecules to study enzymatic reactions and to act as metabolic inhibitors.[35] Briley and Barnett have used fluorinated analogs in the study of binding sites and reaction mechanisms in carbohydrate derivatives.[35] 4,4-difluorinated analogues of L-

arginine and *N*-hydroxy-L-arginine have been used in the mechanistic study of nitric oxide synthase.[36]

We needed a substrate that would bind to Fe in LolO like 2-OH-AcAP but would not undergo the second C(7)–H abstraction. The 6,6-difluorinated analog of 2-OH-AcAP would stop the cycloetherification provided that two highly electronegative F atoms at C(6) were sufficient enough to inhibit the C(7)–H abstraction. The 7,7-difluorinated analog of 2-OH-AcAP would prevent the cycloetherification completely, as there would not be any H atoms to abstract from C(7). However, we feared that the synthesis of 7,7-F_2-AcAP would much challenging than that of 6,6-F_2-AcAP because of possible β-elimination of HF during the Dieckmann condensation step. In Chapters 2 and 3, I describe how I synthesized the 6,6- and 7,7- difluorinated analogs of AcAP and subjected them to oxidation catalyzed by LolO. We did also consider making monofluorinated derivatives of AcAP, but we quickly rejected this approach due to the difficulty of controlling the stereochemistry of the monofluorinated C(6) and C(7).

CHAPTER 2. **SYNTHESIS OF 6,6-F_2-ACAP AND ITS OXIDATION CATALYZED BY LOLO**

2.1 Introduction

Initially, I thought the C(7)–H abstraction in the second step of LolO cyclization might be retarded or prevented if I used the 6,6-difluorinated analog of 2-hydroxy-AcAP (**1**) (Scheme 2.1).

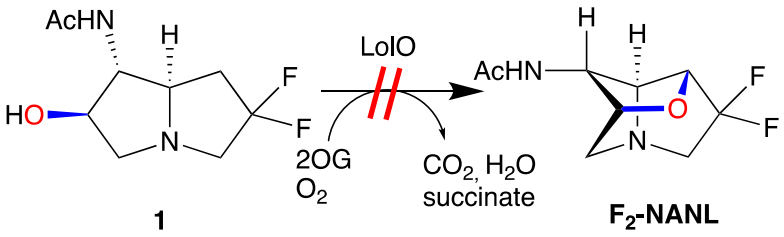

Scheme 2.1 LolO-catalyzed cyclization of 6,6-F_2-OH-AcAP.

The assumption was that the two highly electronegative F atoms on C(6), adjacent to the reactive center C(7), would inhibit C(7)–H abstraction by destabilizing the carbocation or radical formed after hydrogen or hydride abstraction at C(7) (Scheme 2.2).

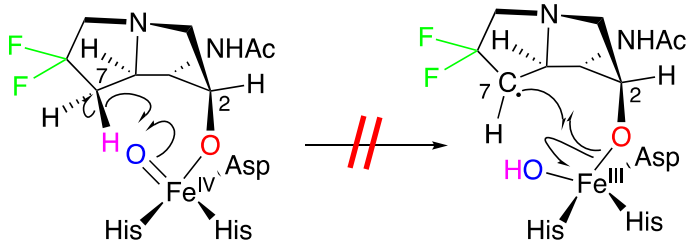

Scheme 2.2 Proposed inhibition of C(7)-H abstraction using 6,6-F_2-AcAP.

2.2 Results and discussion

Because I thought that it would be extremely challenging to synthesize the densely functionalized and stereochemically complex **1** through chemical methods, I decided to rely on LolO to install the hydroxy group on what I thought would be the much more easily

prepared 6,6-F_2-AcAP (**2**) (Figure 2.1). I would then subject **2** to LolO-catalyzed hydroxylation at C(2) to give **1**.[10]

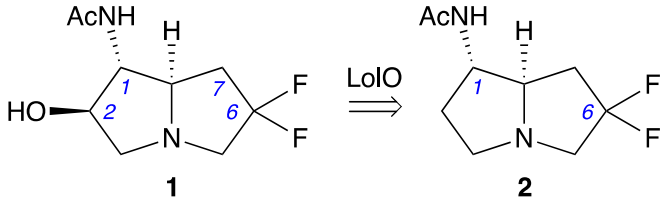

1 **2**

Figure 2.1 Difluorinated analog of 2-OH-AcAP and its preparation from difluorinated analog of AcAP.

I started making **2** by converting L-*trans*-4-hydroxyproline **3** to its *N*-Boc ethyl ester **4**, oxidizing the alcohol of **4** to the ketone with DMP, and then using DAST to obtain L-4,4-difluoroproline derivative **5** (Scheme 2.3). Then, applying the methods we had used previously to prepare AcAP,[37] I deprotected the N atom of **5** and alkylated it with ethyl acrylate to give the 1,6-diester **6**. Following the procedure that our group previously used to make deuterated AcAP analogues, I then induced a Dieckmann reaction of **6** by subjecting it to NaH in toluene;[38] when the starting material had been consumed, I added aqueous acid and heated the mixture to promote β-keto ester hydrolysis and decarboxylation, and then I added NH_2OH and isolated the resulting 6,6-difluorinated 1-oximinopyrrolizidine **8**. Reduction of **8** over Ni_2B and subsequent acetylation provided what I hypothesized was **2a** in 6% yield as well as what I hypothesized was its diastereomer **2b** in 10% yield. I sent **2a** to Penn State University, where Dr. Juan Pan subjected the compound to LolO catalysis under standard conditions.[10] She reported that LolO did not consume **2a** as a substrate.

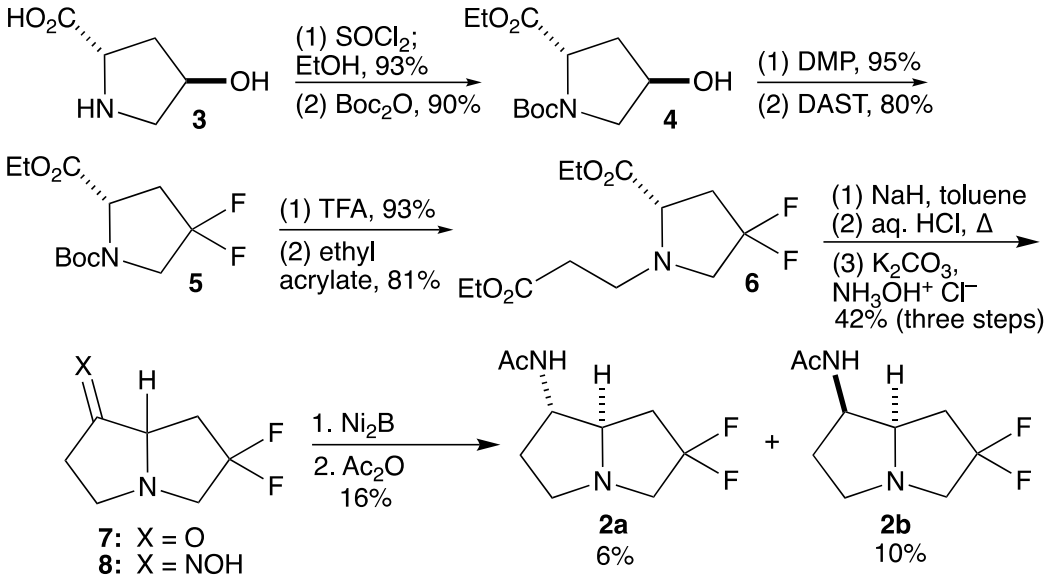

Scheme 2.3 Initial approach towards synthesis of 6,6-F_2-AcAP.

2.2.1 NMR analysis of (± 6,6-F_2-AcAP·BH_3 complex)

Initially, I hypothesized that having two F atoms in the structure might be the reason why LolO did not consume it as a substrate. However, I was able to grow crystals of the endo isomer **2b** over hexane and CH_2Cl_2 (Figure 2.2). The crystal structure of **2b** gave us information regarding why **2a** might not have been consumed by LolO.

2.2.2 Crystal structure of *endo*-6,6-F_2-AcAP·BH_3

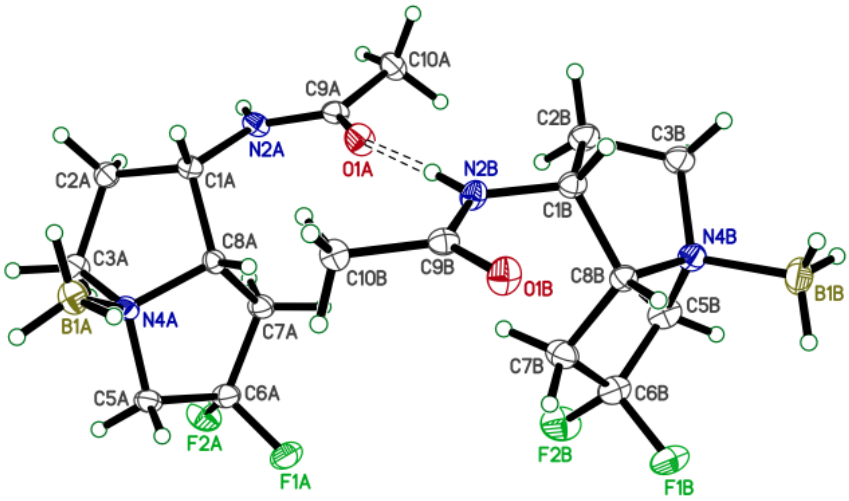

Figure 2.2 Thermal ellipsoid plot of (±) *endo*-6,6-F_2-AcAP·BH_3

To my surprise, the crystal structure of **2b** showed that there was a BH_3 group attached to the pyrrolizidine N. I looked at the ^{1}H NMR spectrum of **2b** once again to find out how I missed those hydrogens in the ^{1}H NMR spectrum. After reading the pertinent literature, I discovered that BH_3 protons appear near 0.5-1.5 ppm which is a common chemical shift for grease and water.[39] This was interesting because I did not observe BH_3 complexation during the synthesis of AcAP even though I was following exactly the same procedure.

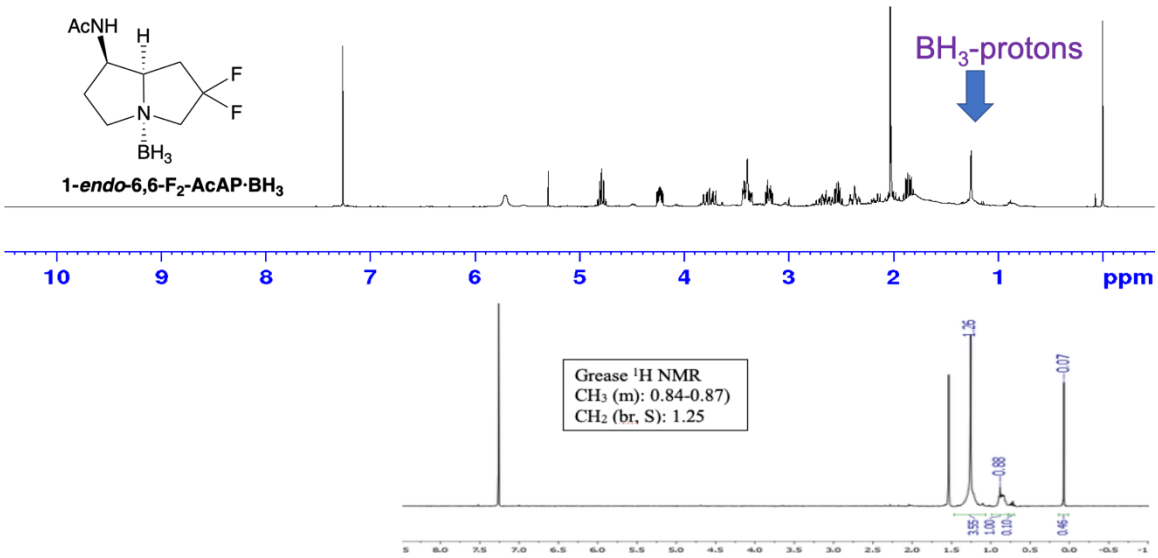

Figure 2.3 Comparison of ^{1}H NMR of (±) *endo*-6,6-F_2-AcAP·BH_3 with ^{1}H NMR of stopcock silicone grease.

After I knew **2b** had a BH_3 group attached to the pyrrolizidine ring, I was curious as to whether the exo isomer **2a** likewise had a BH_3 group attached to the pyrrolizidine ring N. When I closely compared the ^{1}H NMR spectrum of **2a** with that of **2b** (Figure 2.4), it appeared that **2a** had a similar peak pattern where the BH_3 protons appear, suggesting that **2a** might also have a BH_3 group attached to the pyrrolizidine ring N. (I tried to confirm this suggestion by X-ray crystallography, but I was unable to obtain suitable crystals.) Moreover, the presence of a BH_3 group in **2a** might explain why the LolO did not consume **2a**.

The BH_3 could have originated from $NaBH_4$, which I used to make Ni_2B *in situ* in the oxime reduction step (Scheme 2.4).

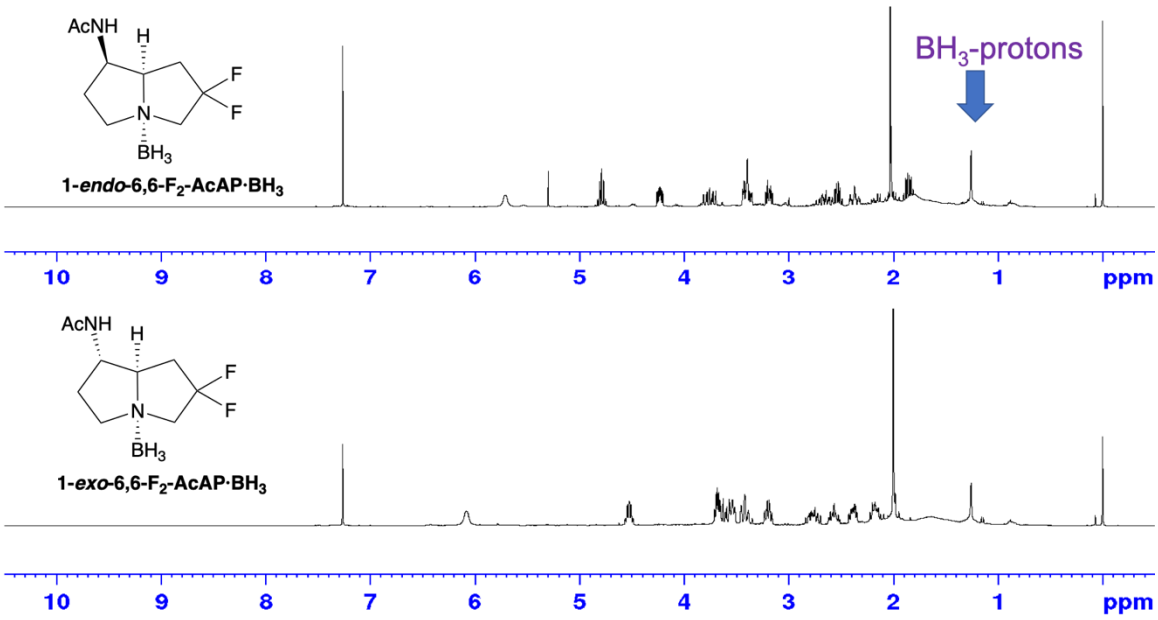

Figure 2.4 Comparison of ^{1}H NMR of (±) *endo*-6,6-F_2-AcAP·BH_3 with ^{1}H NMR of (±) *exo*-6,6-F_2-AcAP·BH_3

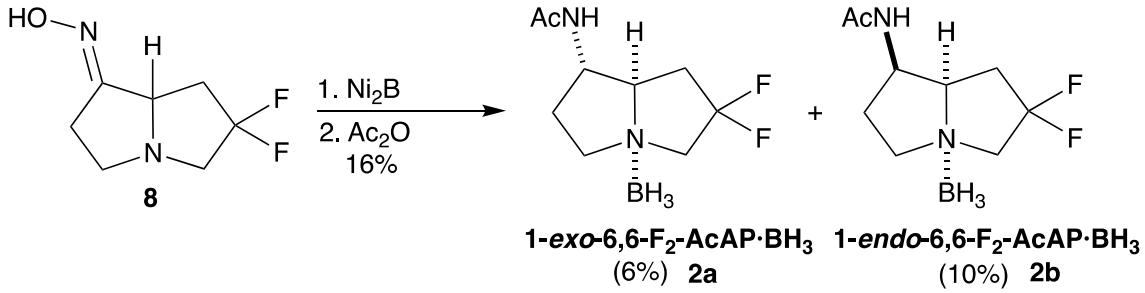

Scheme 2.4 Reduction of 6,6-F_2-oxime with Ni_2B

To prevent a BH_3 complex from forming, I instead reduced **8** with Raney nickel, as shown in Scheme 2.5. Hydrogenation of **8** over Raney Ni and subsequent acetylation provided **2** in 59% yield as a 1.9:1 mixture of diastereomers. The two diastereomers were nearly inseparable, but I was able to separate a small amount of the major diastereomer in pure form as well as a small amount of a 3:1 mixture of the minor and major diastereomers, respectively.

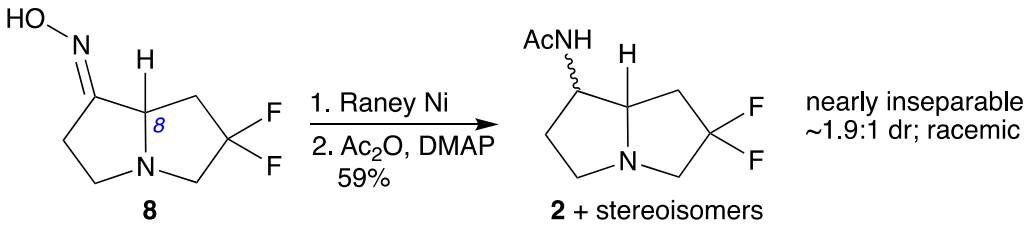

Scheme 2.5 Reduction of 6,6-F_2-oxime with Raney nickel.

Besides the problem of nearly inseparable diastereomers, I also had an absolute configuration problem. From our previous studies, I knew that nascent ketone **7** produced during the decarboxylation would certainly have undergone epimerization at C(8),[10] so **2** and 1-*endo*-**2** were certainly racemic mixtures. This meant that only about 1/3 of my material in hand consisted of **2** itself. Still, I moved forward with the mixture of (±)-**2** and (±)-1-*endo*-**2**, because my next and last step was the LolO-catalyzed hydroxylation of **2** at C(2). I expected that LolO would act only on the stereoisomer of **2** that had the same absolute configuration as the natural substrate. Then, as long as **1** was separable from the three unnatural stereoisomers of **2**, I would be able to obtain **1** as a single diastereomer in enantiopure form.

2.2.3 NMR analysis of (±) *exo*-6,6-F_2-AcAP

To establish the stereochemistry of (±)-6,6-F_2-AcAP (**2**) with absolute certainty, I analyzed its structure and stereochemistry with NMR and obtained its crystal structure.

The ^{1}H NMR spectrum (Figure A.2) showed 14 H atoms. The ^{13}C NMR (Figure A.3) showed the presence of nine C atoms. The HSQC spectrum (Figure 2.5) confirmed the presence of 13 H atoms: two methine groups, four pairs of methylene groups, and one methyl group. The remaining one H atom resonating at 6.18 ppm is from the NH group as

seen in ^{1}H NMR spectrum (Figure A.2). ^{19}F NMR spectrum (Figure A.4) confirmed the presence of two geminal F atoms.

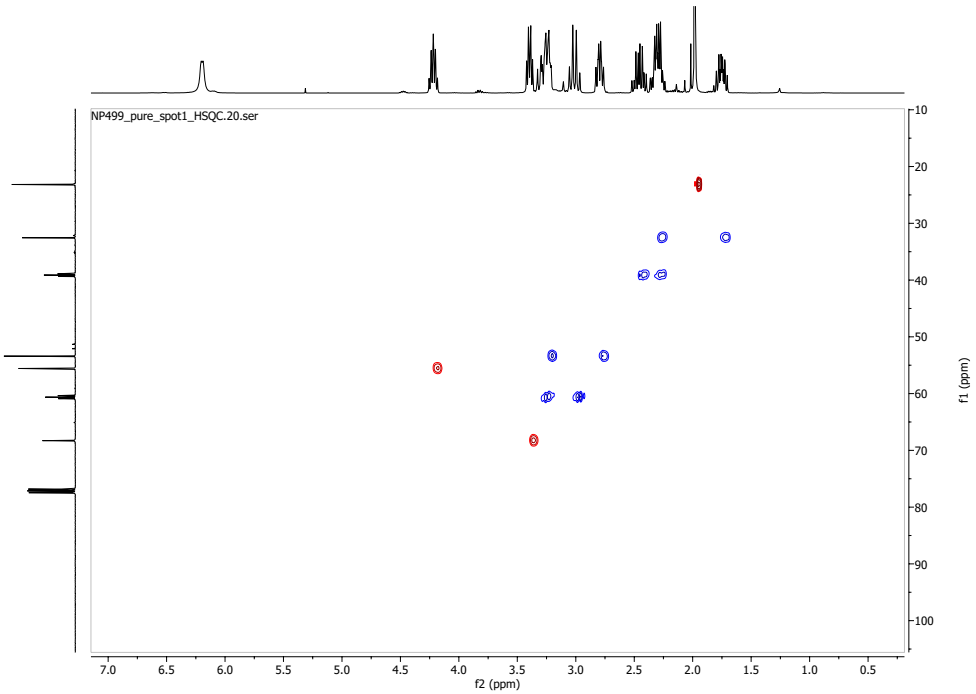

Figure 2.5 400 MHz ^{1}H–^{13}C HSQC NMR spectrum of *exo*-6,6-F_2-AcAP.

From the ^{13}C NMR (Figure A.3) and HSQC spectrum (Figure 2.5), I assigned the ^{13}C resonance at 170.3 ppm to carbonyl carbon C(9). I assigned the resonance at 131.2 ppm to C(6) because of the triplet nature of the peak caused by two geminal F atoms with large coupling constants to C (J = 250.4 Hz). The HSQC spectrum (Figure 2.5) supported this assignment, as neither of these peaks were connected to any H atoms. The next two triplet peaks in the ^{13}C NMR spectrum resonated at 60.6 ppm (J = 26.5 Hz) and 35.2 ppm (J = 24.1 Hz). These resonances could be due to C(5) and C(7), as they were adjacent to C(6) bearing two F atoms. I assigned the downfield resonance at 60.6 ppm to C(5), as it was closer to the ring N than C(7), and the remaining resonance at 35.2 ppm to C(7). The HSQC

spectrum (Figure 2.5) also showed that C(5) is connected to two geminal H atoms resonating at 3.26 ppm and 3.02 ppm, while C(7) is connected to two geminal H atoms resonating at 2.46 ppm and 2.29 ppm. In the ^{13}C NMR spectrum, the effects of two F atoms at C(6) are visible up to two C atoms away. The next triplet peak in the ^{13}C NMR spectrum resonated at 68.3 ppm (J = 4.3 Hz) which could be due to C(8), as it is two C atoms away from C(6). The HSQC spectrum (Figure 2.5) shows that C(8) is connected to one methine H atom resonating at 3.39 ppm, further supporting the assignment of C(8). I assigned the remaining methine H from the HSQC spectrum, which resonated at 4.21 ppm, to the H atom attached to C(1) resonating at 55.6 ppm. H(1) is downfield from H(8) as it is closer to the amido group, further supporting the assignment. The HMBC spectrum (Figure A.5) supported this argument, as there was a correlation between the ^{1}H resonance at 4.21 ppm and the ^{13}C resonance due to the carbonyl C(9), a three-bond coupling (Figure 2.6). By contrast, there was no correlation in the HMBC spectrum between the ^{1}H resonance at 3.39 ppm and the ^{13}C resonance due to C(9).

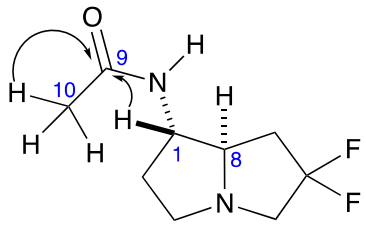

Figure 2.6 HMBC correlations from H(1) and H(10) to C(9) of 6,6-F_2-AcAP

I assigned the remaining resonances to H atoms on the basis of ^{1}H-^{1}H COSY correlations and their chemical shifts (Figure 2.7). There was a strong correlation between the H(1) and the two H(8) atoms in the COSY spectrum and also strong correlation between H(1) and the H atoms resonating at 2.29 ppm and 1.75 ppm, which HSQC showed were a

geminal pair. These data suggested that the latter two H atoms were attached to C(2). The remaining H atoms resonating at 3.39 ppm and 2.79 ppm, which the HSQC spectrum revealed are a geminal pair, can be assigned to H(3). There was also a strong correlation between the H(2) resonances and those assigned to H(3) in the COSY spectrum, which further supported the assignment of the latter resonances.

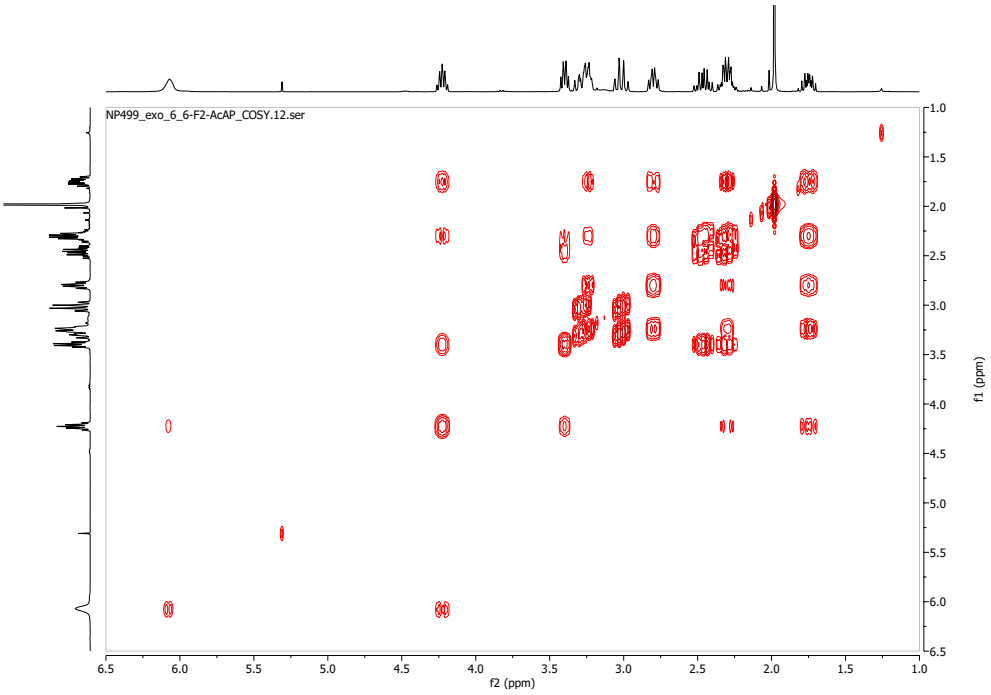

Figure 2.7 400 MHz ^{1}H-^{1}H COSY NMR spectrum of (±)-6,6-F_2-AcAP.

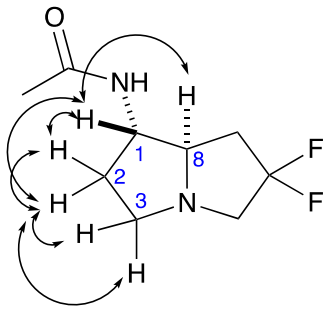

Figure 2.8 COSY correlations between H atoms at C(1), C(2), C(3), and C(8) of 6,6-F_2-AcAP.

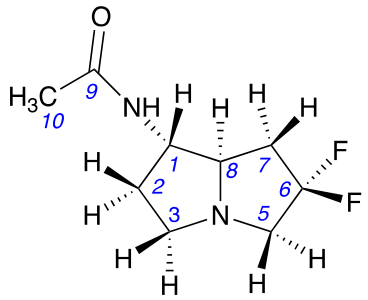

Figure 2.9 ^{13}C NMR and ^{1}H NMR assignment of (±) 1-*exo*-6,6-F_2-AcAP.

Table 2.1 ^{13}C NMR and ^{1}H NMR chemical shift of (±) 1-*exo*-6,6-F_2-AcAP

Carbon	**Chemical shift (ppm)**	**Hydrogen**	**Chemical shift (ppm)**
C(1)	55.6	H(1)	4.21
C(2)	32.6	H(2)	2.29, 1.75
C(3)	53.4	H(3)	3.26, 2.79
C(5)	60.6	H(5)	3.26, 3.02
C(6)	131.2		
C(7)	39.1	H(7)	2.46, 2.29
C(8)	68.3	H(8)	3.39
C(9)	170.3		
C(10)	23.2	H(10)	1.98
		NH	6.18

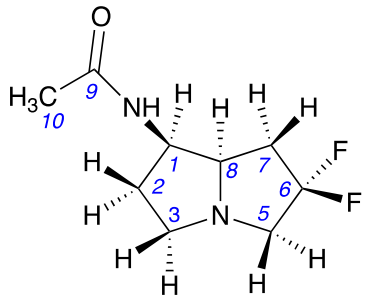

Figure 2.10 ^{13}C NMR and ^{1}H NMR assignment of (±) 1-*endo*-6,6-F_2-AcAP.

Table 2.2 ^{13}C NMR and ^{1}H NMR chemical shift of (±) 1-*endo*-6,6-F_2-AcAP.

Carbon	**Chemical shift (ppm)**	**Hydrogen**	**Chemical shift (ppm)**
C(1)	52.1	H(1)	4.49
C(2)	32.5	H(2)	2.17, 1.81
C(3)	51.3	H(3)	3.11, 2.76
C(5)	60.7	H(5)	3.29, 3.03
C(6)	131.6		
C(7)	35.1	H(7)	2.26, 2.11
C(8)	65.1	H(8)	3.82
C(9)	169.8		
C(10)	23.2	H(10)	2.02
		NH	5.71

2.2.4 Stereochemistry analysis of *exo*-6,6-F_2-AcAP and *endo*-6,6-F_2-AcAP

Even though the minor isomer was not pure, I could assign H(1) and H(8), as they appear downfield in the spectrum and do not overlap with the peaks from the major isomer. The HSQC spectrum (Figure A.8) of the minor isomer showed two methine groups, four methylene groups, and one methyl group. I assigned the methine resonance at 4.47 ppm to

H(1) due to its proximity to an amido group. The remaining methine resonance at 3.81 ppm is due to H(8).

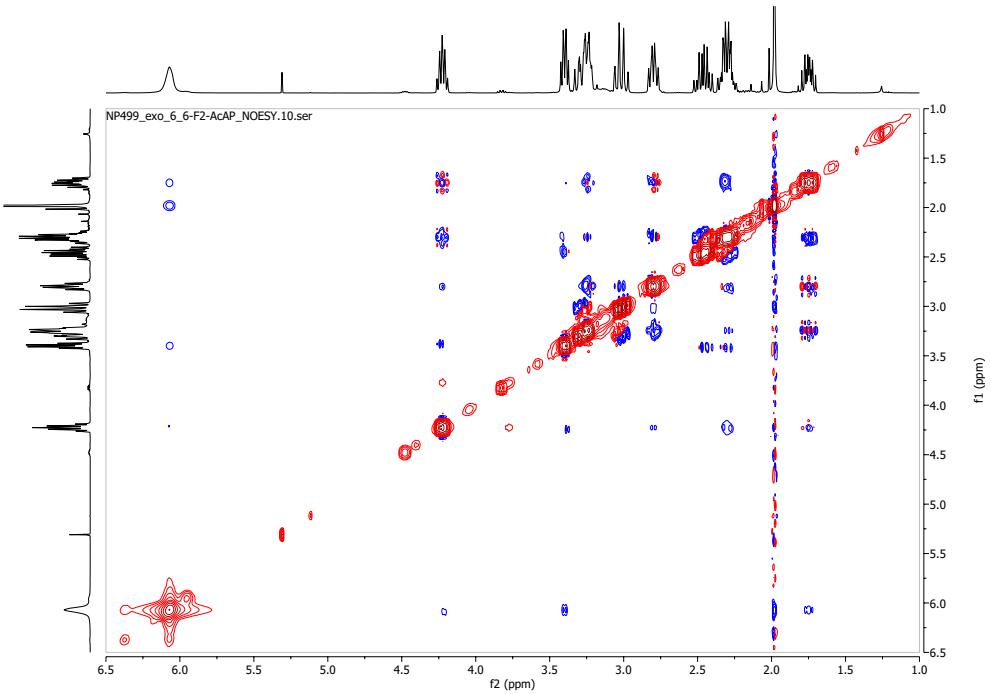

Figure 2.11 400 MHz 1H-1H NOESY NMR spectrum of (±)-exo-6,6-F_2-AcAP.

The NOESY spectrum of **2a** and **2b** (Figure 2.9 and 2.10) helped me to determine the relative stereochemistry of the H atoms at C(1) and C(8) in the two diastereomers. I looked for the NOE interactions between H(1) and NH; H(8) and NH; H(1) and H(8). The NOESY spectrum of the major diastereomer revealed a strong interaction between NH and H(8) and a weak interaction between H(1) and H(8) (Figure 2.9), whereas the NOESY spectrum of the minor diastereomer revealed a strong interaction between H(1) and H(8) and no interaction between NH and H(8). These results unambiguously identified the major diastereomer as (±)-**2**, the desired 1-*exo* diastereomer, and the minor diastereomer as the undesired 1-*endo*-**2**.

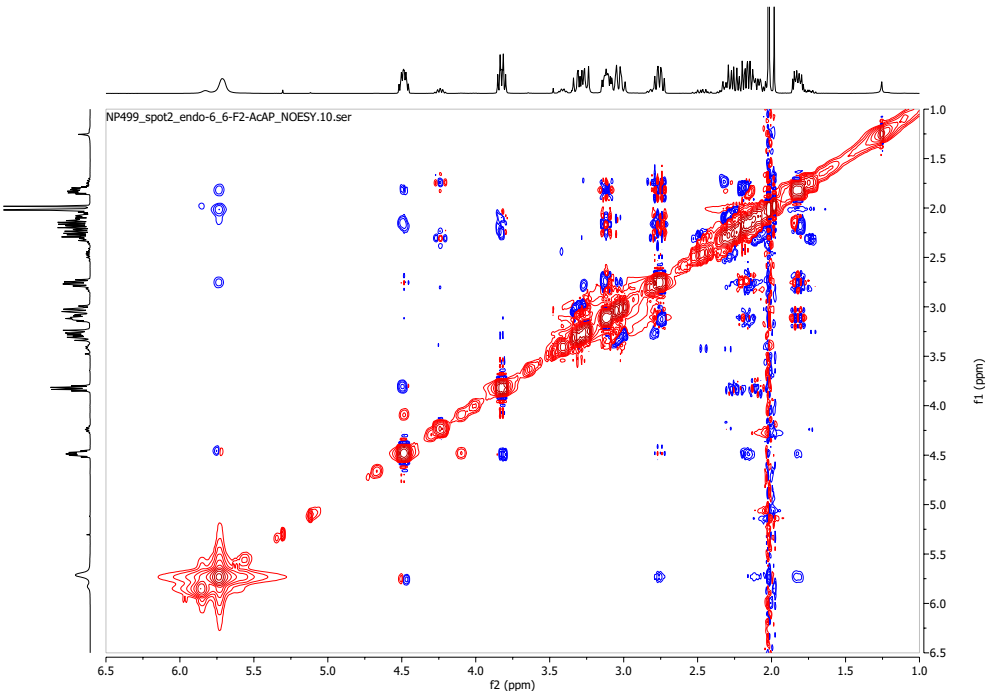

Figure 2.12 400 MHz ^{1}H-^{1}H NOESY NMR spectrum of (±)-1-*endo*-6,6-F2-AcAP (major diastereomer)

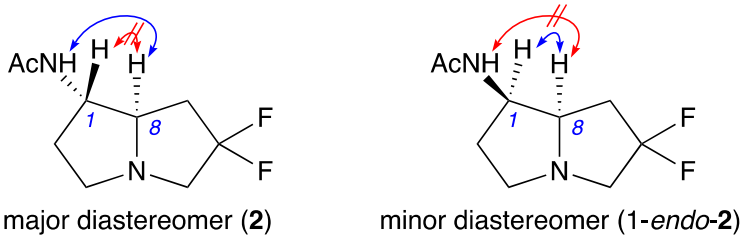

Figure 2.13 Observed and unobserved interactions in the NOESY spectra of the major and minor diastereomers that establish them as **2** and 1-*endo*-**2**, respectively.

2.2.5 Crystal structure of (±)-*exo*-6,6-F_2-AcAP

I was able to crystallize the major diastereomer of **2** from CH_2Cl_2 with slow diffusion of petroleum ether. These crystals allowed me to use X-ray crystallography to assign its stereochemistry unequivocally. The crystal structure clearly showed the stereochemistry of

the amido group at C(1) of 6,6-F_2-AcAP was exo to H(8), further supporting its assignment as the *exo*-isomer (Figure 2.14).

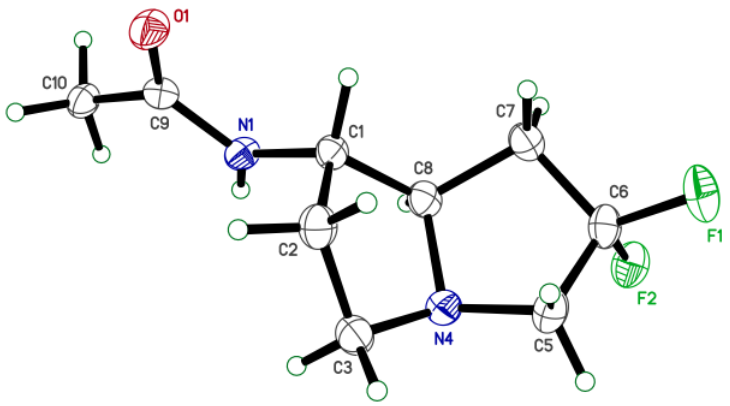

Figure 2.14 ORTEP diagram of **2**

2.2.6 Chemoenzymatic conversion of 6,6-F_2-AcAP catalyzed by LolO

Eliott S. Wenger at Penn State helped me to run these enzymatic assays. With (±)-**2** in hand, we were ready to use LolO to introduce an endo OH group at C(2) of **2**. We first combined LolO with the mixture of (±)-**2** and (±)-1-*endo*-**2** and O_2 in the absence of 2-OG following the reported procedure,[10] and we analyzed the reaction mixture by LC–MS. We observed two peaks with *m/z* values of 205, representing the two diastereomers. (The starting material and products described here all have a basic N atom, so the LC-MS detects their conjugate acids, leading to *m/z* values 1 amu greater than the molecular weights of the uncharged compounds.) After providing 2-OG in two-fold excess over the substrate, we detected new products with *m/*z values of 221, 219, and 237, respectively (Figure 2.13).

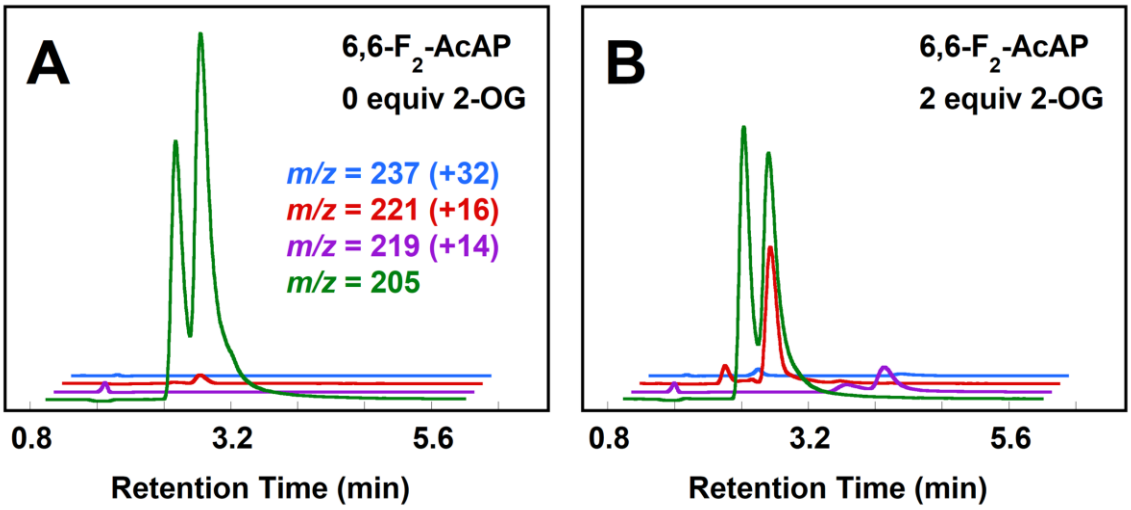

Figure 2.15 Selected LC–MS traces showing the substrate consumption and product formation by LolO in a reaction with a mixture of (±)-**2** and (±)-1-*endo*-**2** in the absence (panel A) and presence (B) of 2-OG.

In order to tentatively identify the products, we conducted similar assays with varying amounts of 2-OG from limiting to excess, which allowed us to monitor the dependence of each species on 2-OG concentration (Figure 2.14). As we increased the concentration of 2-OG, the initially more abundant *m/z* = 205 species (retention time = 2.5 min) was partially consumed, whereas the initially less abundant *m/z* = 205 species (retention time = 2.8 min) remained unaffected. This observation suggested that the 2.5 min species corresponded to (±)-**2**, whereas the 2.8 min species corresponded to (±)-1-*endo*-**2**. We reasoned that LolO consumed only half of the 2.5 min species at excess 2-OG because it was able to hydroxylate only the natural enantiomer of **2**. We also observed two different species with *m/z* values of 221, a shift of +16 likely corresponding to hydroxylation by LolO. The amount of major hydroxylation product (retention time = 2.6 min) was highest with limiting amount of 2-OG and was present in decreasing amounts as 2-OG was increased. Because the LolO catalyzed reaction consumed this species (retention time = 2.6 min) in

further oxidations, this peak can be assigned as 2-OH-6,6-F_2-AcAP (**1**). The other minor hydroxylation product, with retention time = 2.1 min, formed in a smaller quantity and was clearly not a substrate for further oxidations. This species could be an inefficient hydroxylation product of one of the enantiomers of 1-*endo*-**2,** or it could have formed by hydroxylation at C(7), as it was observed that LolO catalyzes hydroxylation at the C(7) position in the native reaction with AcAP in a small fraction of events.[10]

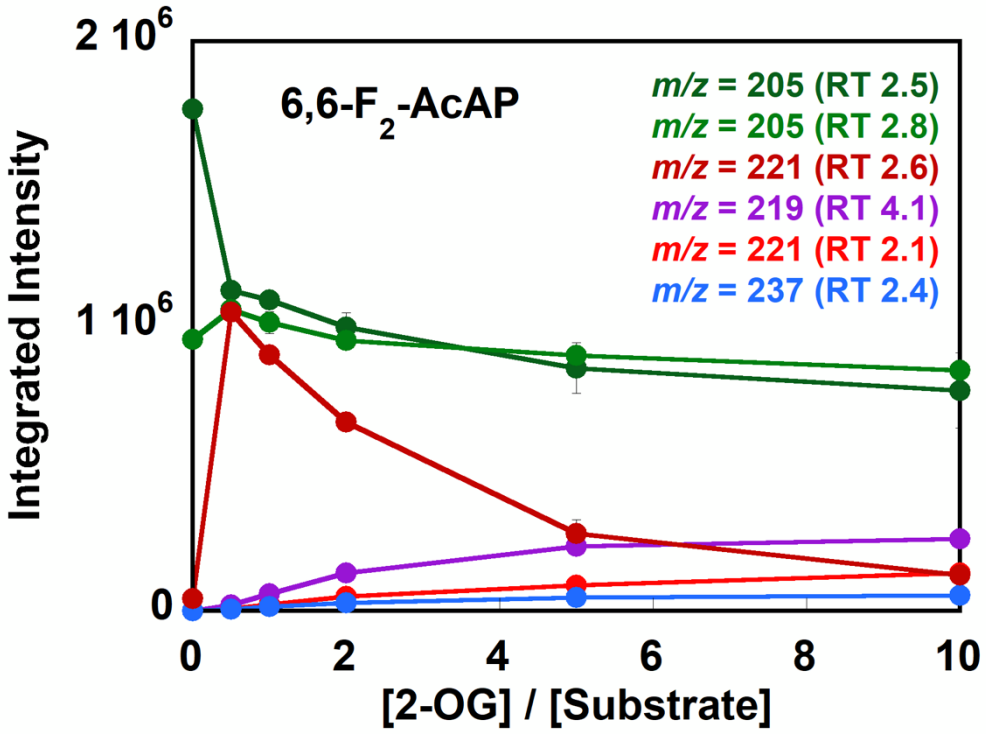

Figure 2.16 Oxidation of (±)-**2** by LolO with varying amounts of 2-OG. LC–MS total ion counts of ions with the indicated m/z values. Each data point is an average of two identical trials.

When we provided an excess amount of 2-OG, we observed a product with *m/*z = 219, which corresponded to the difluorinated analog of NANL, the first fully cyclized intermediate in loline alkaloid biosynthesis. The concentration of presumed 6,6-F_2-NANL increased as the concentration of **2** decreased, consistent with the formation of 6,6-F_2-

NANL from the major hydroxylation product, **1**. The apparent cycloether formation from **2** suggests that the ferryl intermediate in the active site of LolO is strongly oxidizing, as it is able to abstract a hydrogen atom from C(7) even with two F atoms on an adjacent carbon. Finally, we observed a small amount of a species with *m/*z = 237, most likely the dihydroxylated analog of **2** (M + 32), showcasing the ability of LolO to hydroxylate **2** at both C(2) and C(7).[40]

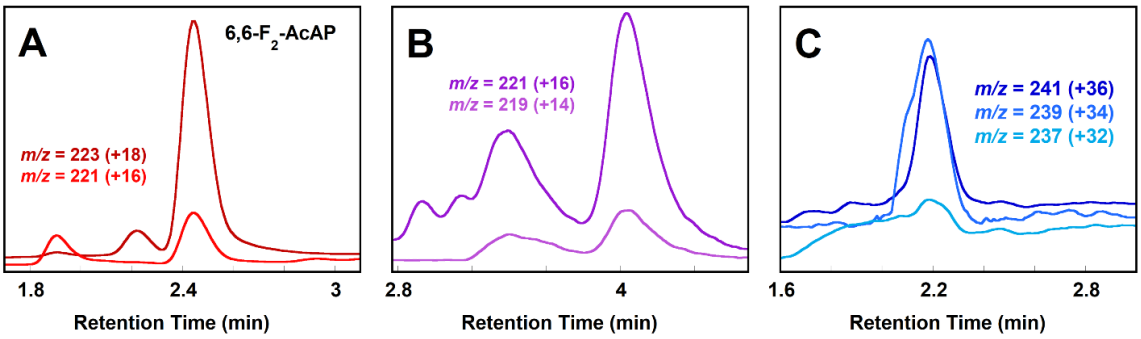

Figure 2.17 Products formed from (±)-**2** by LolO in the presence of $^{16}O_2$ (bottom graph) and $^{18}O_2$ (top graph). Panel A shows the two hydroxylation products, panel B shows the two cycloetherification product, and panel C shows the dihydroxylation product with $^{16}O_2$ (bottom), incorporation of one $^{18}O_2$ (middle) and incorporation of two $^{18}O_2$ (top).

By doing the identical assays using $^{18}O_2$ in place of natural O_2, we gathered further evidence for the assignment of these products (Figure 2.15). A substantial portion of the signal of **2** was increased from *m/z* = 221 to *m/z* = 223 in the presence of $^{18}O_2$, suggesting considerable incorporation of ^{18}O into the product. Similarly, the signal for 6,6-F_2-NANL increased from *m/z* = 219 to *m/z* = 221 in the presence of $^{18}O_2$, reflecting considerable incorporation of ^{18}O into **1**. Further evidence for the assignment of a dihydroxylated species was obtained from shift of the *m/*z = 237 species to *m/*z = 239 *and m/z* = 241 while doing assays with $^{18}O_2$ in place of O_2, showing incorporation of up to two ^{18}O atoms. Interestingly, the minor hydroxylated species (retention time = 2.1 min) showed far less

incorporation of the ^{18}O label compared to the major product. We previously observed differential incorporation of ^{18}O in two hydroxylation products formed from a single ferryl intermediate in the native LolO reaction.[40] This result also shows the different efficiencies with which two hydroxylation products are formed from **2**.

2.3 Conclusion

I have prepared 6,6-F_2-AcAP (**2**) from *N*,*O*-protected 4-oxoproline in eight steps where the key step was Dieckmann condensation that annulated the A ring onto the B ring, and I have shown that LolO catalyzes the hydroxylation of **2** at C(2) to give **1**. Furthermore, I have shown that LolO consumes **1** further to give a species whose mass corresponds to the cycloetherification product, 6,6-difluoro-NANL, a difluorinated analog of the natural loline alkaloid NANL.[10] It seems that two F atoms at C(6) are enough to prevent C–H activation of **1**. The abstraction of an H atom from a C atom adjacent to the CF_2 group suggests that the iron-oxo complex (ferryl intermediate) should have high oxidizing power. Likewise, this result also suggests that the cycloetherification reaction does not proceed through a C(7) carbocation intermediate, which would be severely destabilized by the two neighboring F atoms on C(6). Even though the conversion of **2** to F_2-NANL did not stop at **1** as we hoped, I did learn that LolO accepted the 6,6-difluorinated analog as a substrate. In the next chapter, I describe how I prepare 7,7-F_2-AcAP and how it undergoes LolO-catalyzed hydroxylation but not cycloetherification.

2.4 Experimental

General

Unless otherwise specified, all reagents were purchased from commercial sources and were used without further purification. Anhydrous THF, EtOH, MeOH were purchased from Sigma Aldrich and VWR while CH_2Cl_2 was distilled from CaH_2. All reactions were carried out under a nitrogen atmosphere unless otherwise mentioned. Completion of the reaction was checked with Sorbtech Silica G TLC Plates (UV254). Flash chromatography was carried out using Sorbtech silica gel (60A°, 230-400 mesh). Deuterated solvents were purchased from Cambridge Isotope Laboratories (Andover, MA). NMR spectra were recorded on a Bruker Avance NEO 400 MHz spectrometer and samples calibrated for; ^{1}H NMR ($CDCl_3$, δ = 7.26 ppm), ^{13}C NMR ($CDCl_3$, δ = 77.36). ^{19}F NMR internally referenced to C_6F_6, δ = –164.9 ppm vs $CFCl_3$.

1-tert-butyl 2-ethyl (2*S*,4*R*)-4-hydroxyproline-1,2-dicarboxylate (4)

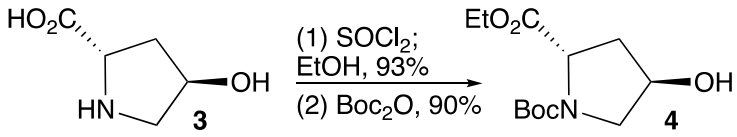

To the suspension of *trans*-4-hydroxy-L-proline (**3**) (10.0 g, 76.3 mmol) in anhydrous ethanol (80 mL) at 0 °C, thionyl chloride (22.1 mL, 305 mmol) was added dropwise via addition funnel. The reaction mixture was heated to reflux (74 °C) overnight. Then, the reaction mixture was cooled in ice bath and ether (20 mL) was added with vigorous stirring. The precipitate was filtered, washed with additional cold ether and dried to get the colorless solid **3a** (13.8 g, 70.6 mmol, 93%) as hydrochloride salt, taken to the next step without further purification. The spectroscopic data for the compound were identical to those

previously reported.[41] ^{1}H NMR (400 MHz, D_2O) δ 4.68 – 4.60 (m, 2H), 4.27 (q, J = 7.1 Hz, 2H), 3.49 (dd, J_d = 12.6, 3.8 Hz, 1H), 3.38 (dt, J_d = 12.7 Hz, J_t = 1.6 Hz, 1H), 2.46 (ddt, J_d = 14.3, 7.8 Hz, J_t = 1.8 Hz, 1H), 2.26 (ddd, J_d = 14.5, 10.5, 4.4 Hz, 1H), 1.26 (t, J = 7.1 Hz, 3H). ^{13}C NMR (101 MHz, D_2O) δ 169.9, 69.5, 64.0, 58.4, 53.6, 36.8, 13.2.

To the suspension of **3a** (13.8 g, 70.5 mmol) in 1,4-dioxane (150 mL) at 0 °C, a saturated solution of $NaHCO_3$ (150 mL) was added followed by Boc anhydride (16.9 g, 77.5 mmol). The reaction mixture was warmed to room temperature and stirred overnight. Solid colorless precipitate was filtered and discarded while the filtrate was evaporated to get the residue. To the concentrated residue, 10 mL of H_2O was added and extracted with CH_2Cl_2 (3 × 50 mL). The combined organic layer was dried with $MgSO_4$, and evaporated to get (2*S*,4*R*)-4-hydroxyproline-1,2-dicarboxylic acid 1-tert-butyl 2-ethyl ester **4** as a colorless oil (16.4 g, 63.2 mmol, 90%) in analytically pure form. The spectroscopic data for the compound were identical to those previously reported.[42] ^{1}H NMR (400 MHz, $CDCl_3$) δ 4.53 – 4.25 (m, 2H), 4.15 (m, 2H), 3.70 – 3.28 (m, 2H), 3.03 (m, 1H), 2.37 – 2.12 (m, 1H), 2.02 (m, 1H), 1.42, 1.37 (2 × s, 9H), 1.23 (q, J = 7.0 Hz, 3H). ^{13}C NMR (101 MHz, $CDCl_3$) δ 173.3, 172.9, 154.6, 154.2, 80.4, 80.2, 70.0, 69.3, 67.1, 61.1, 61.0, 58.1, 57.8, 54.7, 54.7, 39.2, 38.5, 28.4, 28.3, 14.2, 14.1.

1-*tert*-butyl 2-ethyl (*S*)-4-oxopyrrolidine-1,2-dicarboxylate (4a)

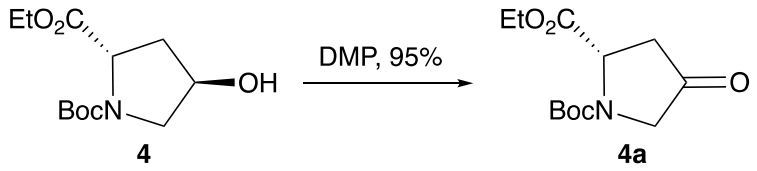

4 **4a**

The procedure was adapted from Hofman *et. al*.[43] To the solution of **4** (9.45 g, 36.5 mmol) in CH_2Cl_2 (100 mL) at room temperature, freshly prepared Dess–Martin periodinane[44] (17.0 g, 40.1 mmol) was added over 15 min. After 2 h, the reaction was quenched with a saturated aqueous solution of $Na_2S_2O_3$ (50 mL) and a saturated aqueous solution of $NaHCO_3$ (50 mL) (pH 8). The organic layer was separated, and the aqueous layer was extracted with CH_2Cl_2 (2 × 50 mL). The combined organic layer was dried over $MgSO_4$, filtered, and evaporated to get the crude product. Flash chromatography of the crude product over silica gel using 20% EtOAc in hexanes gave the 1-*tert*-butyl 2-ethyl (*S*)-4-oxopyrrolidine-1,2-dicarboxylate **4a** (8.95 g, 34.8 mmol, 95%) as a yellow oil. ^{1}H NMR (400 MHz, $CDCl_3$), mixture of rotamers, δ 4.74 (dd, J_d = 35.2, 10.5 Hz, 1H), 4.21 (m, 2H), 4.00 – 3.66 (m, 2H), 2.94 (ddd, J_d = 18.6, 14.3, 10.0 Hz, 1H), 2.57 (dd, J_d = 18.9, 2.7 Hz, 1H), 1.47 (s, 9H), 1.28 (t, J = 7.2 Hz, 3H). ^{13}C NMR (101 MHz, $CDCl_3$), mixture of rotamers, δ 208.5, 207.7, 171.8, 154.3, 153.6, 81.2, 61.7, 56.4, 55.8, 52.9, 52.5, 41.3, 40.8, 28.3, 14.2. IR (ATR): 1736, 1693 cm^{-1}. GC-MS (EI): 9.15 min, 100%; 201 (13%), 184 (24%), 156 (20%), 128 (16%), 84 (47%), 57 (100%).

1-*tert*-butyl 2-ethyl (*S*)-4,4-difluoropyrrolidine-1,2-dicarboxylate (5)

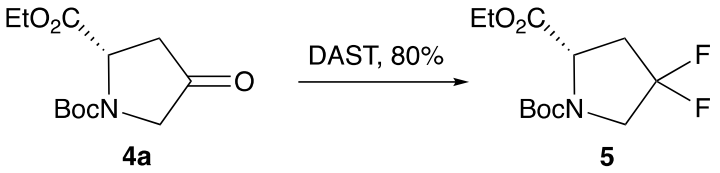

4a **5**

The procedure was adapted from Doebilin *et. al*.[34] To a solution of **4a** (6.40 g, 24.9 mmol) in dry CH_2Cl_2 (20 mL) under N_2 at 0 °C, DAST (9.90 mL, 74.6 mmol) was added dropwise over 15 minutes. The reaction was allowed to warm to room temperature overnight. At 0 °C, the solution was diluted with CH_2Cl_2 (40 mL) and quenched with the dropwise addition of a saturated aqueous solution of $NaHCO_3$ (pH 8). The mixture was stirred at 0 °C for 30 minutes, and the resulting biphasic mixtures were separated. The aqueous layer was extracted with CH_2Cl_2 (2 × 50 mL). The combined organic layer was washed with brine, dried with $MgSO_4$, filtered, and evaporated. Flash chromatography of the material over silica gel with 5-10% EtOAc in hexanes gave **5** (5.54 g, 19.9 mmol, 80%) as a colorless oil. ^{1}H NMR (400 MHz, $CDCl_3$), mixture of rotamers, δ 4.48 (ddd, J_d = 37.7, 9.3, 4.9 Hz, 1H), 4.33 – 4.09 (m, 2H), 3.99 – 3.57 (m, 2H), 2.70 (m, 1H), 2.46 (qd, Jq = 13.3 Hz, J_d = 5.0 Hz, 1H), 1.47, 1.43(s, 9H), 1.28 (q, J = 7.0 Hz, 3H). ^{13}C NMR (101 MHz, $CDCl_3$), mixture of rotamers, δ 171.1, 170.7, 153.7, 153.2, 129.2, 128.4, 126.7, 125.9, 124.2, 123.4, 81.1, 80.9, 61.6, 57.3, 56.8, 53.9, 53.6, 53.4, 53.26, 53.1, 52.8, 39.1, 38.9, 38.6, 38.5, 38.2, 37.9, 28.3, 28.2, 14.2, 14.1. ^{19}F NMR (376 MHz, $CDCl_3$), mixture of rotamers, δ (-101.1) – (-102.1) (m, 1F), (-102.4) – (-102.8) (m, 1F). IR (ATR): 1751, 1704 cm^{-1}. GC-MS (EI):): 7.81 min, 99.4%; 259 (1%), 206 (33%), 178 (32%), 150 (14%), 106 (89%), 86 (12%), 57 (100%). HRMS-ESI *(m/z)*: $[M\text{-Boc} + H]^+$ Calcd for $C_7H_{12}F_2NO_2$ 180.0836; found 180.0836.

Ethyl (2*S*)-*N*-(3-ethoxy-3-oxopropyl)-4,4-difluoroprolinate (6)

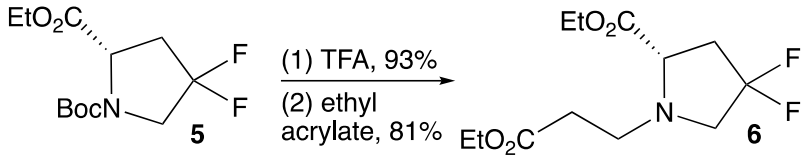

To the solution of **5** (5.51 g, 19.7 mmol) in CH_2Cl_2 (70 mL), trifluoroacetic acid (21 mL) was added at room temperature and stirred until completion. After 3 h, solvent was evaporated and the crude material was treated with CH_2Cl_2 (30 mL), H_2O (7 mL), and NH_4OH (9 mL) (pH 8) at 0 °C. After 1 h, the organic layer was separated, and the aqueous layer was extracted with CH_2Cl_2 (2 × 25 mL). The combined organic layer was dried with $MgSO_4$, filtered, and evaporated to get the yellow crude oil **5a** (3.30 g, 18.4 mmol, 93%) which was taken to the next step without further purification. ^{1}H NMR (400 MHz, $CDCl_3$) δ 4.23 (q, J = 7.1 Hz, 2H), 3.97 (dd, J_d = 8.8, 6.3 Hz, 1H), 3.58 – 3.27 (m, 1H), 3.19 (q, J = 12.9 Hz, 1H), 2.68 – 2.50 (m, 1H), 2.48 – 2.31 (m, 2H), 1.29 (t, J = 7.1 Hz, 3H). ^{13}C NMR (101 MHz, $CDCl_3$) δ 172.8, 130.3 (t, J = 252.7 Hz), 61.6, 58.2 (t, J = 4.5 Hz), 53.9 (t, J = 29.1 Hz), 39.1, (t, J = 26.4 Hz), 14.2. ^{19}F NMR (376 MHz, $CDCl_3$), δ (-101.8) (J_{F-F} = 230.7 Hz, J_{H-F} = 12.5, 15.3 Hz, 1F), (-102.8) (J_{F-F} = 231.4 Hz, J_{H-F} = 12.5, 14.9 Hz, 1F), 1F). IR (ATR): 3362, 1732 cm^{-1}. GC-MS (EI): 5.01 min, 95.2%; 159 (1%), 106 (100%), 86 (31%).

Excess ethyl acrylate (20 mL) was added to ethyl 4,4-difluoroprolinate **5a** (3.23 g, 18.0 mmol) under nitrogen and refluxed at 115 °C for four days. After the reaction was complete, excess ethyl acrylate was evaporated. Flash chromatography of the residue over silica gel using 15-20% EtOAc in petroleum ether gave 4,4-difluoro diester **6** (4.06 g, 14.5

mmol, 81%) as a yellow oil. ^{1}H NMR (400 MHz, $CDCl_3$) δ 4.18 (dq, J_d = 28.5 Hz, J_q = 7.1 Hz, 4H), 3.58 (t, J = 7.5 Hz, 1H), 3.46 (td, J_t = 12.7 Hz, J_d = 10.8 Hz, 1H), 3.11 (dt, J_d = 12.5 Hz, J_t = 7.4 Hz, 1H), 3.01 – 2.72 (m, 2H), 2.69 – 2.29 (m, 4H), 1.28 (dt, J_d = 14.4 Hz, J_t = 7.2 Hz, 6H). ^{13}C NMR (101 MHz, $CDCl_3$) δ 171.9, 171.4, 128.0 (t, J = 248.4 Hz), 63.6 (t, J= 7.9 Hz), 61.2, 60.6, 59.9, (t, J = 29.2 Hz), 48.7, 39.6, (t, J= 26.4 Hz) 33.4, 14.2. ^{19}F NMR (376 MHz, $CDCl_3$), δ (-95.6) ((J_{F-F} = 230.5 Hz, J_{H-F} = 13.1, 17.1 Hz, 1F), (-97.8) ((J_{F-F} = 230.0 Hz, J_{H-F} = 10.8, 12.3 Hz, 1F). IR (ATR): 1728 cm^{-1}. GC-MS (EI): 8.35 min, 100%; 279 (1%), 206 (100%), 192 (34%), 186 (6%), 140 (13%), 118 (17%), 98 (16%), 73 (10%), 55 (10%). HRMS-ESI *(m/z)*: $[M+H]^+$ Calcd for $C_{12}H_{20}F_2NO_4$ 280.1360; found 280.1357.

(±)-6,6-difluoro-1-oximinopyrrolizidine (8)

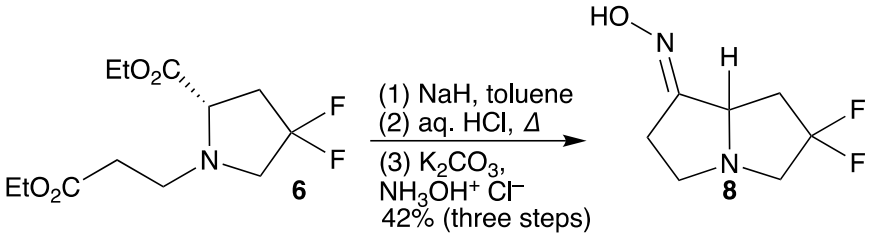

The procedure was adapted from McHugh *et. al*. for the Dieckmann condensation.[38] To NaH (60% oil dispersion, 0.131 g, 3.48 mmol) in anhydrous toluene (8.0 mL) under N_2 was added **6** (0.485 g, 1.74 mmol) in anhydrous toluene (5 mL) over 15 minutes. The reaction mixture was stirred for 18 h at room temperature and then quenched with 2 mL of glacial acetic acid followed by 15 mL of 2 N HCl. The organic layer was separated and washed with water. The combined aqueous layers were evaporated under the reduced pressure. The residue was then treated with acetone and filtered, and the filtrate was then

evaporated under reduced pressure. The residue was then treated with 6 N HCl (10 mL) and refluxed for 2 h. The reaction mixture was adjusted to pH 9 by adding a saturated solution of K_2CO_3 in H_2O at 0 °C. Hydroxylamine hydrochloride (0.145 g, 2.09 mmol) was added to the reaction mixture, and the mixture was allowed to reflux for 2 h and then allowed to stir at room temperature for 20 h. Solvents and water were evaporated under reduced pressure and extracted with CH_2Cl_2. The combined organic layers were dried over $MgSO_4$ and evaporated under reduced pressure. The residue was then purified by flash chromatography in CH_2Cl_2: CH_3OH: NH_4OH (20:1:0.2) to afford (±)-6,6-difluoro-1-oximinopyrrolizidine (0.129 g, 0.732 mmol, 42%) as a yellow solid consisting of an inseparable mixture of diastereomers, **8**, mp 74-75 °C. ^{1}H NMR (^{19}F decoupled) (400 MHz, $CDCl_3$), mixture of diastereomers, δ 10.62 – 9.63 (m, 1H), 4.60 – 3.87 (m, 1H), 3.39 (d, *J* = 12.8 Hz, 1H), 3.33 – 3.18 (m, 1H), 3.07 – 2.91 (m, 2H), 2.91 – 2.55 (m, 4H), 2.41 (ddd, J_d = 28.1, 14.8, 6.4 Hz, 1H). ^{13}C NMR (101 MHz, $CDCl_3$), mixture of diastereomers, δ 163.9, 163.6, 133.8, 133.2, 131.3, 131.2, 130.7, 128.8, 128.2, 63.4, 63.4, 63.3, 61.3, 61.2, 59.9, 59.9, 59.7, 59.6, 59.4, 53.4, 51.8, 50.6, 39.5, 39.3, 39.0, 38.3, 38.1, 37.8, 29.2, 25.7. ^{19}F NMR (376 MHz, $CDCl_3$) mixture of diastereomers, δ (-95.25) – (-96.75) (m, 1F), (-97.21) – (-97.97) (m, 2F), (-99.70) – (-101.12) (m, 1F). IR (ATR): 3185, 3070, 1677 cm^{-1}. GC-MS (EI): 6.94 min, 98.1%; 176 (49%), 159 (100%), 138 (30%), 118 (47%), 112 (47%), 98 (59%), 68 (13%), 55 (19%). HRMS-ESI *(m/z)*: $[M+H]^+$ Calcd for $C_7H_{11}F_2N_2O$ 177.0839; found 177.0836.

(±)-1-*exo*-6,6-difluoro-1-acetamidopyrrolizidine (2) and (±)-1-*endo*-6,6-difluoro-1-acetamidopyrrolizidine

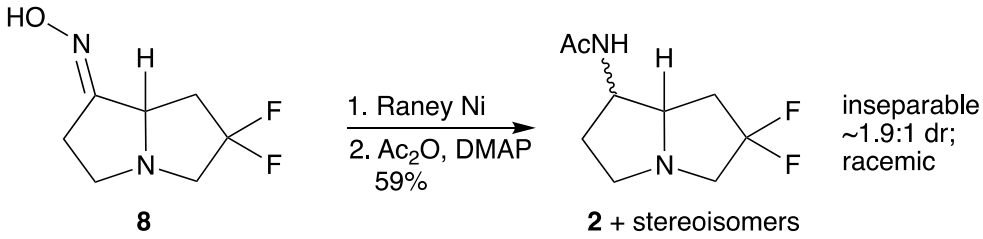

8 **2** + stereoisomers

To a mixture of (±)-**8** (0.165 g, 0.940 mmol) in THF (14 mL), Raney Ni (in excess) was added and stirred for 14 h at room temperature as indicated by TLC for the completion of reduction to amine. Acetic anhydride (0.100 mL, 1.03 mmol) and DMAP (0.115 g, 0.940 mmol) were added to the reaction mixture, and the mixture was stirred for 3 h at room temperature. The mixture was diluted with CH_2Cl_2 and filtered through the short pad of Celite. The Celite pad was washed several times with CH_2Cl_2. The combined organic layer was adjusted to pH 12 by adding 1 M NaOH, followed by addition of saturated $NaHCO_3$ and brine. The phases were allowed to separate for 30 min, and the aqueous layer was extracted with CH_2Cl_2 (2 × 20 mL). The combined organic layers were dried over $MgSO_4$, filtered, and concentrated under reduced pressure. The crude mixture was purified with flash chromatography using 10% MeOH in CH_2Cl_2 with 2% NH_4OH to afford (±)-6,6-difluoro-1-acetamidopyrrolizidine as a yellow solid consisting of a mixture of diastereomers (0.113 g, 0.555 mmol, 59%). The two diastereomers were nearly inseparable, but, after considerable effort, we were able to obtain a small amount of the major diastereomer in pure form as well as a small amount of a 3:1 mixture of the minor and major diastereomers, respectively.

1-*exo*-6,6-F_2-AcAP (major diastereomer) [(±)-2]

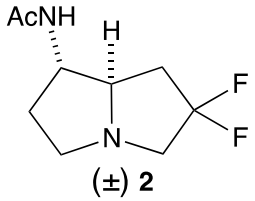

(±) **2**

^{1}H NMR (400 MHz, $CDCl_3$) δ 6.19 (br s, 1H), 4.22 (p, *J* = 7.2 Hz, 1H), 3.40 (dt, J_d = 8.1Hz, J_t = 6.2 Hz, 1H), 3.35 – 3.18 (m, 2H), 3.12 – 2.93 (m, 1H), 2.86 – 2.73 (m, 1H), 2.54 – 2.38 (m, 1H), 2.38 – 2.20 (m, 2H), 1.98 (s, 3H), 1.86 – 1.66 (m, 1H). ^{13}C NMR (101 MHz, $CDCl_3$) δ 170.3, 131.2 (t, *J* = 250.9 Hz), 68.3 (t, *J* = 4.4 Hz), 60.6 (t, *J* = 26.7 Hz), 55.6, 53.4, 39.1 (t, *J* = 24.8 Hz), 32.6, 23.2. ^{19}F NMR (376 MHz, $CDCl_3$), δ (-100.1) ((J_{F-F} = 232.1 Hz, J_{H-F} = 14.1 Hz, 1F), (-103.0) (J_{F-F} = 232.05 Hz, J_{H-F} = 11.4, 14.2 Hz, 1F). IR (ATR): 3281, 3069, 1629, 1548 cm^{-1}. GC-MS (EI): 8.18 min, 98.8%; 185 (1%) 145 (100%), 144 (65%), 119 (62%), 55 (31%), mp 113-114 °C. HRMS-ESI *(m/z)*: $[M+H]^+$ Calcd for $C_9H_{15}F_2N_2O$ 205.1152; found 205.1156.

1-*endo*-6,6-F_2-AcAP (minor diastereomer) [(±)-1-*endo*-2]

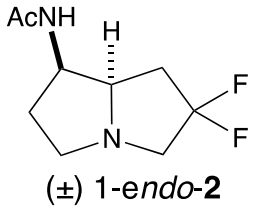

(±) 1-e*ndo*-**2**

^{1}H NMR (400 MHz, $CDCl_3$) δ 5.77 (br s, 1H), 4.62 – 4.38 (m, 1H), 3.82 (dt, *J*d = 8.6 Hz, J_t = 6.3 Hz, 1H), 3.37 – 3.19 (m, 1H), 3.18 – 2.94 (m, 2H), 2.88 – 2.68 (m, 1H), 2.38 – 2.06 (m, 3H), 2.02 (s, 3H), 1.90 – 1.68 (m, 1H). ^{13}C NMR (101 MHz, $CDCl_3$) δ 169.8, 131.6 (t, *J* = 251.1 Hz), 65.1 (t, *J* = 4.1 Hz), 60.7 (t, *J* = 26.7 Hz), 52.1, 51.3, 35.1 (t, *J* =

24.1 Hz), 32.5, 23.2. ^{19}F NMR (376 MHz, $CDCl_3$), δ (-99.8) ((J_{F-F} = 232.3 Hz, J_{H-F} = 15.4 Hz, 1F), (-102.8) ((J_{F-F} = 230.9 Hz, J_{H-F} = 12.5, 1F). IR (ATR): 3269, 3176, 1737, 1659, 1549 cm^{-1}. GC-MS (EI): 185 (1%), 145 (95%), 144 (26%), 119 (100%), 55 (43%). HRMS-ESI *(m/z)*: $[M+H]^+$ Calcd for $C_9H_{15}F_2N_2O$ 205.1152; found 205.1155.

Enzymatic Assays

(Eliott S. Wenger from Dr. Bollinger's lab helped me to conducted these enzymatic assays.) The enzyme (LolO) was purified using the published procedure.[10] For the 2-OG titrations, a sequence of six samples were prepared anoxically in an anoxic chamber. Each sample was 100 µL of 6.1 225 µM LolO, 200 µM substrate (6,6-F_2-AcAP), 200 µM Fe^{II} [from $Fe(NH_4)_2(SO_4)_2$], 2 mM ascorbic acid, and a varied 2-OG concentration (0, 100, 200, 400, 1000, and 2000 µM) in buffer containing 5% glycerol, 150 mM NaCl, and 50 mM sodium HEPES buffer at pH 7.5. Each sample was then brought out of the anoxic chamber and diluted with an equal volume of cold (4 °C) air-saturated buffer and stirred at 4 °C open to air for half an hour. The enzyme was then quenched by addition of formic acid to a final concentration of 5%. The enzyme was removed by centrifugation [Microcon centrifugal filter unit with a 10-kDa MWCO filter (MilliporeSigma, Burlington, MA)]. For chromatography, 1 µL of each sample was injected into the LC-MS instrument (Agilent 1200 series LC system coupled to an Agilent 6410 QQQ mass spectrometer). Compounds were examined by electrospray ionization MS in positive mode. A reverse-phase Agilent Extend-C18 column (4.6 mm × 50 mm, 1.8 µm particle size) was used at a flow rate of 0.3 mL/min with 0.1% formic acid in H_2O for mobile phase A and 100% acetonitrile was used for mobile phase B. The column was developed with 100% mobile phase A for 6 minutes; 100%-0% A from 6 minutes to 8 minutes, 0% A for 8 minutes to 10 minutes, 0%-100% A

from 10 minutes to 12 minutes, and 100% A from 12 minutes to 14 minutes. 2OG was thus titrated against each substrate in two identical trials.

For assays using ^{18}O, the LolO solution buffer was saturated with ^{18}O at 4 °C using a Schlenk line. Samples were prepared as described above though in a sealed vial inside the anoxic chamber, and an equal volume of ^{18}O-charged buffer was added to each sample via gas-tight syringe, instead of removing the samples from the glovebox and diluting with air-saturated buffer. Samples were thereafter processed identically, and each substrate was tested at two 2-OG concentrations (50 and 1000 μM final concentrations) in two identical trials.

CHAPTER 3. SYNTHESIS OF 7,7-F_2-ACAP AND ITS OXIDATION CATALYZED BY LOLO

3.1 Introduction

As I discussed earlier, to test our hypothesis on how LolO changes its chemical behavior from the first to the second oxidation of AcAP, I wanted to block the C–H abstraction event in the oxacyclization reaction of 2-hydroxy-AcAP. For this purpose, I chose to synthesize the 7,7-difluorinated analog of 2-hydroxy-AcAP, which, if it bound to the active site of LolO, should completely block the cycloetherification (Scheme 3.1). As a result, the ferryl intermediates whose role it was to abstract H(7) might accumulate in sufficient amounts for direct spectroscopic characterization. Such characterization has historically been key in parsing the mechanisms of enzymes in this subclass, but because the kinetics of native reactions are not always amenable to high intermediate accumulation, substrate analogs have often been employed with modifications to slow intermediate decay.[45]

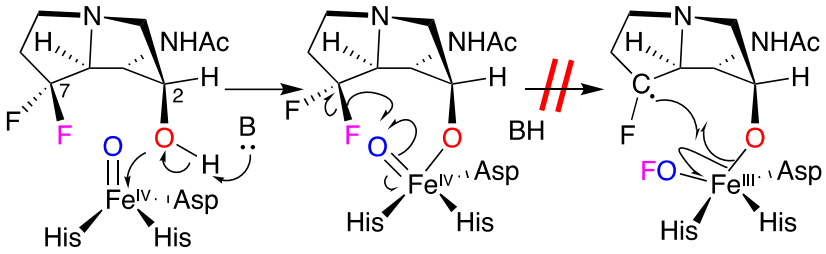

Scheme 3.1 Proposed inhibition of cycloetherification using 2-*endo*-OH-7,7-F_2-AcAP.

Because of the difficulties of constructing the densely functionalized and stereochemically complex 2-*endo*-OH-7,7-F_2-AcAP (**10**), I decided to introduce the endo OH group at C(2) by using LolO-catalyzed hydroxylation of 7,7-F_2-AcAP (**9**), as shown in Scheme 3.2.

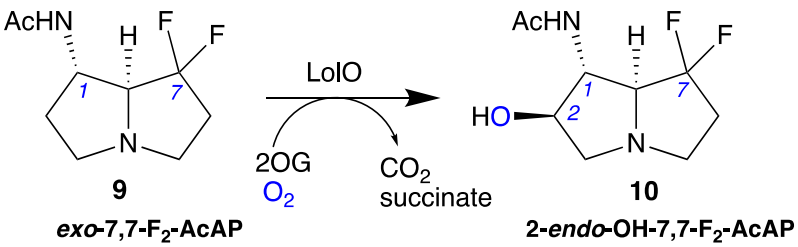

Scheme 3.2 Preparation of 7,7-difluorinated analog of 2-OH-AcAP from 7,7-difluorinated analog of AcAP

3.2 Result and discussion

3.2.1 First route towards synthesis of 7,7-F_2-AcAP

At first, I planned to synthesize **9** via the route that we already used to prepare AcAP[10] and 6,6-F_2-AcAP (**2**). The plan was to make the pyrrolizidine ring using a Dieckmann condensation reaction (Scheme 3.3).

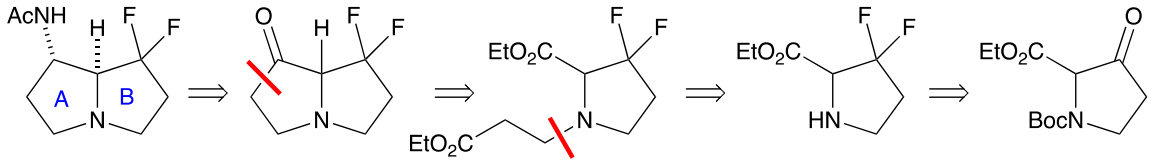

Scheme 3.3 Retrosynthesis of 7,7-F_2-AcAP: first approach

I prepared ethyl (±)-*N*-Boc-3-oxoprolinate[46] **12** from glycine ethyl ester in three steps following a published procedure (Scheme 3.4).[47] I then used DAST to introduce two geminal fluorine atoms to make **13**, removed the Boc group from N, and then alkylated the N with ethyl acrylate to make 3,3-difluoro diester **14**. However, despite using different kinds of base (LDA, LHMDS, K^{t}BuO, NaH, NaOEt), I could not isolate any product that resulted from a Dieckmann reaction, even though the similar transformation of the 4.4-difluorinated diester **6** proceeded smoothly. The failure of **14** to cyclize may have been due to the fact that the two highly electronegative F atoms in **14** are closer to the methine H(2)

than they are in the successfully cyclized **6**, rendering H(2) in **14** much more acidic than H(2) in **6** and possibly thereby thwarting the Dieckmann reaction, which requires deprotonation of the acrylate-derived α-C, not the proline-derived one. The greater acidity of H(2) in **14** may also induce elimination of HF by an E1cb mechanism.

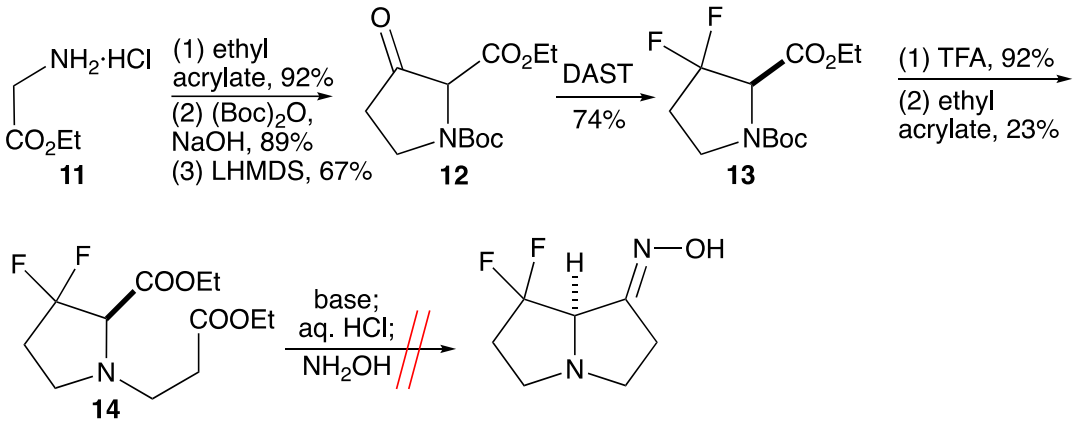

Scheme 3.4 First route towards synthesis of 7,7-F_2-AcAP

3.2.2 Second route towards synthesis of 7,7-F_2-AcAP

After learning that the two F atoms in the B ring thwarted the annulation of the A ring onto the B ring, I decided to construct the A ring of pyrrolizidine first, annulate the B ring onto it, and then introduce the F atoms towards the end of the synthesis (Scheme 3.5). Still, I was relying on the Dieckmann reaction to construct the second ring.

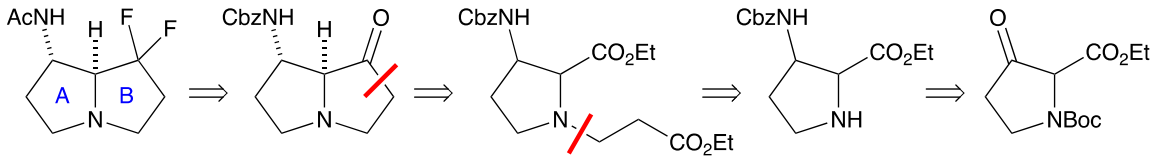

Scheme 3.5 Retrosynthesis of 7,7-F_2-AcAP second approach

I began with reduction of the ketone group of **12** with $NaBH_4$, which had previously been reported to give the cis alcohol **15** (Scheme 3.6).[48] I converted the alcohol of **15** into

a tosylate and then used sodium azide to displace the tosylate with inversion of configuration. I then reduced the azide to a primary amine, protecting the latter with a Cbz group to provide *trans*-3-aminoproline derivative **16** in excellent overall yield. My plan was that the CbzNH group at C(3) of **16** would eventually become the acetamido group at C(1) of **9**. I then deprotected the Boc group followed by alkylating the ring N with ethyl acrylate to make 1,6-diester **17**.

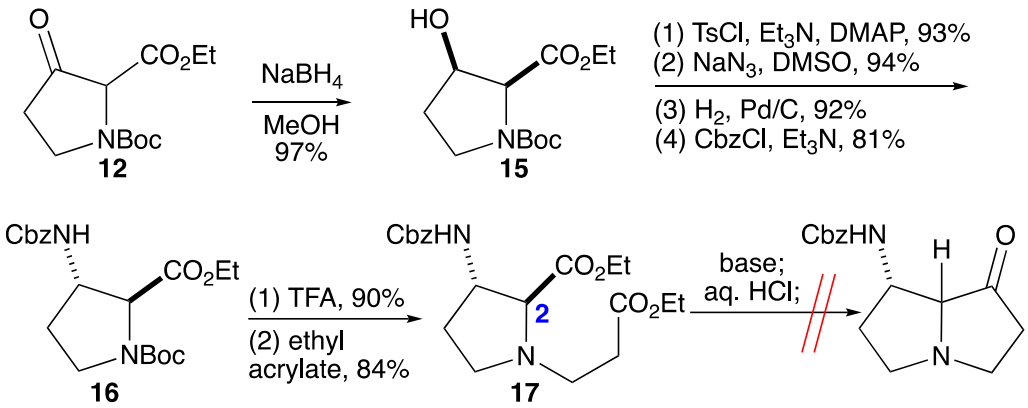

Scheme 3.6 Second routes towards synthesis of 7,7-F_2-AcAP.

Here, again, despite using various kinds of base, I could not isolate any product that could have resulted from the desired Dieckmann reaction. This result, like the previous one, could also be due to the increased acidity of H(2) in **17** compared to **6**.

3.2.3 Third route towards synthesis of 7,7-F_2-AcAP

To avoid the problematic Dieckmann reaction to construct the pyrrolizidine ring, I decided to take a different approach to the annulation. After an extensive literature search, I found that radical cyclization of pyrrolidone **18**, bearing pendant alkynyl and iodo groups, gave pyrrolizidinone **19**.[49]

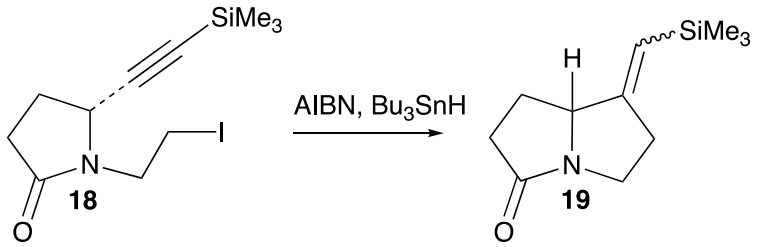

Scheme 3.7 Synthesis of pyrrolizidine ring based on radical cyclization

I decided to use a similar approach to construct the pyrrolizidine ring. In my retrosynthetic approach (Scheme 3.8), I still planned to construct the A ring first and to introduce the geminal F atoms towards the end of the synthesis.

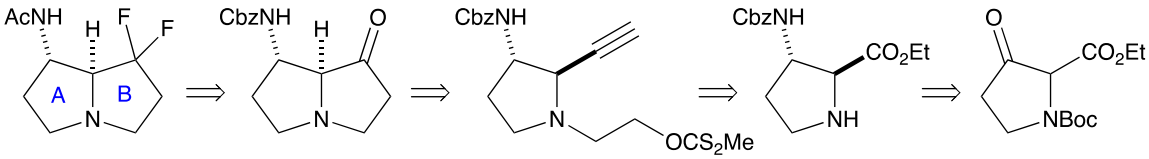

Scheme 3.8 Retrosynthesis of 7,7-F_2-AcAP based on radical cyclization approach

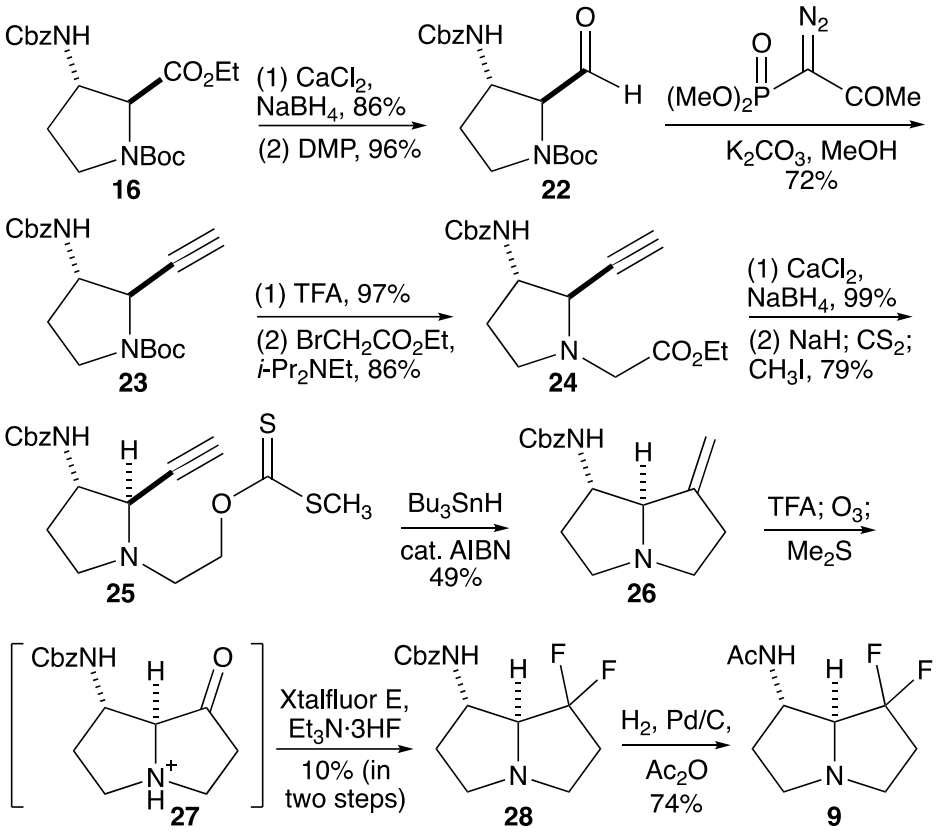

Scheme 3.9 Third route towards the synthesis of 7,7-F_2-AcAP.

In my second approach. The new route (Scheme 3.9) began with reducing the ester moiety of **16**, which I already had prepared in excellent yield. However, this step was challenging, as I could not obtain a satisfactory yield using $LiAlH_4$, perhaps due to coordination of Al with the secondary carbamate in the structure. While searching in the literature for compounds having similar functionality, I found that **20** had been reduced to **21** with $Ca(BH_4)_2$ prepared *in situ* (Scheme 3.10).[50]

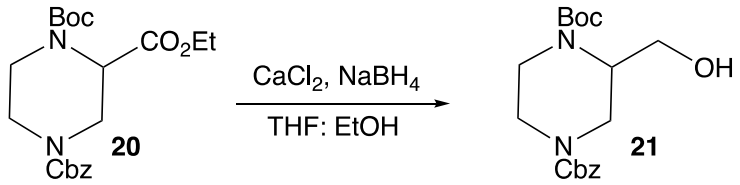

Scheme 3.10 Reducing ester moiety in presence of carbamate using $CaBH_4$.

Following this procedure, I reduced the ester moiety of **16** to the corresponding alcohol in an excellent 86% yield. The alcohol was then oxidized to aldehyde **22** using freshly prepared Dess–Martin periodinane.[44] My initial approach towards converting the aldehyde of **22** to alkyne **23** using Corey-Fuchs homologation was unsatisfactory in my case because of competing side reactions in the second step.[51, 52] However, combining the aldehyde **22** with freshly prepared Ohira-Bestmann reagent[53] gave alkyne **23**, which has an ethynyl group that I could use as a radical acceptor, in good yield. I then deprotected the ring *N* of **23** and alkylated it with ethyl bromoacetate to make **24**. I reduced the ester of **24** to the alcohol with $Ca(BH_4)_2$ and converted the alcohol to xanthate **25**. I then treated **25** with tributyltin hydride and AIBN to make alkene **26** in moderate yield. In this reaction, the nascent C radical generated by cleavage of the xanthate C–O bond added to the nearby alkene in *5-exo-dig* fashion. This step completed the annulation of the B ring onto the A ring.

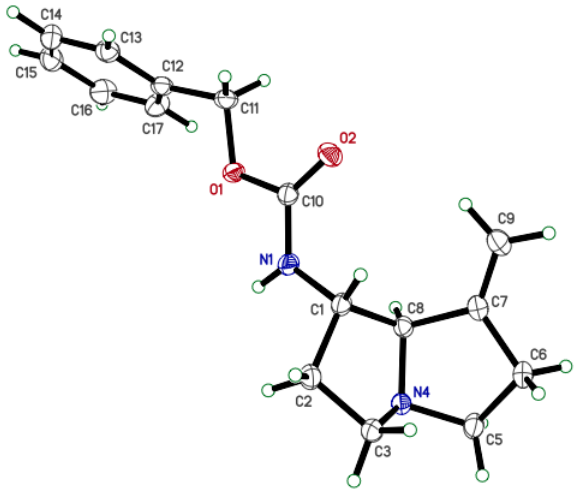

Figure 3.1 Thermal ellipsoid plot of **26**.

I was able to grow the crystals of **26** in CH_2Cl_2 with slow diffusion of petroleum ether. The crystal that I obtained showed that the CbzNH group at C(1) was exo, as desired and expected (Figure 3.1). This result also showed that the relative configuration established in the reduction of **12** to **15** was maintained throughout the synthesis.

Having **26** in hand, I subjected it to ozonolysis in TFA and CH_2Cl_2 as solvent, making ketone **27**, which I quickly treated with Xtalfluor E and triethylamine trihydrofluoride to make **28**, the Cbz analog of our desired **9**, as a single diastereomer in unfortunately poor yield. Finally, I deprotected the Cbz group of **28** by hydrogenolysis and acetylated the resulting primary amine using acetic anhydride to make **9**, my desired product, in 19 steps from glycine ethyl ester hydrochloride. My route to **9** was admittedly long, but the yields of most steps (except the last few) were excellent, so I was able to obtain sufficient amount of **9** for enzymatic assays.

3.2.4 NMR analysis of (±)-7,7-F_2-AcAP (**9**)

I used NMR to confirm the expected structure and stereochemistry of (±)-7,7-F_2-AcAP (**9**). The ^{1}H NMR spectrum (Figure A.10) showed 14 H atoms. The ^{13}C NMR spectrum (Figure A.11) confirmed the presence of nine C atoms. The HSQC spectrum (Figure 3.2) confirmed the presence of 13 H atoms: two methine groups, four pair of methylene groups, and one methyl group. The remaining one H is from the NH group as seen in the ^{1}H NMR spectrum (Figure A.10). The ^{19}F NMR spectrum (Figure A.12) confirmed the presence of two geminal F atoms.

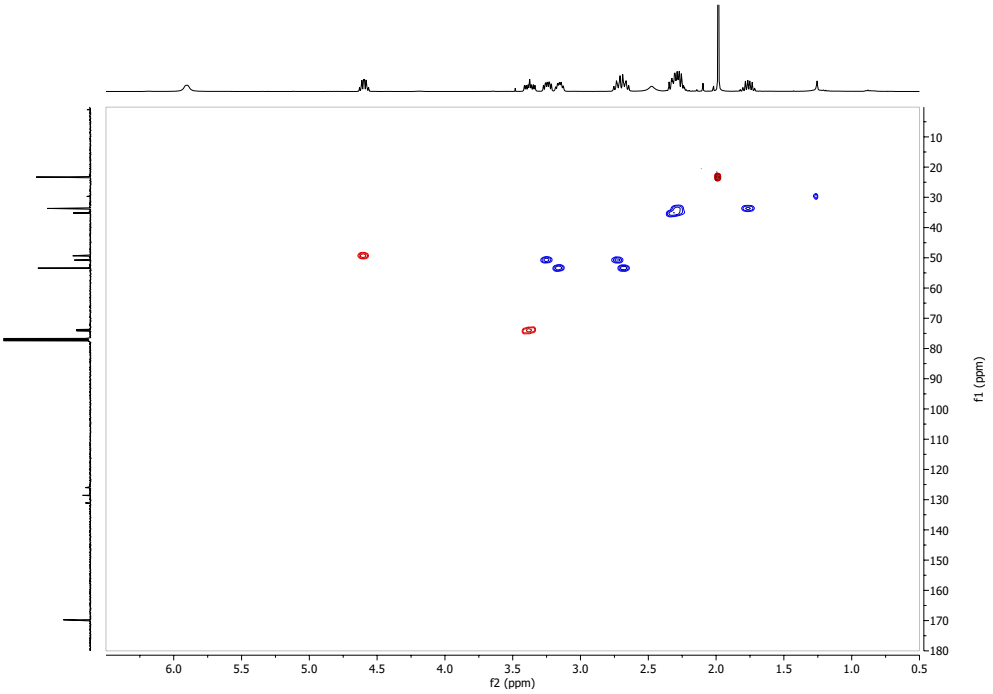

Figure 3.2 400 MHz ^{1}H–^{13}C HSQC NMR spectrum of (±)-7,7-F_2-AcAP.

Using the ^{13}C NMR (Figure A.11) and HSQC spectra (Figure 3.2), I assigned the ^{13}C resonance at 169.8 ppm to the carbonyl carbon. I assigned the resonance at 128.6 to C(7) because of the triplet nature of the peak caused by two geminal F atoms with large coupling constants (J = 251 Hz). The HSQC spectrum (Figure 3.2) supported this assignment, as C(7) is not connected to any H atoms. The next two doublet of doublet peaks in the ^{13}C NMR spectrum resonated at 73.9 ppm (J = 22.9, 6.1 Hz) and 35.2 ppm (J = 23.9, 1.9 Hz). These resonances could be assigned to C(8) and C(6), as they are next to C(7) bearing two F atoms. I assigned the resonance at 73.9 ppm to C(8) as it was closer to the ring N than C(6) was. The HSQC spectrum (Figure 3.2) supported this assignment, as C(8) is connected to one H resonating at 3.36 ppm while C(6) is connected to two geminal H atoms resonating at 2.28 ppm. I assigned the remaining methine H in the HSQC spectrum

resonating at 4.59 ppm to C(1) (49.4 ppm, dd, J = 8.7, 1.2 Hz) which is downfield compared to H(8) as it is closer to the amido group, further supporting the assignment.

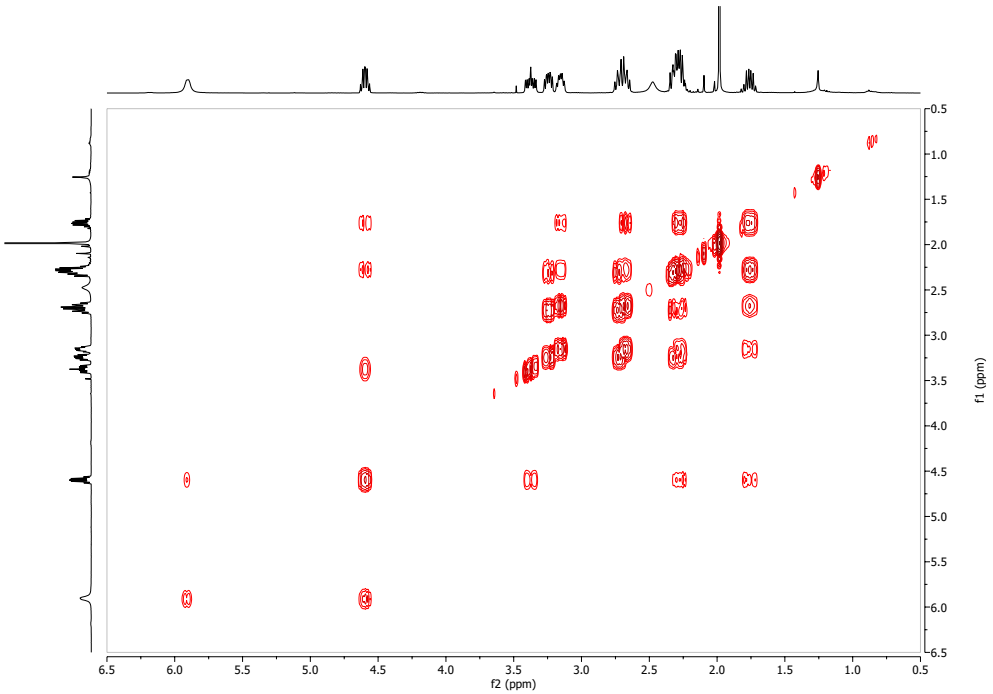

Figure 3.3 400 MHz ^{1}H-^{1}H COSY NMR spectrum of (±) *exo*-7,7-F_2-AcAP.

In the ^{13}C NMR spectrum, the effects of the two F atoms at C(7) are visible up to two C atoms away. I used the HSQC spectrum to assign the resonance at 49.4 ppm to C(1) . The next quartet peak in ^{13}C NMR resonating at 50.8 ppm (J = 2.83 Hz) could be due to C(5), as it is two C atoms away from C(7). The HSQC spectrum (Figure 3.2) shows that C(5) is connected to two H atoms resonating at 3.23 ppm and 2.69 ppm.

I assigned the remaining ^{1}H NMR resonances on the basis of chemical shifts and ^{1}H-^{1}H COSY correlations (Figure 3.3). In the COSY spectrum, there was a strong correlation between H(1) and H(8) and also between H(1) and the H atoms resonating at 2.28 ppm and 1.75 ppm, which HSQC showed were a geminal pair. These data suggested that the H

atoms resonating at 1.75 ppm and 2.28 ppm were H(2). The remaining H atoms resonating at 3.14 ppm and 2.69 ppm, which according to the HSQC spectrum are a geminal pair, can be assigned to H(3). In the COSY spectrum, there was also a strong correlation between the H(2) resonances and those assigned to H(3), which further supported the assignment of the latter resonances.

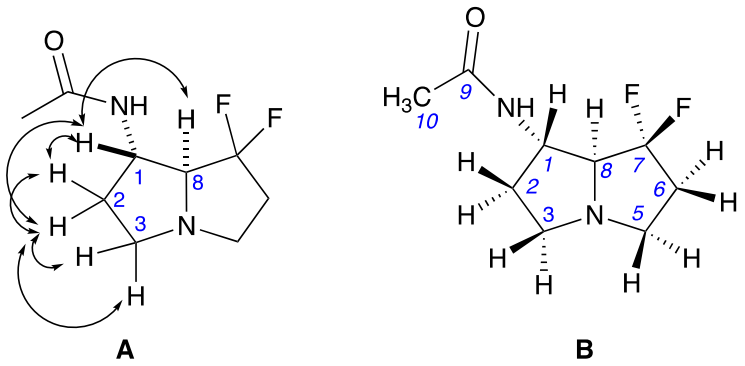

Figure 3.4 **A**. COSY correlations between H atoms at C(1), C(2), C(3), and C(8) of (±)-*exo*-7,7-F_2-AcAP. **B**. ^{13}C NMR and ^{1}H NMR assignment of (±) *exo*-7,7-F_2-AcAP

Table 3.1 ^{13}C NMR and ^{1}H NMR chemical shift of (±)-7,7-F_2-AcAP

Carbon	**Chemical shift (ppm)**	**Hydrogen**	**Chemical shift (ppm)**
C(1)	49.4	H(1)	4.59
C(2)	29.7	H(2)	2.28, 1.75
C(3)	53.4	H(3)	3.14, 2.69
C(5)	50.8	H(5)	3.23, 2.69
C(6)	35.2	H(6)	2.28
C(7)	128.6		
C(8)	73.9	H(8)	3.36
C(9)	169.8		
C(10)	23.3	H(10)	1.98
		NH	5.94

The NOESY spectrum (Figure 3.5) helped me to discern the relative stereochemistry of the H atoms at C(1) and C(8) by looking at the NOE interactions between H(1) and NH; H(8) and NH; and H(1) and H(8). The NOESY spectrum showed a strong interaction between NH and H(8) and a weak interaction between H(1) and H(8) (Figure 3.6). This is only possible if the NH group is cis to H(8), confirming the stereochemistry of the compound as exo. This conclusion was further supported by the fact that LolO accepted the compound as a substrate (see below), and we had never seen LolO accept 1-*endo*-AcAP or analogue as a substrate.[10]

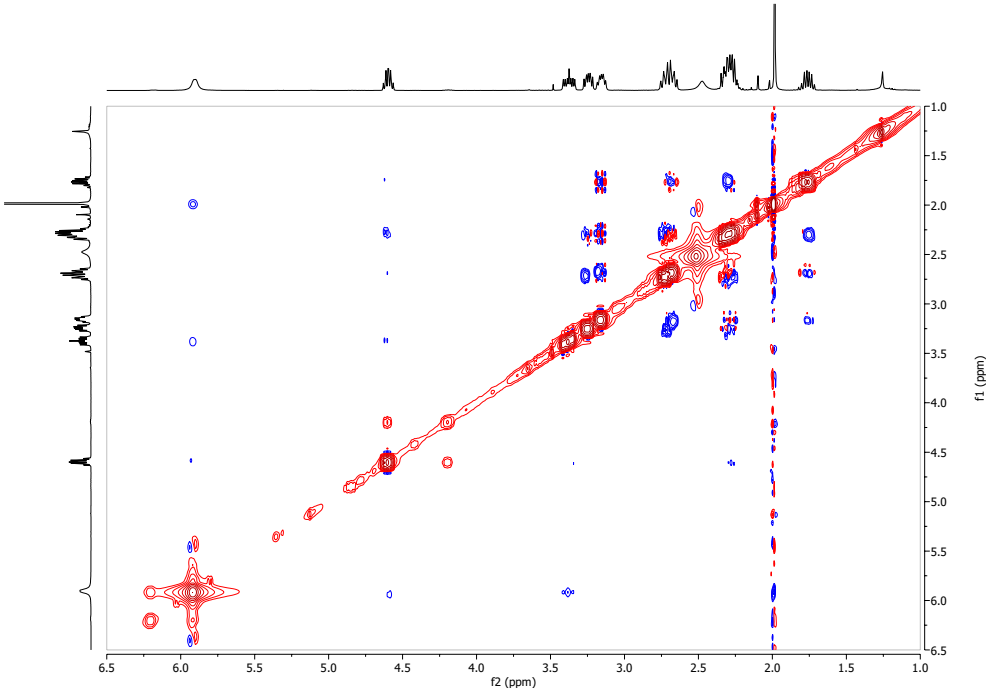

Figure 3.5 400 MHz ^{1}H-^{1}H NOESY spectrum of (±) 1-*exo*-7,7-F_2-AcAP.

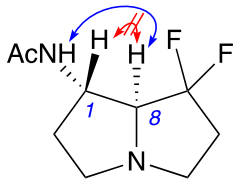

Figure 3.6 Observed and unobserved interactions in the NOESY spectra of (±)-1-*exo*-7,7-F_2-AcAP

3.2.5 Chemoenzymatic conversion of (±)-7,7-F_2-AcAP catalyzed by LolO

Eliott S. Wenger (from Dr. Bollinger's lab) helped me with enzymatic assays at Penn State. We subjected (±)-7,7-F_2-AcAP [(±)-**9**] to the same reaction conditions as we did with 6,6-F_2-AcAP [(±)-**2**] and analyzed the mixture by LC-MS. The only product that we observed had *m/*z = 221, a shift of +16 likely reflecting hydroxylation of **9** by LolO to form **10** (Figure 3.7).

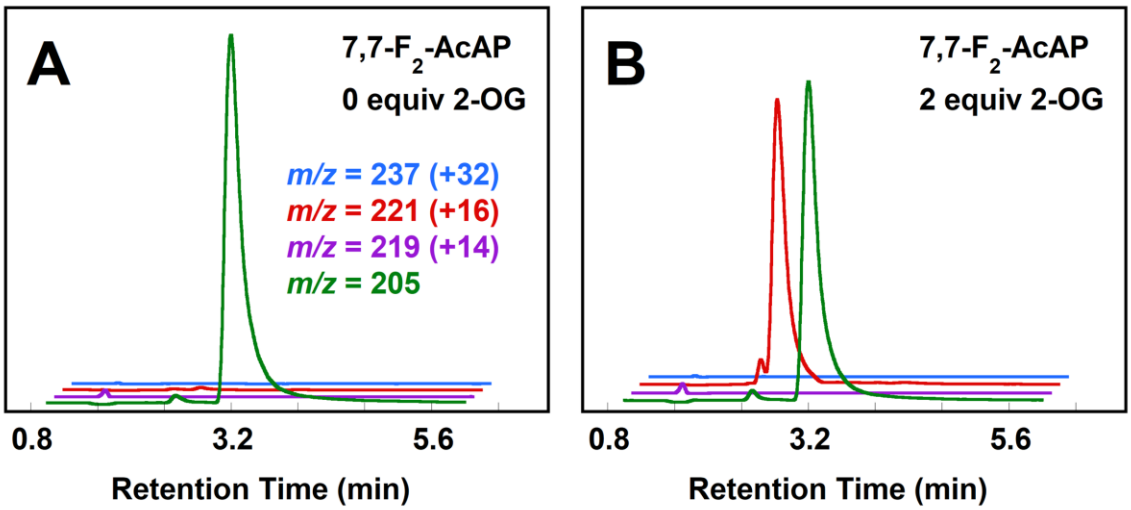

Figure 3.7 Selected LC–MS traces showing the substrate consumption and product formation catalyzed by LolO in a reaction with (±)-**9** in the absence (Panel A) and presence (B) of 2-OG.

The concentration of (±)-**9** decreased by about half as the concentration of 2-OG was increased, as expected due to the racemic nature of the compound, and the concentration

of **10** increased accordingly (Figure 3.8). We did not observe consumption of **10**. We also did not observe any species with a *m/*z value that corresponded to the product of a second LolO-catalyzed oxidation. When we did the assay with $^{18}O_2$ in place of natural O_2, the hydroxylation product (**10**) peak shifted from *m/*z = 221 to *m/*z = 223 (Figure 3.9), further confirming its assignment.

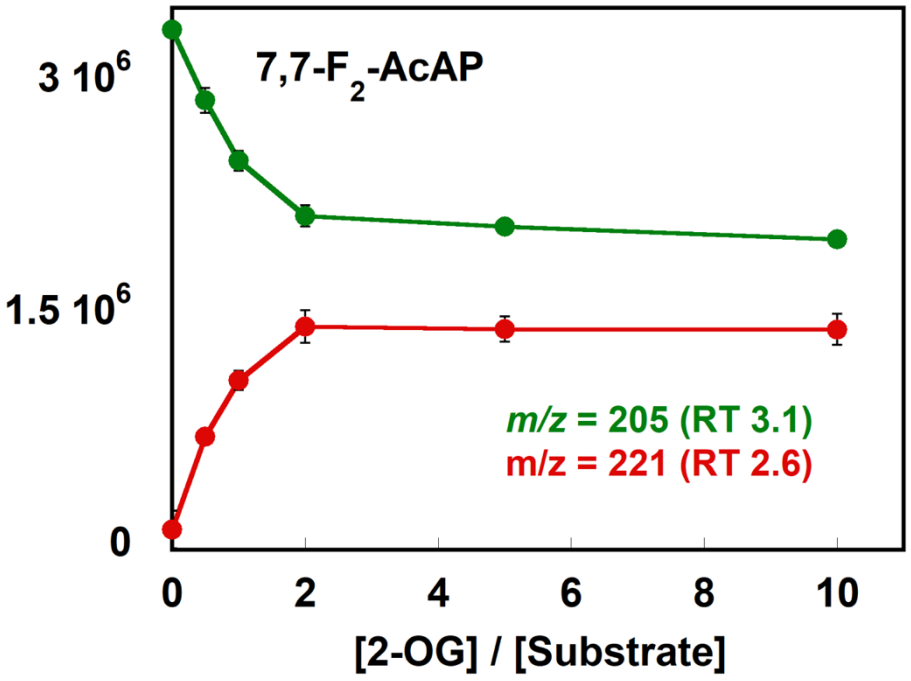

Figure 3.8 Oxidation of **9** by LolO with varied amounts of 2-OG. LC–MS total ion counts of ions with the indicated *m/z* values. Each data point is an average of two identical trials.

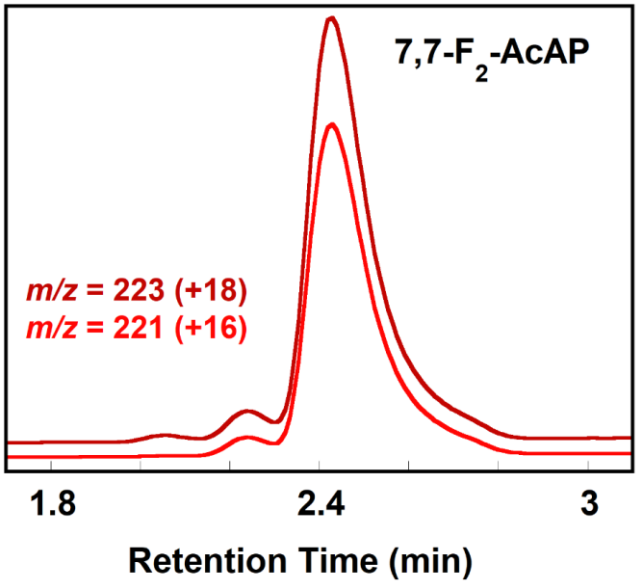

Figure 3.9 Products formed by LolO acting on **9** in the presence of $^{18}O_2$.

3.3 Experimental

1-*tert*-Butyl 2-ethyl (2*S*,3*R*)-3-hydroxypyrrolidine-1,2-dicarboxylate (15)

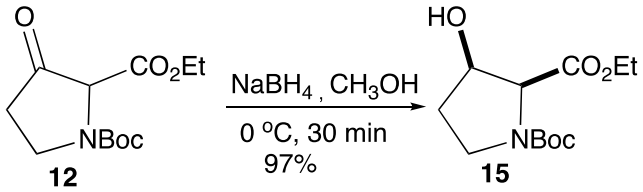

The starting material 1-*tert* butyl-2-ethyl (2*S*)-3-oxopyrrolidine-1,2-dicarboxylate (**12**) was prepared using the published procedure.[47] ^{1}H NMR (400 MHz, $CDCl_3$) δ (mixture of rotamers) 4.54 (s), 4.47 (s, 1H), 4.37 – 4.12 (m, 2H), 4.00 – 3.66 (m, 2H), 2.69 (dd, *J* = 8.4, 6.8 Hz, 2H), 1.49 (s), 1.44 (2 × s, 9H), 1.31 (t, *J* = 7.2 Hz, 3H). ^{13}C NMR (101 MHz, $CDCl_3$) δ (mixture of rotamers) 204.8, 204.2, 166.3, 166.1, 154.1, 153.9, 81.1, 81.0, 65.8, 65.5, 62.2, 42.3, 41.6, 37.2, 36.5, 28.3, 28.2, 14.2, 14.1.

The procedure for reduction was adapted from Greshock *et. al*.[54] To the solution of **12** (1.95 g, 7.60 mmol) in dry MeOH (25 mL) at 0 °C, $NaBH_4$ (0.287 g, 7.60 mmol) was added in two portions in 5 min interval and stirred for 25 min at 0 °C after last addition. The reaction was quenched with saturated NH_4Cl solution (pH 7-8), and MeOH was evaporated in vacuum. The aqueous layer was extracted with EtOAc. The combined organic layer was dried with Na_2SO_4 and evaporated. Flash chromatography of the residue over silica gel with EtOAc:hexanes (8:2) gave **15** (1.92 g, 7.39 mmol, 97%) as colorless viscous oil. The spectroscopic data for the compound were identical to those previously reported.[54] ^{1}H NMR (400 MHz, $CDCl_3$) δ (mixture of rotamers) 4.69 – 4.52 (m, 1H), 4.48 – 4.08 (m, 3H), 3.76 – 3.56 (m, 1H), 3.56 – 3.36 (m, 1H), 2.48 (br s, 1H), 2.23 – 1.87 (m, 2H), 1.46, 1.43 (2 × s, 9H), 1.35 – 1.21 (m, 3H). ^{13}C NMR (101 MHz, $CDCl_3$) δ (mixture of rotamers)

170.5, 170.3, 154.3, 153.9, 80.2, 80.1, 75.4, 72.4, 71.5, 68.2, 63.9, 63.4, 61.3, 61.2, 60.4, 53.4, 44.3, 43.8, 32.9, 32.3, 28.4, 28.3, 21.1, 14.4, 14.2.

1-*tert*-Butyl 2-ethyl (2*S*,3*R*)-3-toluenesulfonyloxypyrrolidine-1,2-dicarboxylate (15a)

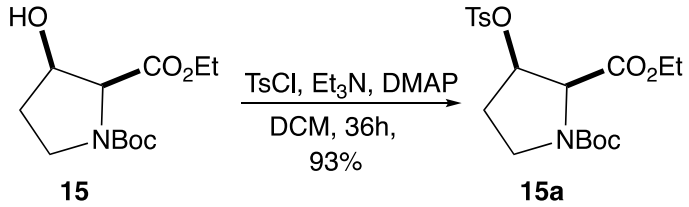

15 **15a**

The tosylation procedure was adapted from Souza *et. al*.[55] To the solution of **15** (4.08 g, 15.8 mmol) in dry CH_2Cl_2 at 0 °C under N_2, *p*-toluenesulfonyl chloride (3.60 g, 18.9 mmol), freshly dried Et_3N (6.60 mL, 47.2 mmol) and DMAP (0.385 g, 3.15 mmol) were added in order and stirred at 0 °C to room temperature until completion (28 h). The reaction was quenched with 0.1 N HCl (80 mL) (pH 8-9). The organic layer was separated and aqueous layer extracted with CH_2Cl_2. The combined organic layer washed with saturated $NaHCO_3$ (50 mL), brine (50 mL) and dried with $MgSO_4$. The solvent was evaporated in vacuum. Flash chromatography of the residue over silica gel with EtOAc:hexanes (3:7) gave **15a** (6.04 g, 14.6 mmol, 93%) as light-yellow color oil. ^{1}H NMR (400 MHz, $CDCl_3$) δ (mixture of rotamers) 7.97 – 7.64 (m, 2H), 7.41 – 7.30 (m, 2H), 5.345 – 4.94 (m, 1H), 4.42 (d, *J* = 6.9 Hz, 1H), 4.30 – 3.94 (m, 2H), 3.73 – 3.28 (m, 2H), 2.46 (s, 3H), 2.35 – 1.90 (m, 2H), 1.43, 1.39 (2 × s, 9H), 1.30 – 1.14 (m, 3H). ^{13}C NMR (101 MHz, $CDCl_3$) δ (mixture of rotamers) 168.3, 167.9, 153.9, 153.4, 145.3, 145.2, 133.4, 130.1, 129.9, 127.9, 127.9, 127.8, 82.9, 80.7, 80.5, 79.0, 78.3, 62.0, 61.7, 61.5, 43.9, 43.5, 30.9, 30.1, 28.3, 28.2, 21.7, 14.2, 14.0. IR (ATR): 1744, 1689 cm^{-1}. GC-MS (EI): 8.77 min, 95.4%; 241 (3%),

168 (9%), 141 (100%), 140 (45%), 113 (17%), 95 (23%), 68 (57%), 57 (88%). HRMS-ESI *(m/z)*: $[M+Na]^+$ Calcd for $C_{19}H_{27}NNaO_7S$ 436.1406; found 436.1396.

1-*tert*-Butyl 2-ethyl (2*S*,3*S*)-3-(benzyloxycarbonylamino)-pyrrolidine-1,2-dicarboxylate (16)

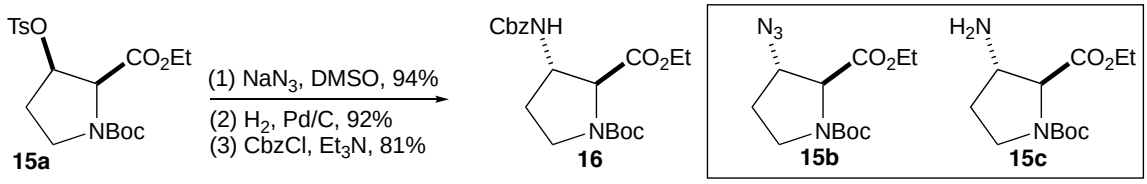

To the solution of **15a** (6.01 g, 14.6 mmol) in dry DMSO (50 mL) under N_2, NaN_3 (1.42 g, 21.8 mmol) was added and stirred at 80 °C for 5 h. The reaction mixture was cooled to room temperature and quenched with 55 mL of H_2O and extracted with ether. The combined organic layers were washed with H_2O (50 mL), dried with $MgSO_4$, and solvent evaporated to get the crude product **15b** (3.55 g, 12.5 mmol, 86%) as a clear oil which was taken to the next step without further purification. ^{1}H NMR (400 MHz, $CDCl_3$) δ (mixture of rotamers) 4.31 – 4.11 (m, 4H), 3.70 – 3.43 (m, 2H), 2.25 – 2.11 (m, 1H), 2.05 – 1.92 (m, 1H), 1.47, 1.42 (2 × s, 9H), 1.38 – 1.24 (m, 3H). ^{13}C NMR (101 MHz, $CDCl_3$) δ (mixture of rotamers) 170.5, 170.2, 154.2, 153.5, 137.01, 119.2, 81.1, 80.5, 80.4, 64.9, 64.7, 64.5, 63.6, 61.7, 61.6, 61.1, 48.4, 44.5, 44.3, 41.0, 30.2, 29.5, 28.5, 28.4, 28.3, 28.2, 14.2, 14.1. IR (ATR): 2098, 1745, 1697 cm^{-1}.

To the solution of **15b** (1.99 g, 6.99 mmol) in EtOAc (30 mL) under nitrogen, 10% palladium on activated charcoal (0.794 g, 0.4 weight equivalent) was added. The nitrogen was replaced with a balloon of hydrogen and stirred at room temperature until completion. The reaction mixture was filtered through Celite, washed with EtOAc (100 mL) and

evaporated to get the crude **15c** (1.66 g, 6.43 mmol, 92%) as a clear oil which was taken to the next step without further purification. ^{1}H NMR (400 MHz, $CDCl_3$) δ (mixture of rotamers) 4.37 – 4.07 (m, 2H), 3.99, 3.88 (d, J = 3.7 Hz, 1H), 3.77 – 3.39 (m, 3H), 2.14 (ddt, J_d = 12.5, 7.9 Hz, J_t = 6.3 Hz, 1H), 1.84 – 1.54 (m, 3H), 1.46, 1.41 (2 × s, 9H), 1.35 – 1.16 (m, 3H). ^{13}C NMR (101 MHz, $CDCl_3$) δ (mixture of rotamers) 172.0, 171.6, 154.5, 153.9, 79.9, 79.8, 68.5, 68.2, 61.1, 61.0, 57.1, 55.9, 44.8, 44.5, 33.2, 32.9, 28.4, 28.3, 14.3, 14.2. IR (ATR): 3373, 1738, 1689 cm^{-1}. GC-MS (EI): 9.37 min, 93.1%; 258 (2%), 185 (9%), 157 (18%), 129 (30%), 115 (19%), 85 (100%), 56 (97%).

To the solution of **15c** (1.65 g, 6.38 mmol) in anhydrous CH_2Cl_2 (20 mL) at 0 °C, benzyl chloroformate (1.37 mL, 9.57 mmol) was added followed by Et_3N (1.00 mL, 7.02 mmol). The ice bath was removed and stirred for 22 h at room temperature. Water (20 mL) was added, the organic layer was separated, and the aqueous layer was extracted with CH_2Cl_2. The combined organic layers were washed with brine (50 mL), dried with Na_2SO_4 and evaporated. Flash chromatography of the residue over silica gel with EtOAc:hexanes (3:7) gave **16** as a clear oil (2.02 g, 5.15 mmol, 81%). ^{1}H NMR (400 MHz, $CDCl_3$) δ (mixture of rotamers) 7.53 – 7.18 (m, 5H), 5.35 – 4.94 (m, 3H), 4.51 – 3.97 (m, 4H), 3.73 – 3.32 (m, 2H), 2.20 (dq, J_d = 14.3 Hz, Jq = 7.0 Hz, 1H), 2.00 – 1.69 (m, 1H), 1.45, 1.40 (2 × s, 9H), 1.33 – 1.07 (m, 3H). ^{13}C NMR (101 MHz, $CDCl_3$) δ (mixture of rotamers) 171.1, 170.7, 155.5, 154.3, 153.8, 136.1, 128.6, 128.3, 128.2, 80.4, 80.3, 67.0, 65.4, 64.9, 61.5, 61.4, 55.6, 54.7, 52.8, 44.4, 44.2, 43.7, 30.9, 30.1, 29.2, 28.4, 28.3, 14.2, 14.1. IR (ATR): 3315, 3061, 1739, 1682 cm^{-1}. HRMS-ESI *(m/z)*: $[M+Na]^+$ Calcd for $C_{20}H_{28}N_2NaO_6$ 415.1845; found 415.1835.

***tert*-Butyl (2*R*,3*S*)-3-(benzyloxycarbonylamino)-2-ethynylpyrrolidine-1-carboxylate (23)**

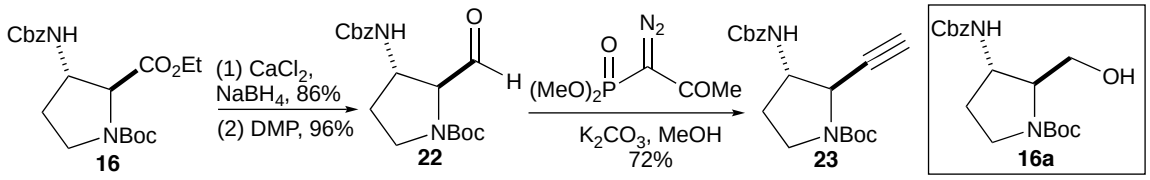

To the solution of **16** (1.34 g, 3.41 mmol) in 30 mL THF/EtOH (1:1) under nitrogen at room temperature, $CaCl_2$ (0.606 g, 5.46 mmol) was added and stirred until fully dissolved. The reaction mixture was brought to 0 °C and $NaBH_4$ (0.548 g, 14.5 mmol) was added, stirring for 1.5 h at 0 °C and 1.5 h at room temperature. The reaction mixture was carefully quenched with dropwise addition of saturated NH_4Cl (pH 8) and extracted with EtOAc. The combined organic layers were washed with a saturated solution of $NaHCO_3$ and dried with Na_2SO_4. The solvent was evaporated to give the crude product **16a** (1.02 g, 2.92 mmol, 86%) as a sticky solid which was taken to next step without further purification. ^{1}H NMR (400 MHz, $CDCl_3$) δ 7.62 – 7.10 (m, 5H), 5.39 – 4.86 (m, 3H), 4.56 – 3.16 (m, 7H), 2.17 (br s, 1H), 1.89 – 1.63 (m, 1H), 1.46 (s, 9H). ^{13}C NMR (101 MHz, $CDCl_3$) δ 156.3, 155.9, 136.1, 128.6, 128.3, 128.2, 125.5, 80.6, 67.1, 65.8, 65.0, 53.3, 45.2, 30.6, 30.3, 28.5, 28.4. IR (ATR): 3421, 3270, 3059, 1694, 1675 cm^{-1}.

To the solution of **16a** (0.953 g, 2.72 mmol) in anhydrous CH_2Cl_2 (40 mL) under nitrogen, Dess–Martin periodinane (1.39 g, 3.27 mmol) was added in one portion. The reaction was stirred at room temperature until completion. After 3h, the reaction mixture was quenched with saturated solution of $Na_2S_2O_3$ (25 mL) and saturated solution of $NaHCO_3$ (25 mL) (pH 8). The organic layer was separated and the aqueous layer was

extracted with CH_2Cl_2 (2 × 40 mL). The combined organic layers were dried with $MgSO_4$ and the solvent was evaporated to get the product **22** (0.909 g, 2.61 mmol, 96%) as sticky solid which was taken to the next step without further purification. ^{1}H NMR (400 MHz, $CDCl_3$) δ (mixture of rotamers) 9.58, 9.52 (2 × s (br), 1H), 7.58 – 7.07 (m, 5H), 5.44 – 4.86 (m, 3H), 4.61 – 3.79 (m, 2H), 3.74 – 3.26 (m, 2H), 2.46 – 1.97 (m, 1H), 1.96 – 1.61 (m, 1H), 1.46, 1.40 (2 × s, 9H). ^{13}C NMR (101 MHz, $CDCl_3$) δ (mixture of rotamers) 197.7, 197.6, 155.6, 154.5, 153.7, 135.9, 128.6, 128.4, 128.3, 81.2, 80.8, 70.4, 70.2, 67.2, 65.9, 52.5, 51.5, 44.7, 44.4, 31.1, 30.3, 30.2, 29.7, 28.3, 28.2, 15.3. IR (ATR): 3310, 3064, 3059, 1681 cm^{-1}.

To the solution of aldehyde **22** (1.23 g, 3.54 mmol) in dry MeOH (20 mL) under nitrogen at room temperature, K_2CO_3 (0.979 g, 7.08 mmol) was added followed by dropwise addition of freshly prepared Ohira–Bestmann reagent (0.816 g, 4.23 mmol) in 5 mL methanol (dark yellow color was observed on addition) and stirred at room temperature overnight. The reaction mixture was quenched with H_2O (20 mL) and MeOH was evaporated in vacuum. The aqueous layer was extracted with EtOAc (3 × 30 mL) and dried with Na_2SO_4. The solvent was evaporated to get the crude product which was purified with EtOAc:hexanes (3:7) to get the pure product **23** (0.882 g, 2.56 mmol, 72%) as colorless solid; mp 113-114 °C. ^{1}H NMR (400 MHz, $CDCl_3$) δ 7.49 – 7.27 (m, 5H), 5.31 – 4.81 (m, 3H), 4.54 – 4.12 (m, 2H), 3.71 – 3.21 (m, 2H), 2.59 – 2.21 (m, 2H), 1.86 (br s, 1H), 1.47 (s, 9H). ^{13}C NMR (101 MHz, $CDCl_3$) δ 171.2, 155.5, 154.1, 136.1, 128.6, 128.3, 81.4, 80.4, 72.1, 71.7, 67.1, 60.4, 57.7, 54.8, 43.6, 43.3, 30.3, 29.4, 28.4, 21.1, 14.2. IR (ATR): 3289, 3263, 3056, 1717, 1674 cm^{-1}. HRMS-ESI *(m/z)*: $[M\text{-Boc}+H]^+$ Calcd for $C_{14}H_{17}N_2O_2$ 245.1290; found 245.1286.

Ethyl 2-[(2*R*,3*S*)-3-(benzyloxycarbonylamino)-2-ethynylpyrrolidin-1-yl]acetate (24)

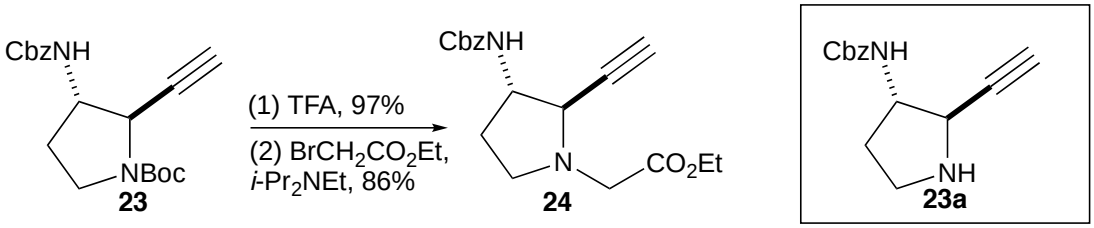

To the solution of **23** (0.165 g, 0.480 mmol) in CH_2Cl_2 (15 mL) at 0 °C, TFA (4 mL) was added dropwise and stirred at 0 °C until the starting material had been consumed completely (1 h). The solvent was evaporated and the crude material was extracted using 15 mL CH_2Cl_2, 5 mL H_2O and few drops of NH_4OH (pH 8). The aqueous layer was extracted with CH_2Cl_2 (2 × 15 mL). The combined organic layers were dried with Na_2SO_4, filtered and solvent evaporated to give **23a** (0.114 g, 0.465 mmol, 97%) in analytically pure form which was taken to the next step without further purification. ^{1}H NMR (400 MHz, $CDCl_3$) δ 7.58 – 7.03 (m, 5H), 5.43 – 4.91 (m, 3H), 4.35 – 4.04 (m, 1H), 3.75 (s, 1H), 3.28 – 2.90 (m, 2H), 2.32 (p, *J* = 6.1 Hz, 2H), 1.85 (s, 1H), 1.71 – 1.48 (m, 1H). ^{13}C NMR (101 MHz, $CDCl_3$) δ 155.7, 136.4, 128.5, 128.2, 83.,6 72.1, 66.8, 57.6, 55.2, 43.8, 31.6. IR (ATR): 3285, 3180, 3065, 1682, cm^{-1}.

To the solution of **23a** (0.555 g, 2.27 mmol) in dry THF (25 mL) at 0 °C, diisopropylethylamine (0.5 mL, 2.95 mmol) was added followed by ethyl bromoacetate (0.3 mL, 2.73 mmol). The mixture was heated at 55 °C for 2 days. The reaction was quenched with H_2O at room temperature and extracted with EtOAc (3 × 30 mL). The combined organic layer was washed with saturated $NaHCO_3$ (15 mL), dried with Na_2SO_4, filtered and solvent evaporated in reduced pressure. Flash chromatography of the residue

over silica gel with EtOAc:hexanes (4:6) gave **24** (0.815 g, 2.40 mmol, 99%) as light-yellow solid; mp 76-77 °C. ^{1}H NMR (400 MHz, $CDCl_3$) δ 7.60 – 7.05 (m, 5H), 5.63 (d, J = 8.8 Hz, 1H), 5.28 – 4.90 (m, 2H), 4.31 (t, J = 7.5 Hz, 1H), 4.16 (qd, J_q = 7.1 Hz, J_d = 1.2 Hz, 2H), 3.78 (s, 1H), 3.58 – 3.27 (m, 2H), 3.06 (td, J_t = 8.7 Hz, J_d = 4.9 Hz, 1H), 2.65 (td, J_t = 9.1 Hz, J_d = 6.0 Hz, 1H), 2.48 – 2.14 (m, 2H), 1.87 – 1.56 (m, 1H), 1.25 (t, J = 7.1 Hz, 3H). ^{13}C NMR (101 MHz, $CDCl_3$) δ 170.6, 155.6, 136.5, 128.5, 128.1, 128.0, 79.1, 74.8, 66.6, 60.7, 59.9, 56.8, 52.4, 49.4, 30.8, 14.2. IR (ATR): 3305, 3252, 3228, 3065, 1745, 1682 cm^{-1}. HRMS-ESI *(m/z)*: $[M+H]^+$ Calcd for $C_{18}H_{22}N_2NaO_4$ 353.1477; found 353.1473.

Benzyl *N*-[(2*R*,3*S*)-2-ethynyl-1-(2-{[(methylsulfanyl)methanethioyl]oxy}ethyl)pyrrolidin-3-yl]carbamate (25)

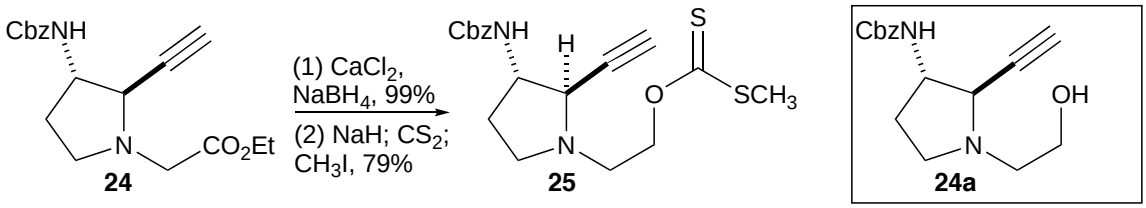

To the solution of **24** (0.0884g, 0.270 mmol) in THF:EtOH (1:1) (10 mL) under nitrogen at room temperature, $CaCl_2$ (0.0480 g, 0.430 mmol) was added and stirred until it dissolved. The reaction mixture was brought to 0 °C and $NaBH_4$ (0.0430g, 1.15 mmol) was added, and the mixture was allowed to warm to room temperature overnight. The reaction mixture was carefully quenched with dropwise addition of saturated NH_4Cl (pH 8) and extracted with EtOAc. The combined organic layer washed with saturated solution of $NaHCO_3$ and dried with Na_2SO4. The solvent was evaporated to give **24a** (0.0770g, 0.267 mmol, 99%) as a colorless solid which was taken to next step without further purification.

^{1}H NMR (400 MHz, $CDCl_3$) δ 7.63 – 7.07 (m, 5H), 5.60 – 4.85 (m, 3H), 4.29 (s, 1H), 3.99 – 3.39 (m, 3H), 3.16 – 2.69 (m, 3H), 2.61 (q, *J* = 8.7 Hz, 1H), 2.50 – 2.07 (m, 3H), 1.86 – 1.52 (m, 1H). ^{13}C NMR (101 MHz, $CDCl_3$) δ 155.6, 136.4, 128.5, 128.2, 78.9, 74.8, 66.8, 60.4, 59.7, 56.7, 53.5, 49.2, 30.6, 30.3.

To the solution of **24a** (0.103 g, 0.357 mmol) in THF (15 mL) at 0 °C, NaH, 60% dispersion in oil (0.0170g, 0.428 mmol) was added all at once. The reaction mixture was warmed to room temperature. After 3 h, CS_2 (0.11 mL, 1.79 mmol) was added. The mixture was allowed to stir for 2h at room temperature, and then CH_3I (0.11 mL, 1.79 mmol) was added. The mixture was allowed to stir at room temperature overnight. The reaction mixture was quenched with dropwise addition of saturated NH_4Cl (pH 8), water to dissolve insoluble precipitate and extracted with EtOAc. The combined organic layer was washed with saturated solution of $NaHCO_3$, dried with Na_2SO_4, and the solvent was evaporated. Flash chromatography of the residue over silica gel with EtOAc:hexanes (3:7) gave product **25** (0.107 g, 0.283 mmol, 79%) as a light yellow solid; mp 72-73 °C. ^{1}H NMR (400 MHz, $CDCl_3$) δ 7.48 – 7.12 (m, 5H), 5.36 (d, *J* = 8.9 Hz, 1H), 5.19 – 4.94 (m, 2H), 4.85 – 4.56 (m, 2H), 4.28 (q, *J* = 18.5, 13.4 Hz, 1H), 3.62 (s, 1H), 3.15 – 2.83 (m, 3H), 2.60 (td, J_t = 9.4 Hz, J_d = 6.2 Hz, 1H), 2.55 (s, 3H), 2.45 – 2.17 (m, 2H), 1.76 – 1.45 (m, 1H). ^{13}C NMR (101 MHz, $CDCl_3$) δ 215.9, 155.4, 136.4, 128.5, 128.2, 128.1, 78.5, 75.0, 72.0, 66.7, 60.51, 56.4, 49.6, 49.5, 30.6, 19.0. IR (ATR): 3296, 3278, 3253, 3082, 1745, 1683, 1553 cm^{-1}. HRMS-ESI *(m/z)*: $[M+H]^+$ Calcd for $C_{18}H_2N_2O_3S_2$ 379.1150; found 379.1149.

Benzyl *N*-[(1*S*,7a*R*)-7-methylidenepyrrolizidin-1-yl]carbamate (26)

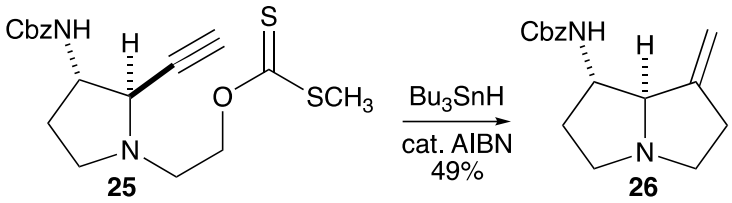

To the solution of **25** (0.153 g, 0.405 mmol) in anhydrous benzene (40 mL), tributyltin hydride (0.13 mL, 0.486 mmol) was added at room temperature followed by AIBN (0.010 g, 0.041 mmol) under nitrogen. The reaction mixture was sparged with nitrogen for 10 minutes and transferred to 80 °C preheated oil bath. After the mixture was allowed to reflux for 8 h, tributyltin hydride (0.060 mL, 0.240 mmol) and AIBN (0.010g, 0.041 mmol) were again added, and the mixture was allowed to reflux overnight. The reaction mixture was brought to room temperature and evaporated to get the crude product, purified using 10% MeOH in CH_2Cl_2 with 2% NH_4OH to get **26** (0.0540 g, 0.198 mmol, 49%) as a yellow solid; mp 104-105 °C. ^{1}H NMR (400 MHz, $CDCl_3$) δ 7.48 – 7.12 (m, 5H), 5.92 (d, J = 8.3 Hz, 1H), 5.23 – 4.88 (m, 4H), 4.23 – 3.88 (m, 1H), 3.72 – 3.49 (m, 1H), 3.27 – 2.90 (m, 2H), 2.83 – 2.31 (m, 4H), 2.27 – 2.01 (m, 1H), 1.68 (dq, J_d = 13.4 Hz, J_q = 6.9 Hz, 1H). ^{13}C NMR (101 MHz, $CDCl_3$) δ 156.0, 150.4, 136.5, 128.5, 128.1, 128.0, 107.1, 74.0, 66.6, 57.8, 52.5, 52.3, 32.9, 31.6. IR (ATR): 3169, 3028, 1700, 1656, 1562 cm^{-1}. GC-MS (EI): 12.28 min, 100%; 272 (27%), 121 (12%), 95 (100%), 91 (18%), 77 (10%). HRMS-ESI (*m/z*): $[M+H]^+$ Calcd for $C_{16}H_{21}N_2O_2$ 273.1603; found 273.1599.

(±)-Benzyl *N*-[(1*S*,7a*S*)-7,7-difluoropyrrolizidin-1-yl]carbamate (28)

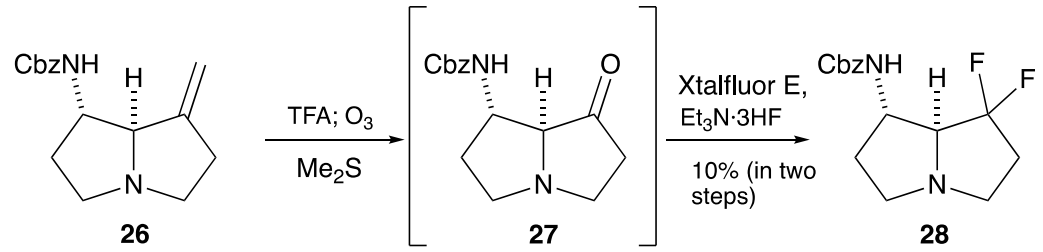

To the solution of **26** (0.365 g, 1.33 mmol) in anhydrous CH_2Cl_2 (10 mL), CF_3COOH (5 mL) was added at room temperature. After stirring for 5 min, the reaction mixture was brought to –78 °C, and ozone was passed through the solution until it maintained a persistent blue color (1 h). Ozone was removed by sparging with nitrogen, and dimethyl sulfide (0.20 mL, 2.74 mmol) was added. The mixture was stirred for 1 h at –78 °C and 3 h at room temperature. The solvent was evaporated, the crude TFA salt was dissolved in CH_2Cl_2 and saturated $NaHCO_3$ (10 mL) was added at 0 °C. The organic layer was separated, and the aqueous layer was extracted with CH_2Cl_2 (2 × 20 mL). The combined organic layers were dried with Na_2SO_4 and evaporated to give the crude product **27**, which was taken to the next step without further purification. A small amount of the compound was purified for characterization by NMR. ^{1}H NMR (400 MHz, $CDCl_3$) δ 7.75 – 6.96 (m, 5H), 5.87 – 5.34 (m, 1H), 5.23 – 4.89 (m, 2H), 4.20 (t, *J* = 6.7 Hz, 1H), 3.51 – 3.03 (m, 3H), 3.03 – 2.76 (m, 1H), 2.65 (q, *J* = 8.3 Hz, 1H), 2.55 – 2.04 (m, 3H), 1.86 – 1.53 (m, 1H). ^{13}C NMR (101 MHz, $CDCl_3$) δ 216.0, 155.7, 136.4, 136.3, 128.5, 128.3, 128.2, 74.3, 66.9, 54.2, 53.9, 52.9, 52.8, 50.1, 48.5, 37.4, 34.9, 33.5, 29.7

To a solution of triethylamine trihydrofluoride (0.43 mL, 2.66 mmol) in 1,2-dichloroethane (1.5 mL), Xtalfluor E (0.914 g, 3.99 mmol) was added at room temperature,

and the mixture was brought to 80 °C. Compound **27** (0.365 g, 1.33 mmol) in 1,2-dichloroethane (2 mL) was added dropwise to the reaction mixture, which was allowed to reflux overnight. The reaction mixture was diluted with CH_2Cl_2 (10 mL), and saturated $NaHCO_3$ (15 mL) was added at 0 °C. The mixture was stirred for 1 h. The organic layer was separated, and aqueous layer was extracted with CH_2Cl_2 (2 × 20 mL). The combined organic layers were dried with Na_2SO_4, and the solvent was evaporated. The residue was purified with 5% MeOH in CH_2Cl_2 with 2% NH_4OH to get **28** (0.0390 g, 0.132 mmol, 10% in two steps) as yellow solid; mp 97-98 °C. ^{1}H NMR (400 MHz, $CDCl_3$) δ 7.54 – 7.12 (m, 5H), 5.49 – 4.90 (m, 3H), 4.39 (q, J = 6.6 Hz, 1H), 3.35 (ddd, J_d = 16.4, 10.2, 4.7 Hz, 1H), 3.21 (dt, Jd = 10.6 Hz, J_t = 6.0 Hz, 1H), 3.10 (dt, J_d = 11.5 Hz, J_t = 6.1 Hz, 1H), 2.77 – 2.55 (m, 2H), 2.37 – 2.10 (m, 3H), 1.87 – 1.65 (m, 1H). ^{13}C NMR (101 MHz, $CDCl_3$) δ 155.7, 136.3, 130.9, 128.5, 128.2, 128.1, 125.9, 74.4, 74.1, 73.9, 66.9, 53.3, 50.9, 50.7, 50.6, 35.5, 35.3, 35.0, 33.8, 29.7. ^{19}F NMR (376 MHz, $CDCl_3$), δ (-106.3) (J_{F-F} = 233.1 Hz, J_{H-F} = 7.5 Hz, 1F), (-110.5) (J_{F-F} = 229.4 Hz, J_{H-F} = 18.8 Hz, 1F). IR (ATR): 3306, 3062, 3037, 1686, 1534 cm^{-1}. GC-MS (EI): 11.84 min, 100%; 276 (56%), 185 (7%), 145 (100%), 119 (47%), 91 (47%). HRMS-ESI *(m/z)*: $[M+H]^+$ Calcd for $C_{15}H_{19}F_2N_2O_2$ 297.1415; found 297.1412.

(±)-7,7-Difluoro-1-*exo*-acetamidopyrrolizidine (9)

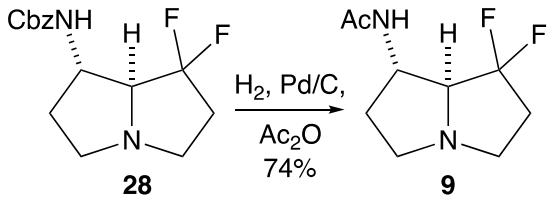

To a solution of **28** (0.0331 g, 0.112 mmol) in anhydrous ethyl acetate (8.0 mL) at room temperature, 10% Pd/C (0.0331 g) was added under nitrogen. Nitrogen was replaced with hydrogen, and the mixture was stirred until the completion of the reaction (3 h). Excess acetic anhydride (0.10 mL) was added, and the mixture was stirred overnight. The reaction mixture was filtered through a short pad of Celite and washed with EtOAc (25 mL) and methanol (25 mL). The solvent was evaporated, and the residue was purified with 8% MeOH in CH_2Cl_2 with 2% NH_4OH to get **9** (0.0168 g, 0.0823 mmol, 74%) as light-yellow solid; mp 117-118 °C. ^{1}H NMR (400 MHz, $CDCl_3$) δ 5.94 (br s, 1H), 4.59 (qd, J_q = 7.1 Hz, J_d =4.9 Hz, 1H), 3.36 (ddd, J_d = 15.6, 10.7, 5.0 Hz, 1H), 3.29 – 3.07 (m, 2H), 2.68 (ddd, J_d = 17.5, 10.6, 7.3 Hz, 2H), 2.38 – 2.13 (m, 3H), 1.98 (s, 3H), 1.85 – 1.65 (m, 1H). ^{13}C NMR (101 MHz, $CDCl_3$) δ 169.8, 131.1, 128.6, 126.0, 74.2, 74.0, 73.9, 73.7, 53.4, 50.8, 50.8, 50.7, 50.7, 49.4, 49.4, 49.3, 49.2, 35.4, 35.2, 35.1, 34.9, 33.7, 23.3. ^{19}F NMR (376 MHz, $CDCl_3$), δ (-105.5) (J_{F-F} = 229.4 Hz, J_{H-F} = 9.9 Hz, 1F), (-110.7) (J_{F-F} = 233.1 Hz, J_{H-F} = 16.4 Hz, 1F). IR (ATR): 3275, 3089, 1650, 1548 cm^{-1}. GC-MS (EI): 8.23 min, 100%; 184 (12%), 145 (100%), 144 (65%), 119 (30%), 100 (6%), 81 (11%), 55 (18%). HRMS-ESI (*m/z*): $[M+H]^+$ Calcd for $C_9H_{15}F_2N_2O$ 205.1152; found 205.1155.

Enzymatic Assays for (±)-7,7-F2-AcAP

(Eliott S. Wenger from Dr. Bollinger's lab helped me to conducted these enzymatic assays.) The enzyme (LolO) was purified using the published procedure.[10] For the 2-OG titrations, a sequence of six samples were prepared anoxically in an anoxic chamber and assay was conducted in exactly similar way as described in Chapter 2 for 6,6-F_2-AcAP.

Enzymatic Production and Purification of 2-OH-7,7-F_2-AcAP

Four Eppendorf tubes were anaerobically prepared in an anoxic chamber containing 700 µL each of 10 mM 7,7-F_2-AcAP, 225 µL LolO (purified according to previously published methods), 200 µM Fe^{II} [from $Fe(NH_4)_2(SO_4)_2$], 100 mM 2-oxoglutarate, and 20 mM ascorbic acid (concentrations *after* final dilution with air-saturated buffer) in a buffer containing 5% glycerol, 150 mM NaCl, and 50 mM sodium HEPES buffer at pH 7.5. The tubes were brought out of the glovebox, and 300 µL of cold (4 °C) air-saturated buffer was added to each tube. The solution was then split into eight tubes with equal (500 µL) volume, and a small stir bar was added. The tubes were stirred at 4 °C open to air for one hour. The solution was light purple but turned pale yellow with greater O_2 exposure. To ensure complete conversion to the hydroxylated product, additional enzyme was added (50 µL of 1 mM LolO, 1 mM Fe^{II}, and 10 mM ascorbic acid added to each tube of 500 uL). After an additional 30 minutes of stirring, all tubes were pooled, and formic acid was added to a final concentration of 5%. The enzyme was removed by centrifugation (spin filter with 10k molecular weight cutoff), though a significant amount of material precipitated above the filter. More product was recovered by resuspending the precipitated material in water and additional centrifugation. After three cycles of resuspension and centrifugation, all the

flow-thru was pooled and lyophilized. When all the water had been removed, the remaining solid was resuspended in 900 µL of water and injected onto a prep-scale Agilent reverse-phase C18 column (21.2 mm × 150 mm, 10 µm particle size). The column was developed at 40 mL/min using the same program and mobile phases as in the small-scale assays. Fractions were collected every ~8 seconds and their composition were determined by LC-MS using methods identical to those used for the small-scale assays. The fractions with >95% 2-OH-7,7-F_2-AcAP were pooled and dried with N_2, yielding a transparent solid that was used for NMR analysis. However, the product obtained is contaminated with the HEPES buffer, which halted the analysis of structure because of overlapped peaks. Further purification of 2-OH-7,7-F_2-AcAP is ongoing.

CHAPTER 4. CONCLUSIONS AND FUTURE DIRECTIONS

As described in Chapter 2, I have prepared 6,6-F_2-AcAP from *N*,*O*-protected 4-oxoproline in eight steps where the key step was Dieckmann condensation that annulated the A ring onto the B ring. I have shown that LolO accepted the 6,6-difluorinated analogs of natural AcAP, suggesting that LolO has a flexible active site. These results also suggested that the cycloetherification mechanism most likely involves a C(7) radical as opposed to a C(7) carbocation, further bolstering our hypothesis of a radical coupling pathway.

As described in Chapter 3, I prepared 7,7-F_2-AcAP from 3-oxoproline in 17 steps where the key step was radical cyclization to make pyrrolizidine ring in *5-exo-dig* fashion. I have shown that LolO catalyzes the hydroxylation of 7,7-difluorinated analog of AcAP, (±)-**9**, to make the 7,7-difluorinated analog of 2-OH-AcAP (**10**). The two F atoms at C(7) prevent LolO from acting on **10** at all by completely blocking the cycloetherification step.

The purification of the 7,7-difluorinated analog of 2-OH-AcAP from HEPES (the buffer used in enzymatic assays) currently represents a surmountable challenge. In the future, this molecule may be of use to a collaborator in the Bollinger-Krebs group, who could accumulate the cycloetherification intermediate to high concentration using **10** as a substrate. Such accumulation will ultimately be necessary for characterizing the cycloetherification intermediate and will represent a key experiment in the full mechanistic dissection of LolO.

Since, my current route to make 7,7-diflorocompound is long, and especially low yield during the deoxyfluorination step, one could synthesize the 7,7-F_2-AcAP in better yield in

future using the following route (Scheme 4.1). It would still have challenges regarding the volatility of the difluoro compound after radical cyclization, which can be avoided if one could make the salt of the compound. Also, it would be interesting to see how the Raney Ni reaction would undergo while reducing 7,7-F_2-oxime.

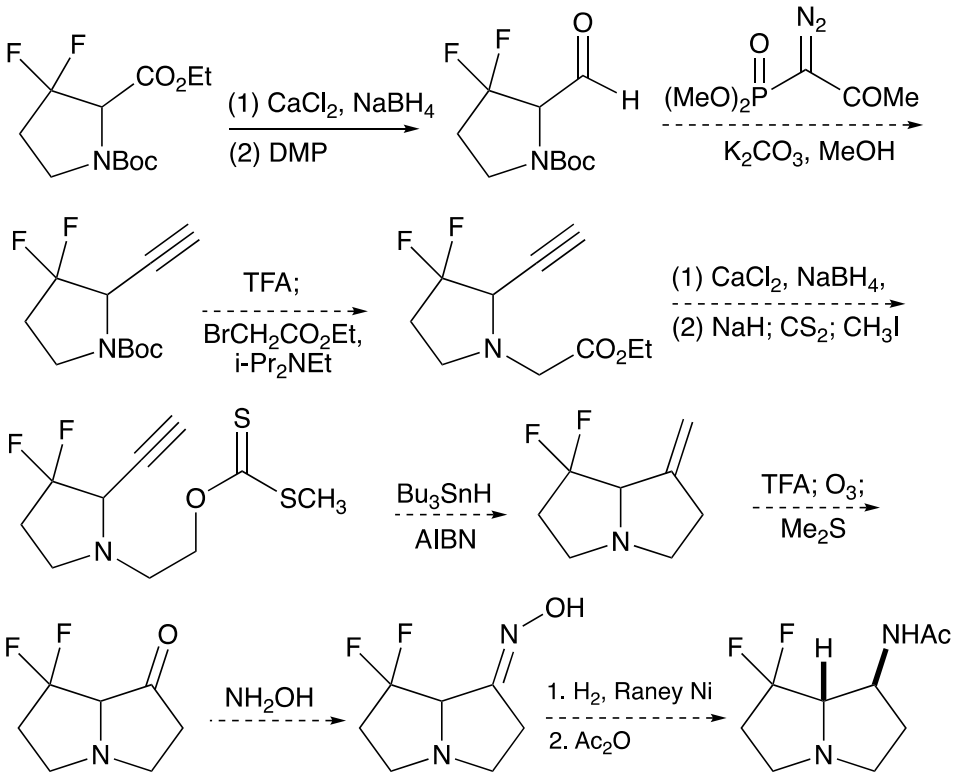

Scheme 4.1 Possible future route to 7,7-F_2-AcAP

APPENDIX: ADDITIONAL SPECTRA OF SELECTED COMPOUNDS

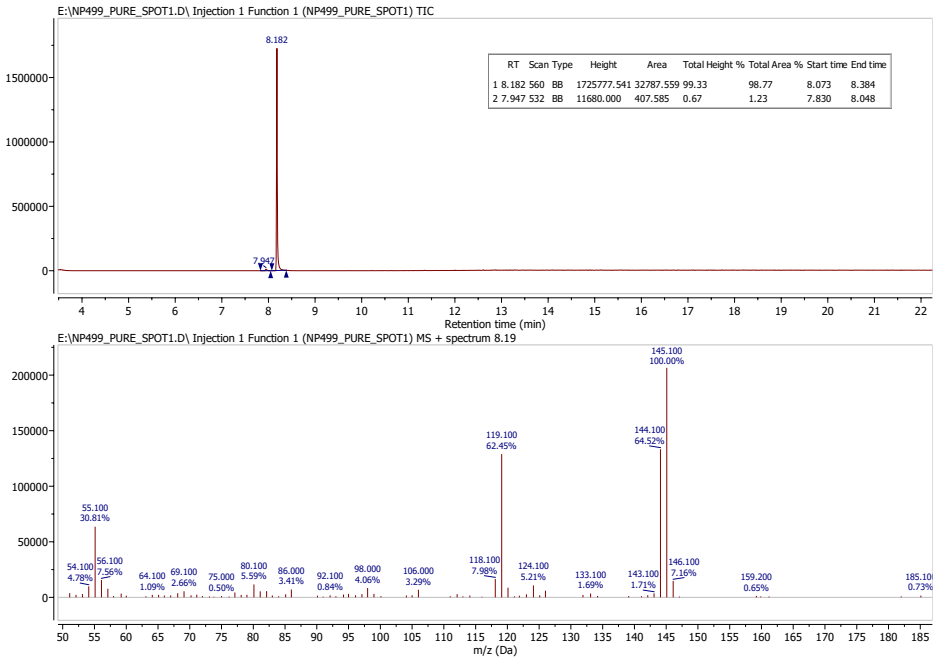

Figure A.1 GCMS spectra of (±) *exo*-6,6-F_2-AcAP

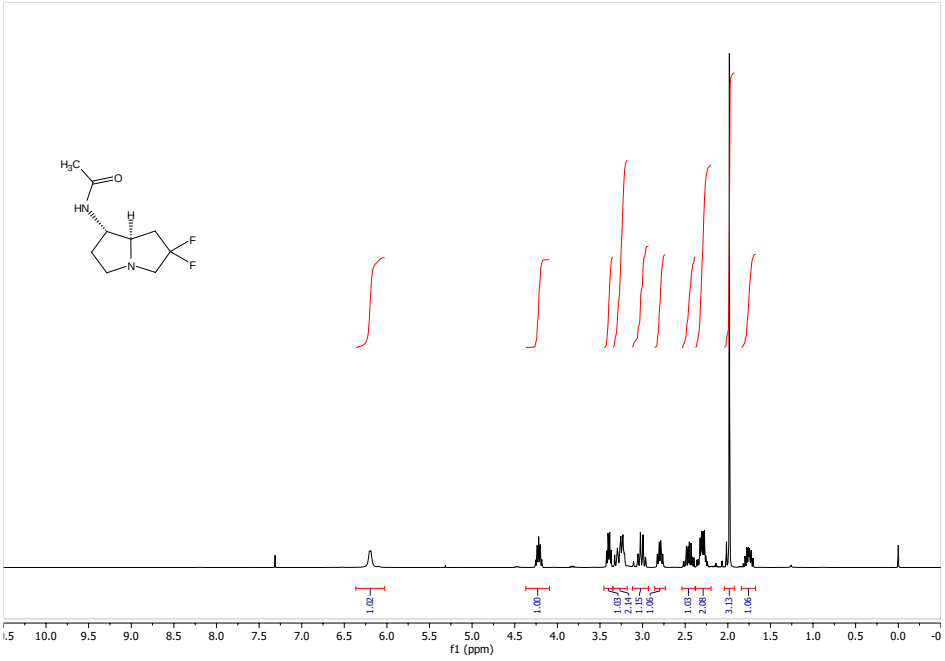

Figure A.2 400 MHz ^{1}H NMR spectra of (±) *exo*-6,6-F_2-AcAP

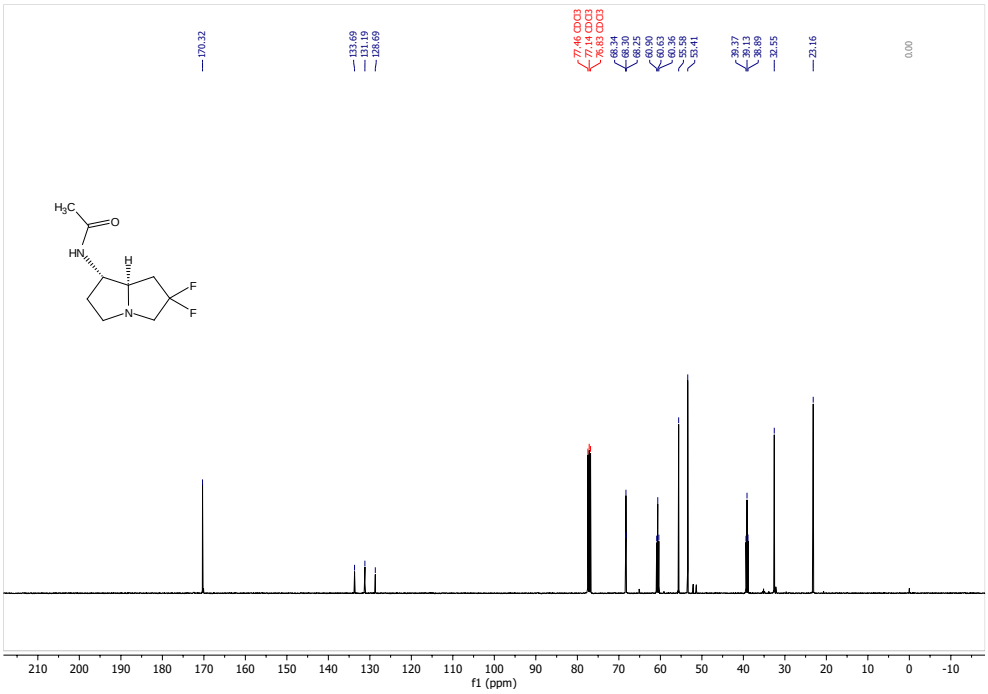

Figure A.3 400 MHz ^{13}C NMR spectra of (±) *exo*-6,6-F_2-AcAP

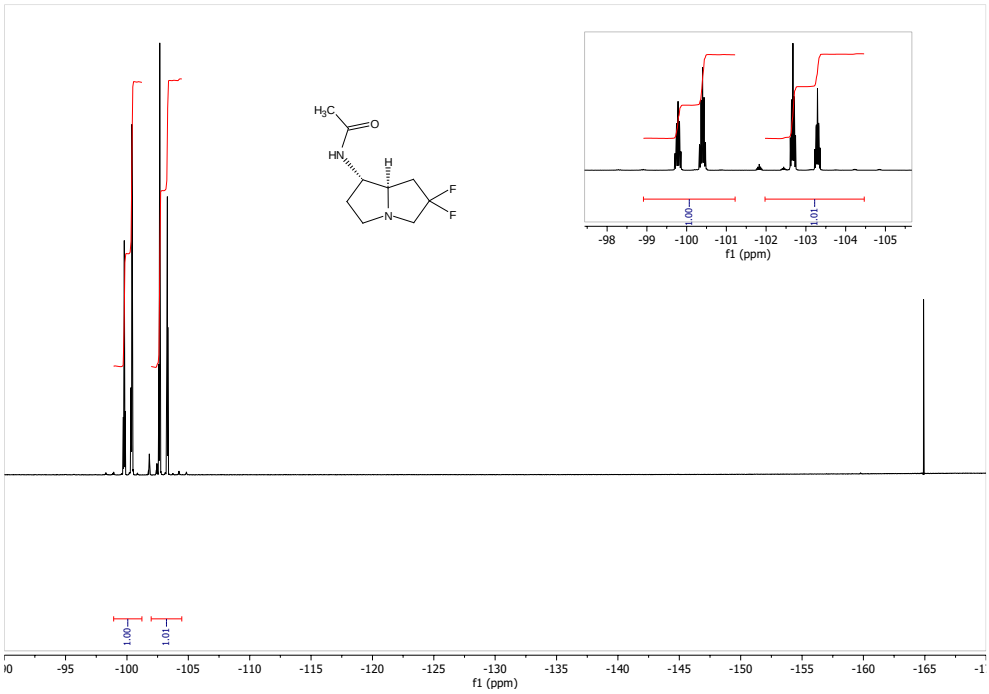

Figure A.4 376 MHz ^{19}F NMR spectra of (±) *exo*-6,6-F_2-AcAP

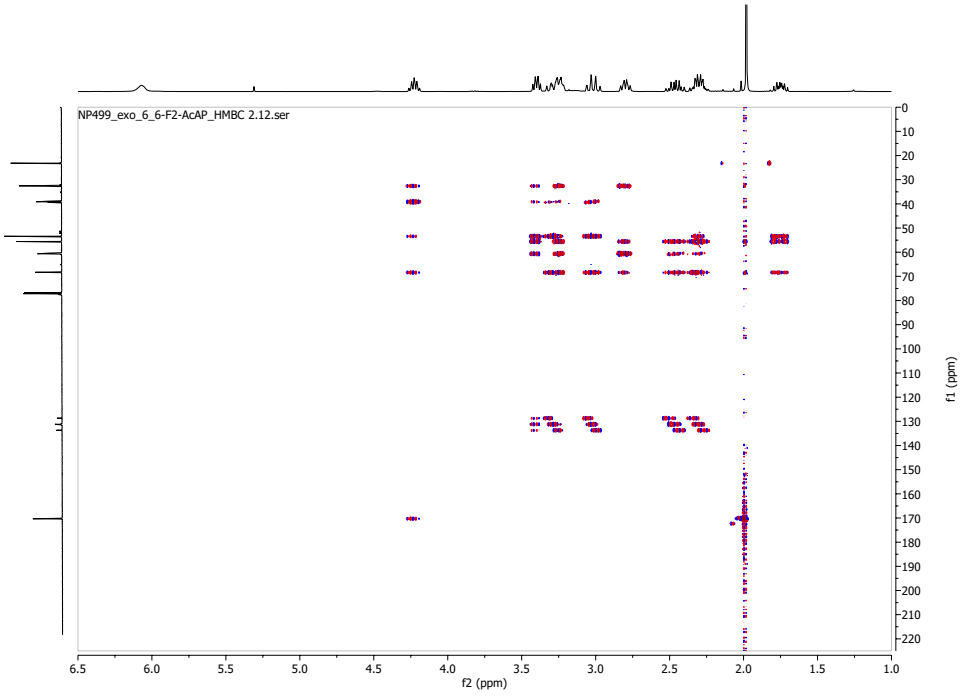

Fig A.5 400 MHz ^{1}H-^{13}C HMBC spectrum of (±) *exo*-6,6-F_2-AcAP.

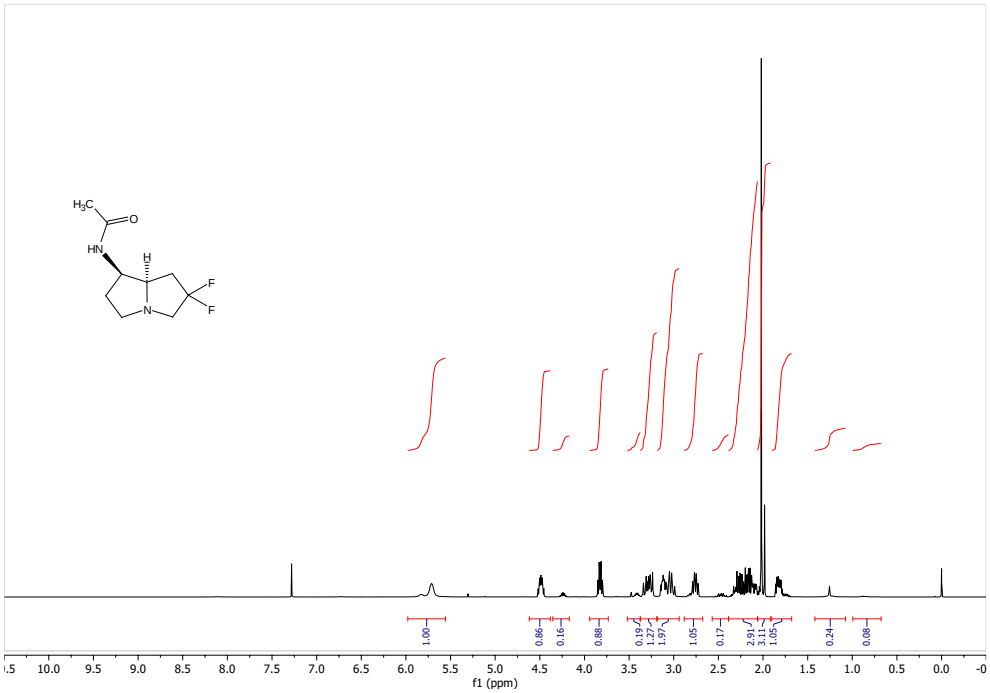

Figure A.6 400 MHz ^{1}H NMR spectra of (±) *endo*-6,6-F_2-AcAP

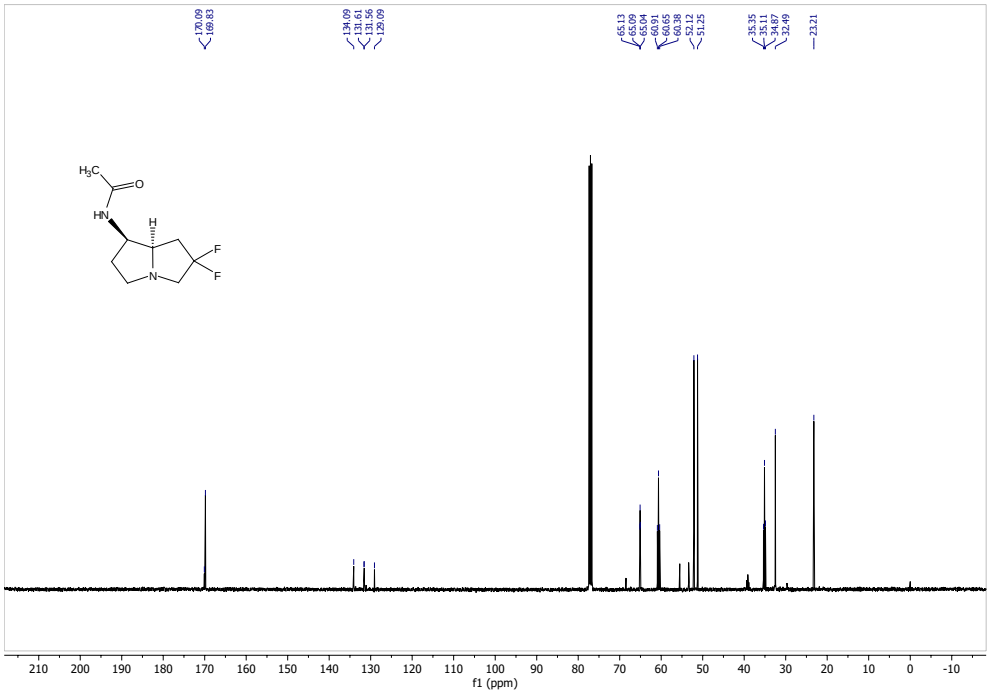

Figure A.7 400 MHz ^{13}C NMR spectra of (±) *endo*-6,6-F_2-AcAP

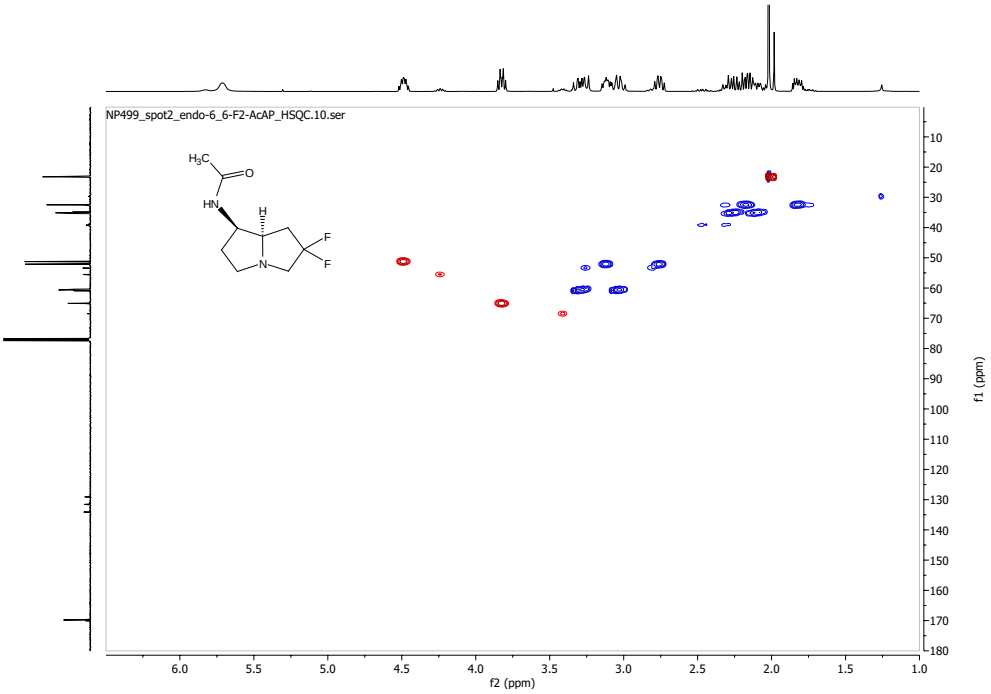

Figure A.8 400 MHz ^{1}H-^{13}C HSQC spectrum of (±) *endo*-6,6-F_2-AcAP

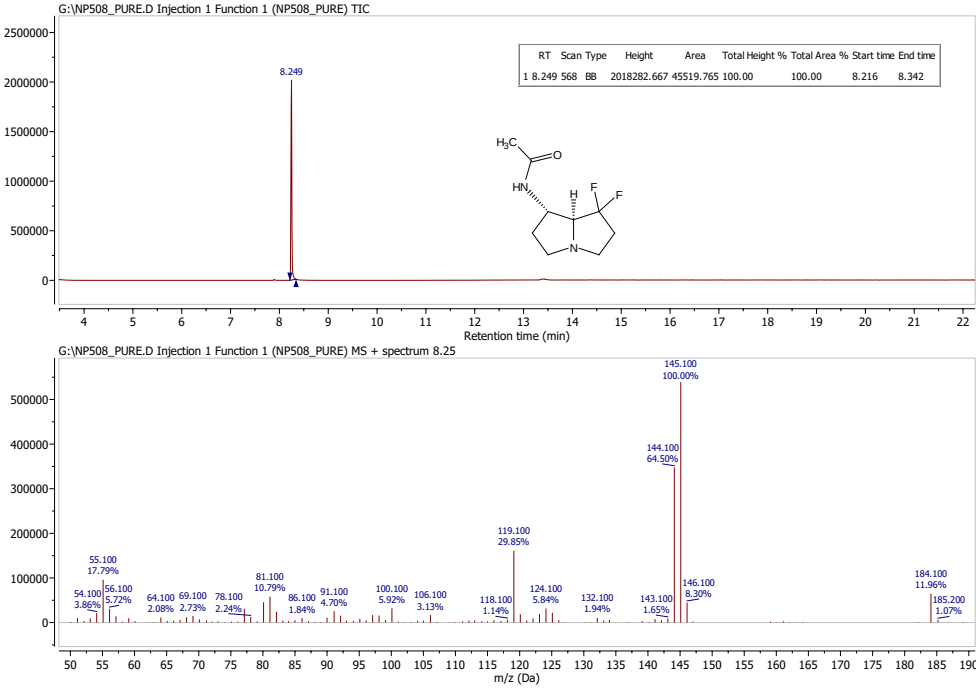

Figure A.9 GCMS spectra of (±) *exo*-7,7-F_2-AcAP

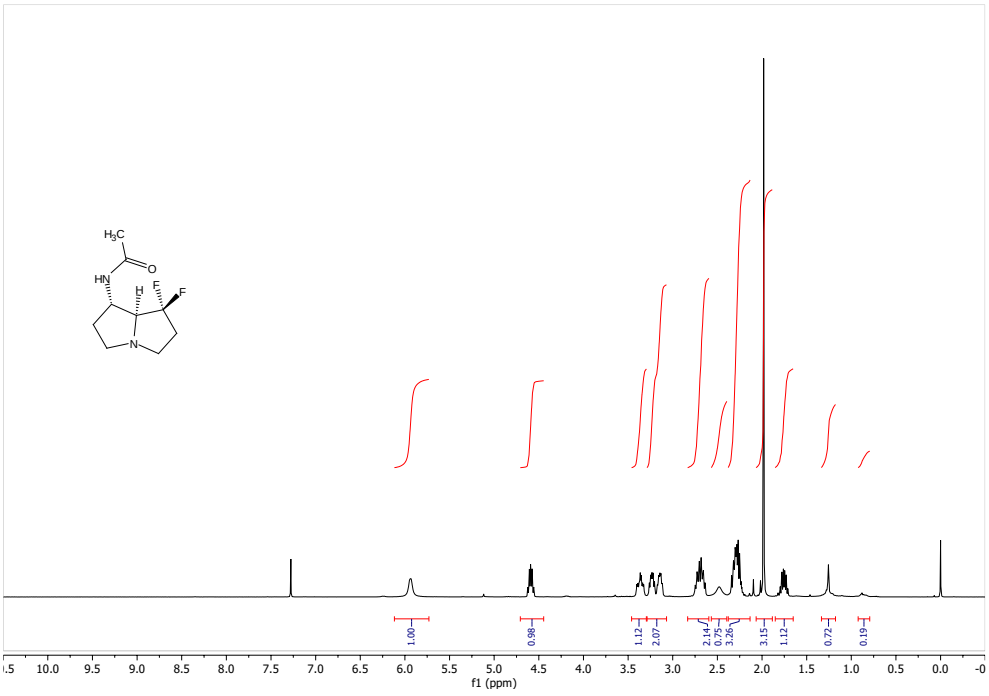

Figure A.10 400 MHz ^{1}H NMR spectra of (±) *exo*-7,7-F_2-AcAP

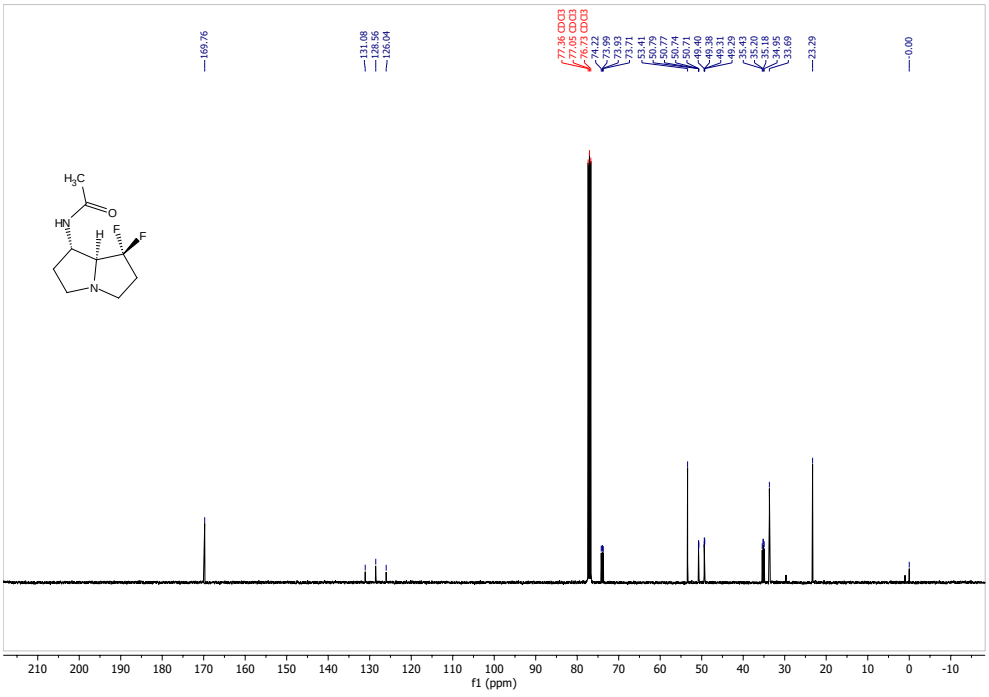

Figure A.11 400 MHz ^{13}C NMR spectra of (±) *exo*-7,7-F_2-AcAP

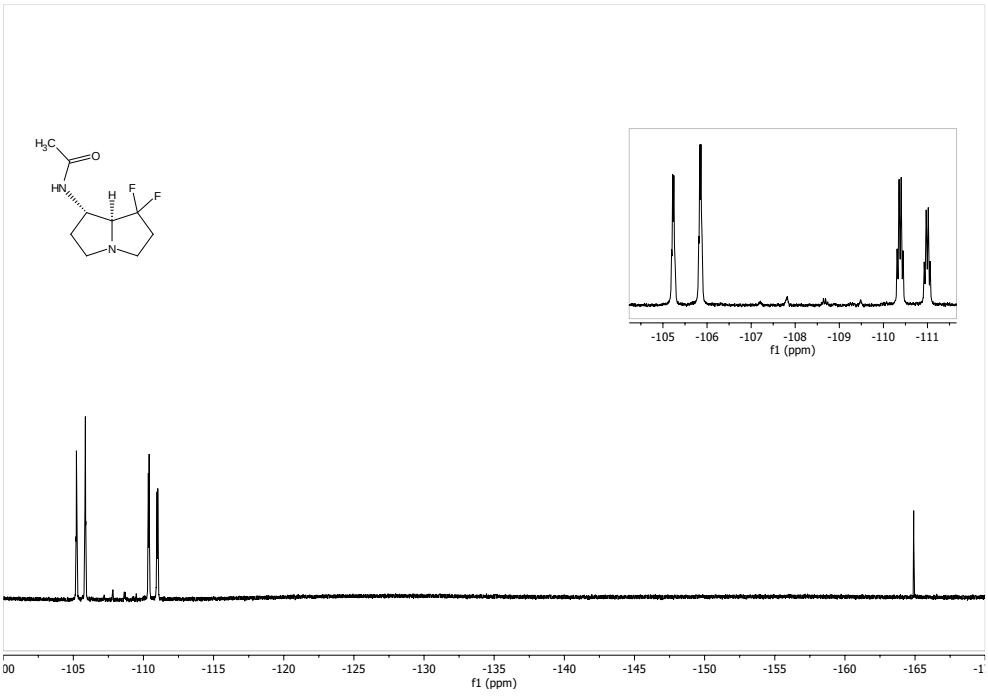

Figure A.12 376 MHz ^{19}F NMR spectra of (±) *exo*-7,7-F_2-AcAP

Table A.1: Crystal data and structure refinement for (±)-*endo*-6,6-F_2-AcAP·BH_3

Empirical formula	C_9 H_{17} B F_2 N_2 O
Formula weight	218.05
Temperature	90.0 (2) K
Wavelength	0.71073 A
Crystal system, space group	Triclinic, P-1
Unit cell dimensions	a = 9.7389(2) A alpha = 74.7529(7) deg.
	b = 10.9170(2) A beta = 78.5454(7) deg.
	c = 11.2419(2) A gamma = 88.9007(7) deg.
Volume	1129.50(4) A^3
Z, Calculated density	4, 1.282 Mg/m^3
Absorption coefficient	0.105 mm^{-1}
F (000)	464
Crystal size	0.250 x 0.240 x 0.100 mm
Theta range for data collection.	2.336 to 27.495 deg.
Limiting indices	-12<=h<=12,
	-14<=k<=14,
	-14<=l<=13

Reflections collected / unique	36263 / 5184 [R(int) = 0.0298]
Completeness to theta = 25.242	99.9 %
Absorption correction	Semi-empirical from equivalents
Max. and min. transmission	0.971 and 0.939
Refinement method	Full-matrix least-squares on F^2
Data / restraints / parameters	5184 / 0 / 284
Goodness-of-fit on F^2	1.046
Final R indices [I>2sigma(I)]	R1 = 0.0363, wR2 = 0.0862
R indices (all data)	R1 = 0.0428, wR2 = 0.0908
Extinction coefficient	0.0131(16)
Largest diff. peak and hole	0.362 and -0.196 $e.A^{-3}$

Table A.2. Atomic coordinates (x 10^4) and equivalent isotropic displacement parameters (A^2 x 10^3) for (±)-*endo*-6,6-F_2-AcAP·BH_3. U(eq) is defined as one third of the trace of the orthogonalized Uij tensor.

	x	y	z	U(eq)
F1A	3227(1)	3312(1)	5886(1)	28(1)
F2A	5358(1)	2779(1)	6032(1)	27(1)
O1A	4503(1)	5911(1)	1233(1)	22(1)

N2A	6576(1)	5080(1)	1513(1)	15(1)
N4A	4922(1)	2037(1)	3480(1)	14(1)
C1A	6031(1)	3780(1)	1802(1)	14(1)
C2A	7162(1)	2811(1)	2139(1)	18(1)
C3A	6472(1)	1821(1)	3336(1)	17(1)
C5A	4195(1)	1782(1)	4823(1)	18(1)
C6A	4444(1)	2978(1)	5217(1)	19(1)
C7A	5012(1)	4012(1)	4028(1)	18(1)
C8A	4835(1)	3450(1)	2956(1)	14(1)
C9A	5761(1)	6068(1)	1223(1)	16(1)
C10A	6444(1)	7372(1)	884(1)	21(1)
B1A	4204(2)	1218(1)	2744(1)	20(1)
F1B	-772(1)	7617(1)	5219(1)	29(1)
F2B	1305(1)	6963(1)	5406(1)	31(1)
O1B	-574(1)	5617(1)	1465(1)	22(1)
N2B	1638(1)	6316(1)	1219(1)	16(1)
N4B	630(1)	9043(1)	2548(1)	18(1)
C1B	1220(1)	7607(1)	1186(1)	16(1)
C2B	2478(1)	8488(1)	1042(1)	20(1)
C3B	1777(1)	9614(1)	1425(1)	21(1)
C5B	1158(1)	8807(1)	3749(1)	23(1)
C6B	531(1)	7525(1)	4527(1)	22(1)
C7B	484(1)	6760(1)	3605(1)	22(1)

C8B	247(1)	7731(1)	2414(1)	16(1)
C9B	684(1)	5388(1)	1379(1)	16(1)
C10B	1212(1)	4069(1)	1484(1)	19(1)
B1B	-700(2)	9967(1)	2555(2)	28(1)

Table A.3. Bond lengths [A] and angles [deg] for (±)-*endo*-6,6-F_2-AcAP·BH_3

F1A-C6A	1.3698(14)
F2A-C6A	1.3752(14)
O1A-C9A	1.2378(14)
N2A-C9A	1.3364(15)
N2A-C1A	1.4562(14)
N2A-H2A	0.859(15)
N4A-C5A	1.4896(14)
N4A-C8A	1.5066(14)
N4A-C3A	1.5074(14)
N4A-B1A	1.6176(16)
C1A-C8A	1.5301(15)
C1A-C2A	1.5452(15)
C1A-H1A	1.0000
C2A-C3A	1.5286(16)

C2A-H2AA	0.9900
C2A-H2AB	0.9900
C3A-H3AA	0.9900
C3A-H3AB	0.9900
C5A-C6A	1.5229(16)
C5A-H5AA	0.9900
C5A-H5AB	0.9900
C6A-C7A	1.5172(16)
C7A-C8A	1.5280(15)
C7A-H7AA	0.9900
C7A-H7AB	0.9900
C8A-H8A	1.0000
C9A-C10A	1.5047(16)
C10A-H10D	0.9800
C10A-H10E	0.9800
C10A-H10F	0.9800
B1A-H1A1	1.133(9)
B1A-H1A2	1.133(9)
B1A-H1A3	1.133(9)
F1B-C6B	1.3676(14)
F2B-C6B	1.3712(14)
O1B-C9B	1.2352(14)
N2B-C9B	1.3407(15)

N2B-C1B	1.4535(15)
N2B-H2B	0.867(15)
N4B-C5B	1.4970(15)
N4B-C3B	1.5107(15)
N4B-C8B	1.5395(14)
N4B-B1B	1.6274(17)
C1B-C2B	1.5287(16)
C1B-C8B	1.5477(15)
C1B-H1B	1.0000
C2B-C3B	1.5133(16)
C2B-H2BA	0.9900
C2B-H2BB	0.9900
C3B-H3BA	0.9900
C3B-H3BB	0.9900
C5B-C6B	1.5076(18)
C5B-H5BA	0.9900
C5B-H5BB	0.9900
C6B-C7B	1.5003(17)
C7B-C8B	1.5282(16)
C7B-H7BA	0.9900
C7B-H7BB	0.9900
C8B-H8B	1.0000
C9B-C10B	1.5028(16)

C10B-H10A	0.9800
C10B-H10B	0.9800
C10B-H10C	0.9800
B1B-H1B1	1.137(10)
B1B-H1B2	1.137(10)
B1B-H1B3	1.137(10)
C9A-N2A-C1A	121.18(10)
C9A-N2A-H2A	119.6(10)
C1A-N2A-H2A	119.2(10)
C5A-N4A-C8A	104.60(8)
C5A-N4A-C3A	112.50(9)
C8A-N4A-C3A	104.12(8)
C5A-N4A-B1A	111.38(9)
C8A-N4A-B1A	113.02(9)
C3A-N4A-B1A	110.89(9)
N2A-C1A-C8A	112.71(9)
N2A-C1A-C2A	111.33(9)
C8A-C1A-C2A	104.56(9)
N2A-C1A-H1A	109.4
C8A-C1A-H1A	109.4
C2A-C1A-H1A	109.4
C3A-C2A-C1A	106.38(9)
C3A-C2A-H2AA	110.5

C1A-C2A-H2AA	110.5
C3A-C2A-H2AB	110.5
C1A-C2A-H2AB	110.5
H2AA-C2A-H2AB	108.6
N4A-C3A-C2A	105.56(9)
N4A-C3A-H3AA	110.6
C2A-C3A-H3AA	110.6
N4A-C3A-H3AB	110.6
C2A-C3A-H3AB	110.6
H3AA-C3A-H3AB	108.8
N4A-C5A-C6A	105.61(9)
N4A-C5A-H5AA	110.6
C6A-C5A-H5AA	110.6
N4A-C5A-H5AB	110.6
C6A-C5A-H5AB	110.6
H5AA-C5A-H5AB	108.7
F1A-C6A-F2A	104.53(9)
F1A-C6A-C7A	112.01(10)
F2A-C6A-C7A	111.0(1)
F1A-C6A-C5A	110.33(10)
F2A-C6A-C5A	111.58(10)
C7A-C6A-C5A	107.45(9)
C6A-C7A-C8A	104.55(9)

C6A-C7A-H7AA	110.8
C8A-C7A-H7AA	110.8
C6A-C7A-H7AB	110.8
C8A-C7A-H7AB	110.8
H7AA-C7A-H7AB	108.9
N4A-C8A-C7A	104.61(9)
N4A-C8A-C1A	104.05(8)
C7A-C8A-C1A	115.02(9)
N4A-C8A-H8A	110.9
C7A-C8A-H8A	110.9
C1A-C8A-H8A	110.9
O1A-C9A-N2A	121.16(11)
O1A-C9A-C10A	121.91(10)
N2A-C9A-C10A	116.93(10)
C9A-C10A-H10D	109.5
C9A-C10A-H10E	109.5
H10D-C10A-H10E	109.5
C9A-C10A-H10F	109.5
H10D-C10A-H10F	109.5
H10E-C10A-H10F	109.5
N4A-B1A-H1A1	109.5
N4A-B1A-H1A2	109.5
H1A1-B1A-H1A2	109.5

N4A-B1A-H1A3	109.5
H1A1-B1A-H1A3	109.5
H1A2-B1A-H1A3	109.5
C9B-N2B-C1B	121.03(10)
C9B-N2B-H2B	120.7(10)
C1B-N2B-H2B	118.1(10)
C5B-N4B-C3B	111.05(9)
C5B-N4B-C8B	106.46(9)
C3B-N4B-C8B	106.06(9)
C5B-N4B-B1B	111.4(1)
C3B-N4B-B1B	109.70(9)
C8B-N4B-B1B	112.02(9)
N2B-C1B-C2B	111.74(9)
N2B-C1B-C8B	113.71(9)
C2B-C1B-C8B	103.69(9)
N2B-C1B-H1B	109.2
C2B-C1B-H1B	109.2
C8B-C1B-H1B	109.2
C3B-C2B-C1B	101.82(9)
C3B-C2B-H2BA	111.4
C1B-C2B-H2BA	111.4
C3B-C2B-H2BB	111.4
C1B-C2B-H2BB	111.4

H2BA-C2B-H2BB	109.3
N4B-C3B-C2B	105.04(9)
N4B-C3B-H3BA	110.7
C2B-C3B-H3BA	110.7
N4B-C3B-H3BB	110.7
C2B-C3B-H3BB	110.7
H3BA-C3B-H3BB	108.8
N4B-C5B-C6B	105.06(9)
N4B-C5B-H5BA	110.7
C6B-C5B-H5BA	110.7
N4B-C5B-H5BB	110.7
C6B-C5B-H5BB	110.7
H5BA-C5B-H5BB	108.8
F1B-C6B-F2B	104.38(9)
F1B-C6B-C7B	111.56(10)
F2B-C6B-C7B	112.04(11)
F1B-C6B-C5B	111.96(11)
F2B-C6B-C5B	111.48(10)
C7B-C6B-C5B	105.58(10)
C6B-C7B-C8B	104.7(1)
C6B-C7B-H7BA	110.8
C8B-C7B-H7BA	110.8
C6B-C7B-H7BB	110.8

C8B-C7B-H7BB	110.8
H7BA-C7B-H7BB	108.9
C7B-C8B-N4B	106.35(9)
C7B-C8B-C1B	114.49(10)
N4B-C8B-C1B	105.10(8)
C7B-C8B-H8B	110.2
N4B-C8B-H8B	110.2
C1B-C8B-H8B	110.2
O1B-C9B-N2B	120.75(11)
O1B-C9B-C10B	122.27(10)
N2B-C9B-C10B	116.95(10)
C9B-C10B-H10A	109.5
C9B-C10B-H10B	109.5
H10A-C10B-H10B	109.5
C9B-C10B-H10C	109.5
H10A-C10B-H10C	109.5
H10B-C10B-H10C	109.5
N4B-B1B-H1B1	109.5
N4B-B1B-H1B2	109.5
H1B1-B1B-H1B2	109.5
N4B-B1B-H1B3	109.5
H1B1-B1B-H1B3	109.5
H1B2-B1B-H1B3	109.5

Symmetry transformations used to generate equivalent atoms:

Table A.4. Anisotropic displacement parameters (A^2 x 10^3) for (±)-*endo*-6,6-F_2-AcAP·BH_3. The anisotropic displacement factor exponent takes the form: $-2\pi^2[h^2 a^{*2}$ U11 + ... + 2 h k a* b* U12]

	U11	U22	U33	U23	U13	U12
F1A	28(1)	27(1)	27(1)	-11(1)	9(1)	-3(1)
F2A	36(1)	27(1)	20(1)	-4(1)	-11(1)	-4(1)
O1A	14(1)	23(1)	27(1)	-2(1)	-7(1)	2(1)
N2A	11(1)	16(1)	17(1)	0(1)	-4(1)	-2(1)
N4A	13(1)	13(1)	15(1)	-2(1)	-3(1)	-1(1)
C1A	13(1)	15(1)	14(1)	-3(1)	-3(1)	-1(1)
C2A	15(1)	18(1)	20(1)	-3(1)	-1(1)	2(1)
C3A	13(1)	18(1)	19(1)	-2(1)	-5(1)	1(1)
C5A	18(1)	17(1)	16(1)	-2(1)	0(1)	-3(1)
C6A	20(1)	21(1)	15(1)	-5(1)	-1(1)	-1(1)
C7A	23(1)	15(1)	16(1)	-5(1)	-1(1)	-4(1)
C8A	13(1)	12(1)	16(1)	-2(1)	-3(1)	0(1)
C9A	15(1)	19(1)	13(1)	-2(1)	-3(1)	0(1)
C10A	20(1)	17(1)	23(1)	0(1)	-4(1)	0(1)
B1A	22(1)	18(1)	24(1)	-8(1)	-9(1)	-3(1)
F1B	22(1)	40(1)	22(1)	-8(1)	2(1)	0(1)
F2B	29(1)	43(1)	23(1)	-5(1)	-12(1)	1(1)
O1B	12(1)	24(1)	31(1)	-8(1)	-6(1)	-1(1)

N2B	11(1)	18(1)	21(1)	-6(1)	-3(1)	1(1)
N4B	16(1)	17(1)	20(1)	-6(1)	-2(1)	-2(1)
C1B	14(1)	18(1)	17(1)	-4(1)	-2(1)	-1(1)
C2B	15(1)	21(1)	22(1)	-6(1)	2(1)	-4(1)
C3B	19(1)	18(1)	22(1)	-4(1)	1(1)	-4(1)
C5B	21(1)	28(1)	21(1)	-10(1)	-5(1)	-3(1)
C6B	18(1)	30(1)	18(1)	-6(1)	-4(1)	1(1)
C7B	28(1)	20(1)	17(1)	-3(1)	-4(1)	-2(1)
C8B	13(1)	16(1)	17(1)	-5(1)	-2(1)	-2(1)
C9B	15(1)	20(1)	13(1)	-4(1)	-4(1)	-1(1)
C10B	20(1)	18(1)	20(1)	-4(1)	-4(1)	1(1)
B1B	22(1)	22(1)	38(1)	-6(1)	-1(1)	6(1)

Table A.5. Hydrogen coordinates (x 10^4) and isotropic displacement parameters (A^2 x 10^3) for (±)-*endo*-6,6-F_2-AcAP·BH_3

	x	y	z	U(eq)
H2A	7446(16)	5212(14)	1503(13)	18
H1A	5694	3649	1058	17
H2AA	7489	2405	1447	22
H2AB	7977	3238	2285	22
H3AA	6679	951	3256	20
H3AB	6817	1936	4073	20
H5AA	4589	1038	5347	21
H5AB	3179	1614	4912	21
H7AA	6011	4219	3975	22
H7AB	4473	4794	4005	22
H8A	3909	3666	2712	17
H10D	7433	7296	947	31
H10E	5968	7850	1463	31
H10F	6377	7820	20	31
H1A1	4186(9)	173(8)	3253(6)	30
H1A2	4831(7)	1377(7)	1749(8)	30
H1A3	3093(9)	1530(7)	2712(8)	30
H2B	2516(16)	6148(14)	1192(14)	20
H1B	737	7937	465	19
H2BA	3116	8087	1606	24

H2BB	3009	8737	163	24
H3BA	2455	10131	1655	25
H3BB	1379	10158	731	25
H5BA	850	9472	4186	27
H5BB	2195	8798	3582	27
H7BA	-293	6113	3928	27
H7BB	1377	6328	3438	27
H8B	-757	7693	2341	19
H10A	851	3698	898	29
H10B	892	3543	2346	29
H10C	2239	4106	1277	29
H1B1	-1533(9)	9566(6)	3434(9)	42
H1B2	-1157(8)	10027(8)	1687(9)	42
H1B3	-341(4)	10954(9)	2549(10)	42

Table A.6. Torsion angles [deg] for (±)-*endo*-6,6-F_2-AcAP·BH_3

C9A-N2A-C1A-C8A	-61.40(13)
C9A-N2A-C1A-C2A	-178.53(10)
N2A-C1A-C2A-C3A	132.72(10)
C8A-C1A-C2A-C3A	10.74(12)
C5A-N4A-C3A-C2A	-145.73(9)
C8A-N4A-C3A-C2A	-33.06(11)

B1A-N4A-C3A-C2A	88.78(11)
C1A-C2A-C3A-N4A	13.52(12)
C8A-N4A-C5A-C6A	-30.88(11)
C3A-N4A-C5A-C6A	81.50(11)
B1A-N4A-C5A-C6A	-153.29(9)
N4A-C5A-C6A-F1A	135.41(10)
N4A-C5A-C6A-F2A	-108.86(10)
N4A-C5A-C6A-C7A	13.03(12)
F1A-C6A-C7A-C8A	-111.7(1)
F2A-C6A-C7A-C8A	131.87(10)
C5A-C6A-C7A-C8A	9.63(12)
C5A-N4A-C8A-C7A	37.13(11)
C3A-N4A-C8A-C7A	-81.12(10)
B1A-N4A-C8A-C7A	158.46(9)
C5A-N4A-C8A-C1A	158.18(9)
C3A-N4A-C8A-C1A	39.93(10)
B1A-N4A-C8A-C1A	-80.49(10)
C6A-C7A-C8A-N4A	-28.51(11)
C6A-C7A-C8A-C1A	-142.0(1)
N2A-C1A-C8A-N4A	-152.09(9)
C2A-C1A-C8A-N4A	-31.02(11)
N2A-C1A-C8A-C7A	-38.27(13)
C2A-C1A-C8A-C7A	82.79(11)

C1A-N2A-C9A-O1A	2.52(17)
C1A-N2A-C9A-C10A	-177.32(10)
C9B-N2B-C1B-C2B	177.95(10)
C9B-N2B-C1B-C8B	60.98(14)
N2B-C1B-C2B-C3B	-163.54(9)
C8B-C1B-C2B-C3B	-40.67(11)
C5B-N4B-C3B-C2B	89.60(11)
C8B-N4B-C3B-C2B	-25.66(12)
B1B-N4B-C3B-C2B	-146.83(10)
C1B-C2B-C3B-N4B	41.26(12)
C3B-N4B-C5B-C6B	-138.13(10)
C8B-N4B-C5B-C6B	-23.11(12)
B1B-N4B-C5B-C6B	99.27(11)
N4B-C5B-C6B-F1B	-86.90(11)
N4B-C5B-C6B-F2B	156.58(10)
N4B-C5B-C6B-C7B	34.69(12)
F1B-C6B-C7B-C8B	89.69(12)
F2B-C6B-C7B-C8B	-153.68(10)
C5B-C6B-C7B-C8B	-32.15(13)
C6B-C7B-C8B-N4B	17.55(12)
C6B-C7B-C8B-C1B	133.15(10)
C5B-N4B-C8B-C7B	3.47(12)
C3B-N4B-C8B-C7B	121.82(10)

B1B-N4B-C8B-C7B	-118.52(11)
C5B-N4B-C8B-C1B	-118.31(10)
C3B-N4B-C8B-C1B	0.04(11)
B1B-N4B-C8B-C1B	119.7(1)
N2B-C1B-C8B-C7B	30.40(14)
C2B-C1B-C8B-C7B	-91.16(11)
N2B-C1B-C8B-N4B	146.73(9)
C2B-C1B-C8B-N4B	25.16(11)
C1B-N2B-C9B-O1B	2.18(16)
C1B-N2B-C9B-C10B	-176.08(10)

Symmetry transformations used to generate equivalent atoms:

Table A.7. Hydrogen bonds for (±)-*endo*-6,6-F_2-AcAP·BH_3 [A and deg.]

D-H... A	d(D-H)	d(H...A)	d(D...A)	<(DHA)
N2B-H2B... O1A	0.867(15)	1.955(16)	2.8188(13)	173.7(14)
N2A-H2A... O1B#1	0.859(15)	1.976(15)	2.8345(13)	176.8(14)

Symmetry transformations used to generate equivalent atoms: #1 x+1, y, z

Table B.1. Crystal data and structure refinement for (±)-*exo*-6,6-F_2-AcAP

Empirical formula	$C_9 H_{14} F_2 N_2 O$
Formula weight	204.22
Temperature	90.0(2) K
Wavelength	1.54178 A
Crystal system, space group	Orthorhombic, Pbca
Unit cell dimensions	a = 9.6610(2) A alpha = 90 deg.
	b = 9.5809(2) A beta = 90 deg.
	c = 20.6859(5) A gamma = 90 deg.
Volume	1914.71(7) A^3
Z, Calculated density	8, 1.417 Mg/m^3
Absorption coefficient	1.030 mm^{-1}
F (000)	864
Crystal size	0.260 x 0.020 x 0.010 mm
Theta range for data collection	4.274 to 74.356 deg.
Limiting indices	-12<=h<=11, -11<=k<=11, -23<=l<=25
Reflections collected / unique	13158 / 1937 [R(int) = 0.0525]
Completeness to theta = 67.679	99.8 %
Absorption correction	Semi-empirical from equivalents
Max. and min. transmission	0.971 and 0.844
Refinement method	Full-matrix least-squares on F^2
Data / restraints / parameters	1937 / 0 / 131
Goodness-of-fit on F^2	1.062

Final R indices [I>2sigma(I)]	R1 = 0.0456, wR2 = 0.1022
R indices (all data)	R1 = 0.0712, wR2 = 0.1159
Extinction coefficient	n/a
Largest diff. peak and hole	0.270 and -0.275 e.A^{-3}

Table B.2. Atomic coordinates (x 10^4) and equivalent isotropic displacement parameters (A^2 x 10^3) for (±)-*exo*-6,6-F_2-AcAP. U(eq) is defined as one third of the trace of the orthogonalized Uij tensor.

	x	y	z	U(eq)
F1	1124(1)	6152(1)	2424(1)	37(1)
F2	766(1)	4187(1)	2918(1)	32(1)
O1	2786(2)	8405(1)	5645(1)	28(1)
N1	2456(2)	6245(2)	5240(1)	20(1)
N4	3040(2)	4888(2)	3772(1)	23(1)
C1	2509(2)	6713(2)	4568(1)	20(1)
C2	3998(2)	6852(2)	4320(1)	26(1)
C3	4317(2)	5383(2)	4083(1)	26(1)
C5	2949(2)	5257(2)	3082(1)	28(1)
C6	1421(2)	5456(2)	2986(1)	25(1)
C7	936(2)	6204(2)	3582(1)	26(1)
C8	1862(2)	5607(2)	4114(1)	22(1)

C9	2586(2)	7143(2)	5729(1)	21(1)
C10	2465(2)	6549(2)	6402(1)	23(1)

Table B.3. Bond lengths [A] and angles [deg] for (±)-*exo*-6,6-F_2-AcAP

F1-C6	1.372(2)
F2-C6	1.377(2)
O1-C9	1.237(2)
N1-C9	1.333(3)
N1-C1	1.462(2)
N1-H1	0.81(2)
N4-C3	1.471(3)
N4-C5	1.471(3)
N4-C8	1.507(2)
C1-C2	1.533(3)
C1-C8	1.547(3)
C1-H1A	1.0000
C2-C3	1.522(3)
C2-H2A	0.9900
C2-H2B	0.9900
C3-H3A	0.9900
C3-H3B	0.9900
C5-C6	1.501(3)

C5-H5A	0.9900
C5-H5B	0.9900
C6-C7	1.499(3)
C7-C8	1.530(3)
C7-H7A	0.9900
C7-H7B	0.9900
C8-H8	1.0000
C9-C10	1.509(3)
C10-H10A	0.9800
C10-H10B	0.9800
C10-H10C	0.9800
C9-N1-C1	121.31(17)
C9-N1-H1	116.6(16)
C1-N1-H1	122.1(16)
C3-N4-C5	113.41(17)
C3-N4-C8	106.26(15)
C5-N4-C8	107.54(15)
N1-C1-C2	112.22(16)
N1-C1-C8	110.68(16)
C2-C1-C8	103.63(16)
N1-C1-H1A	110.0
C2-C1-H1A	110.0
C8-C1-H1A	110.0

C3-C2-C1	102.55(16)
C3-C2-H2A	111.3
C1-C2-H2A	111.3
C3-C2-H2B	111.3
C1-C2-H2B	111.3
H2A-C2-H2B	109.2
N4-C3-C2	105.59(16)
N4-C3-H3A	110.6
C2-C3-H3A	110.6
N4-C3-H3B	110.6
C2-C3-H3B	110.6
H3A-C3-H3B	108.8
N4-C5-C6	102.55(16)
N4-C5-H5A	111.3
C6-C5-H5A	111.3
N4-C5-H5B	111.3
C6-C5-H5B	111.3
H5A-C5-H5B	109.2
F1-C6-F2	104.25(16)
F1-C6-C7	113.51(18)
F2-C6-C7	111.22(17)
F1-C6-C5	112.32(17)
F2-C6-C5	110.66(17)

C7-C6-C5	105.03(17)
C6-C7-C8	103.33(17)
C6-C7-H7A	111.1
C8-C7-H7A	111.1
C6-C7-H7B	111.1
C8-C7-H7B	111.1
H7A-C7-H7B	109.1
N4-C8-C7	105.82(16)
N4-C8-C1	107.06(16)
C7-C8-C1	114.71(17)
N4-C8-H8	109.7
C7-C8-H8	109.7
C1-C8-H8	109.7
O1-C9-N1	122.63(19)
O1-C9-C10	120.71(18)
N1-C9-C10	116.67(18)
C9-C10-H10A	109.5
C9-C10-H10B	109.5
H10A-C10-H10B	109.5
C9-C10-H10C	109.5
H10A-C10-H10C	109.5
H10B-C10-H10C	109.5

Symmetry transformations used to generate equivalent atoms:

Table 4. Anisotropic displacement parameters (A^2 x 10^3) for (±)-*exo*-6,6-F_2-AcAP. The anisotropic displacement factor exponent takes the form: -2 π^2[h^2 a^{*2} U11 + ... + 2 h k a* b* U12]

	U11	U22	U33	U23	U13	U12
F1	38(1)	47(1)	24(1)	12(1)	-7(1)	-5(1)
F2	36(1)	31(1)	27(1)	-3(1)	-1(1)	-8(1)
O1	42(1)	17(1)	25(1)	1(1)	-3(1)	0(1)
N1	27(1)	15(1)	18(1)	2(1)	3(1)	0(1)
N4	24(1)	25(1)	21(1)	0(1)	1(1)	3(1)
C1	24(1)	18(1)	17(1)	2(1)	0(1)	0(1)
C2	26(1)	29(1)	22(1)	2(1)	0(1)	-3(1)
C3	23(1)	31(1)	24(1)	1(1)	-2(1)	2(1)
C5	32(1)	34(1)	19(1)	-1(1)	2(1)	-1(1)
C6	31(1)	28(1)	18(1)	4(1)	-1(1)	-4(1)
C7	24(1)	28(1)	26(1)	1(1)	-4(1)	2(1)
C8	24(1)	23(1)	20(1)	4(1)	1(1)	0(1)
C9	20(1)	21(1)	23(1)	0(1)	1(1)	2(1)
C10	29(1)	22(1)	18(1)	-1(1)	0(1)	0(1)

Table 5. Hydrogen coordinates (x 10^4) and isotropic displacement parameters (A^2 x 10^3) for (±)-*exo*-6,6-F_2-AcAP.

	x	y	z	U(eq)
H1	2350(20)	5430(20)	5336(11)	24
H1A	2011	7622	4521	24
H2A	4058	7539	3964	31
H2B	4636	7134	4671	31
H3A	5092	5396	3770	31
H3B	4571	4770	4450	31
H5A	3309	4496	2806	34
H5B	3465	6126	2988	34
H7A	-52	6005	3669	31
H7B	1064	7225	3539	31
H8	1330	4911	4375	27
H10A	2420	5528	6378	34
H10B	1622	6906	6607	34
H10C	3273	6827	6658	34

Table 6. Torsion angles [deg] for (±)-*exo*-6,6-F_2-AcAP.

C9-N1-C1-C2	83.6(2)
C9-N1-C1-C8	-161.12(17)
N1-C1-C2-C3	86.7(2)
C8-C1-C2-C3	-32.8(2)
C5-N4-C3-C2	88.1(2)
C8-N4-C3-C2	-29.8(2)
C1-C2-C3-N4	39.3(2)
C3-N4-C5-C6	-147.52(17)
C8-N4-C5-C6	-30.3(2)
N4-C5-C6-F1	164.16(16)
N4-C5-C6-F2	-79.79(19)
N4-C5-C6-C7	40.3(2)
F1-C6-C7-C8	-157.28(17)
F2-C6-C7-C8	85.53(19)
C5-C6-C7-C8	-34.2(2)
C3-N4-C8-C7	131.31(17)
C5-N4-C8-C7	9.6(2)
C3-N4-C8-C1	8.5(2)
C5-N4-C8-C1	-113.23(17)
C6-C7-C8-N4	15.2(2)
C6-C7-C8-C1	132.97(18)
N1-C1-C8-N4	-104.93(18)

C2-C1-C8-N4	15.6(2)
N1-C1-C8-C7	138.00(17)
C2-C1-C8-C7	-101.50(19)
C1-N1-C9-O1	-1.5(3)
C1-N1-C9-C10	177.92(17)

Symmetry transformations used to generate equivalent atoms:

Table 7. Hydrogen bonds for (±)-*exo*-6,6-F_2-AcAP [A and deg.]

D-H... A	d(D-H)	d(H...A)	d(D...A)	<(DHA)
N1-H1...O1#1	0.81(2)	2.04(2)	2.856(2)	174(2)
C1-H1A... N4#2	1.00	2.67	3.501(3)	140.7
C7-H7A... O1#3	0.99	2.59	3.459(3)	146.8
C10-H10A... O1#1	0.98	2.55	3.404(2)	146.2
C10-H10B... F1#4	0.98	2.56	3.316(2)	134.1

Symmetry transformations used to generate equivalent atoms: #1 -x+1/2, y-1/2, z #2 -x+1/2, y+1/2, z #3 x-1/2, -y+3/2, -z+1 #4 x, -y+3/2, z+1/2

Table C.1. Crystal data and structure refinement for benzyl *N*-[(1*S*,7a*R*)-7-methylidenepyrrolizidin-1-yl]carbamate.

Empirical formula	$C_{16}H_{20}N_2O_2$
Formula weight	272.34
Temperature	90.0(2) K
Wavelength	0.71073 A
Crystal system, space group	Monoclinic, C2/c
Unit cell dimensions	a = 22.0183(5) A alpha = 90 deg.
	b = 7.3526(2) A beta = 95.590(1) deg.
	c = 17.4828(4) A gamma = 90 deg.
Volume	2816.86(12) A^3
Z, Calculated density	8, 1.284 Mg/m^3
Absorption coefficient	0.085 mm^{-1}
F (000)	1168
Crystal size	0.240 x 0.220 x 0.200 mm
Theta range for data collection	2.844 to 33.201 deg.
Limiting indices	-33<=h<=33, -11<=k<=11, -26<=l<=26
Reflections collected / unique	26635 / 5362 [R(int) = 0.0365]
Completeness to theta = 25.242	99.5 %
Absorption correction	Semi-empirical from equivalents
Max. and min. transmission	0.971 and 0.788
Refinement method	Full-matrix least-squares on F^2
Data / restraints / parameters	5362 / 0 / 185

Goodness-of-fit on F^2	1.017
Final R indices [I>2sigma(I)]	R1 = 0.0377, wR2 = 0.0889
R indices (all data)	R1 = 0.0502, wR2 = 0.0962
Extinction coefficient	n/a
Largest diff. peak and hole	0.344 and -0.204 $e.A^{-3}$

Table C.2. Atomic coordinates (x 10^4) and equivalent isotropic displacement parameters (A^2 x 10^3) for benzyl *N*-[(1*S*,7a*R*)-7-methylidenepyrrolizidin-1-yl]carbamate. U(eq) is defined as one third of the trace of the orthogonalized Uij tensor.

	x	y	z	U(eq)
O1	6348(1)	1359(1)	5221(1)	20(1)
O2	6684(1)	2843(1)	4201(1)	24(1)
N1	5730(1)	3322(1)	4576(1)	20(1)
N4	4991(1)	7389(1)	4136(1)	18(1)
C1	5535(1)	4582(1)	3962(1)	18(1)
C2	4844(1)	4386(1)	3712(1)	21(1)
C3	4634(1)	6323(1)	3534(1)	20(1)
C5	5058(1)	9323(1)	3930(1)	22(1)
C6	5582(1)	9408(1)	3409(1)	21(1)
C7	5969(1)	7767(1)	3655(1)	19(1)
C8	5615(1)	6615(1)	4183(1)	17(1)
C9	6522(1)	7371(1)	3467(1)	24(1)
C10	6288(1)	2561(1)	4627(1)	18(1)

C11	6921(1)	376(1)	5299(1)	22(1)
C12	6880(1)	-1066(1)	5899(1)	19(1)
C13	6906(1)	-2896(1)	5702(1)	22(1)
C14	6894(1)	-4240(1)	6258(1)	28(1)
C15	6846(1)	-3760(1)	7018(1)	30(1)
C16	6817(1)	-1939(2)	7221(1)	29(1)
C17	6838(1)	-599(1)	6665(1)	25(1)

Table 3. Bond lengths [A] and angles [deg] for benzyl *N*-[(1*S*,7a*R*)-7-methylidenepyrrolizidin-1-yl]carbamate

O1-C10	1.360(1)
O1-C11	1.4496(10)
O2-C10	1.2197(10)
N1-C10	1.3442(10)
N1-C1	1.4508(10)
N1-H1N	0.892(13)
N4-C3	1.4760(11)
N4-C5	1.4774(11)
N4-C8	1.481(1)
C1-C2	1.5483(11)
C1-C8	1.5497(11)
C1-H1	1.0000
C2-C3	1.5195(12)

C2-H2A	0.9900
C2-H2B	0.9900
C3-H3A	0.9900
C3-H3B	0.9900
C5-C6	1.5401(12)
C5-H5A	0.9900
C5-H5B	0.9900
C6-C7	1.5136(12)
C6-H6A	0.9900
C6-H6B	0.9900
C7-C9	1.3253(12)
C7-C8	1.5223(11)
C8-H8	1.0000
C9-H9A	0.9500
C9-H9B	0.9500
C11-C12	1.4998(12)
C11-H11A	0.9900
C11-H11B	0.9900
C12-C13	1.3918(12)
C12-C17	1.3949(12)
C13-C14	1.3880(13)
C13-H13	0.9500
C14-C15	1.3899(15)

C14-H14	0.9500
C15-C16	1.3879(15)
C15-H15	0.9500
C16-C17	1.3878(13)
C16-H16	0.9500
C17-H17	0.9500
C10-O1-C11	114.49(6)
C10-N1-C1	121.17(7)
C10-N1-H1N	119.6(8)
C1-N1-H1N	119.1(8)
C3-N4-C5	113.31(7)
C3-N4-C8	105.17(6)
C5-N4-C8	105.70(6)
N1-C1-C2	111.22(7)
N1-C1-C8	114.39(7)
C2-C1-C8	104.11(6)
N1-C1-H1	109.0
C2-C1-H1	109.0
C8-C1-H1	109.0
C3-C2-C1	103.99(6)
C3-C2-H2A	111.0
C1-C2-H2A	111.0
C3-C2-H2B	111.0

C1-C2-H2B	111.0
H2A-C2-H2B	109.0
N4-C3-C2	102.82(6)
N4-C3-H3A	111.2
C2-C3-H3A	111.2
N4-C3-H3B	111.2
C2-C3-H3B	111.2
H3A-C3-H3B	109.1
N4-C5-C6	106.31(7)
N4-C5-H5A	110.5
C6-C5-H5A	110.5
N4-C5-H5B	110.5
C6-C5-H5B	110.5
H5A-C5-H5B	108.7
C7-C6-C5	103.48(6)
C7-C6-H6A	111.1
C5-C6-H6A	111.1
C7-C6-H6B	111.1
C5-C6-H6B	111.1
H6A-C6-H6B	109.0
C9-C7-C6	127.53(8)
C9-C7-C8	124.45(8)
C6-C7-C8	108.01(7)

N4-C8-C7	106.17(6)
N4-C8-C1	105.99(6)
C7-C8-C1	115.94(7)
N4-C8-H8	109.5
C7-C8-H8	109.5
C1-C8-H8	109.5
C7-C9-H9A	120.0
C7-C9-H9B	120.0
H9A-C9-H9B	120.0
O2-C10-N1	126.31(8)
O2-C10-O1	123.75(7)
N1-C10-O1	109.92(7)
O1-C11-C12	107.88(6)
O1-C11-H11A	110.1
C12-C11-H11A	110.1
O1-C11-H11B	110.1
C12-C11-H11B	110.1
H11A-C11-H11B	108.4
C13-C12-C17	118.96(8)
C13-C12-C11	120.24(8)
C17-C12-C11	120.75(8)
C14-C13-C12	120.71(8)
C14-C13-H13	119.6

C12-C13-H13	119.6
C13-C14-C15	119.83(9)
C13-C14-H14	120.1
C15-C14-H14	120.1
C16-C15-C14	119.96(9)
C16-C15-H15	120.0
C14-C15-H15	120.0
C17-C16-C15	120.02(9)
C17-C16-H16	120.0
C15-C16-H16	120.0
C16-C17-C12	120.51(9)
C16-C17-H17	119.7
C12-C17-H17	119.7

Symmetry transformations used to generate equivalent atoms:

Table 4. Anisotropic displacement parameters (A^2 x 10^3) for benzyl *N*-[(1*S*,7a*R*)-7-methylidenepyrrolizidin-1-yl]carbamate. The anisotropic displacement factor exponent takes the form: $-2\pi^2[h^2 a^{*2} U11 + ... + 2 h k a^* b^* U12]$

			U11	U22	U33	U23	U13	U12
O1	18(1)	20(1)	22(1)	6(1)	5(1)	4(1)		
O2	19(1)	29(1)	23(1)	6(1)	6(1)	0(1)		
N1	21(1)	19(1)	21(1)	6(1)	7(1)	4(1)		
N4	18(1)	16(1)	20(1)	2(1)	4(1)	-1(1)		
C1	20(1)	16(1)	18(1)	2(1)	3(1)	0(1)		
C2	21(1)	18(1)	23(1)	2(1)	1(1)	-3(1)		
C3	19(1)	20(1)	22(1)	4(1)	0(1)	-1(1)		
C5	27(1)	16(1)	25(1)	2(1)	9(1)	1(1)		
C6	26(1)	17(1)	20(1)	2(1)	5(1)	-3(1)		
C7	21(1)	19(1)	16(1)	0(1)	2(1)	-4(1)		
C8	17(1)	18(1)	16(1)	2(1)	3(1)	-1(1)		
C9	22(1)	28(1)	23(1)	2(1)	6(1)	-3(1)		
C10	19(1)	17(1)	18(1)	1(1)	3(1)	0(1)		
C11	16(1)	25(1)	24(1)	6(1)	4(1)	5(1)		
C12	15(1)	22(1)	20(1)	3(1)	2(1)	2(1)		
C13	19(1)	24(1)	24(1)	-2(1)	1(1)	0(1)		
C14	25(1)	20(1)	39(1)	3(1)	2(1)	-2(1)		
C15	25(1)	31(1)	34(1)	14(1)	3(1)	0(1)		

C16	32(1)	36(1)	20(1)	5(1)	5(1)	4(1)
C17	30(1)	24(1)	21(1)	0(1)	4(1)	4(1)

Table 5. Hydrogen coordinates (x 10^4) and isotropic displacement parameters (A^2 x 10^3) for benzyl *N*-[(1*S*,7a*R*)-7-methylidenepyrrolizidin-1-yl]carbamate.

	x	y	z	U(eq)
H1N	5482(6)	3094(18)	4938(7)	33(3)
H1	5768	4324	3511	21
H2A	4773	3603	3251	25
H2B	4628	3862	4131	25
H3A	4729	6697	3015	24
H3B	4191	6456	3570	24
H5A	5155	10068	4397	27
H5B	4675	9785	3653	27
H6A	5426	9325	2860	25
H6B	5819	10547	3494	25
H8	5809	6715	4723	20
H9A	6720	8164	3141	29
H9B	6721	6293	3658	29
H11A	7262	1217	5456	26
H11B	6996	-187	4803	26
H13	6933	-3230	5181	27
H14	6919	-5485	6119	34

H15	6832	-4677	7399	36
H16	6783	-1610	7741	35
H17	6823	646	6808	30

Table 6. Torsion angles [deg] for benzyl *N*-[(1*S*,7a*R*)-7-methylidenepyrrolizidin-1-yl]carbamate.

C10-N1-C1-C2	145.68(8)
C10-N1-C1-C8	-96.73(9)
N1-C1-C2-C3	143.19(7)
C8-C1-C2-C3	19.53(8)
C5-N4-C3-C2	157.69(7)
C8-N4-C3-C2	42.73(8)
C1-C2-C3-N4	-38.12(8)
C3-N4-C5-C6	-81.34(8)
C8-N4-C5-C6	33.30(8)
N4-C5-C6-C7	-26.47(9)
C5-C6-C7-C9	-168.96(9)
C5-C6-C7-C8	10.02(8)
C3-N4-C8-C7	93.64(7)
C5-N4-C8-C7	-26.50(8)
C3-N4-C8-C1	-30.21(7)
C5-N4-C8-C1	-150.34(6)
C9-C7-C8-N4	-171.26(8)

C6-C7-C8-N4	9.73(8)
C9-C7-C8-C1	-53.86(11)
C6-C7-C8-C1	127.12(7)
N1-C1-C8-N4	-115.66(7)
C2-C1-C8-N4	5.92(8)
N1-C1-C8-C7	126.85(7)
C2-C1-C8-C7	-111.57(7)
C1-N1-C10-O2	1.76(13)
C1-N1-C10-O1	-176.47(7)
C11-O1-C10-O2	-1.80(12)
C11-O1-C10-N1	176.48(7)
C10-O1-C11-C12	-171.99(7)
O1-C11-C12-C13	116.10(8)
O1-C11-C12-C17	-66.39(10)
C17-C12-C13-C14	-0.26(13)
C11-C12-C13-C14	177.29(8)
C12-C13-C14-C15	0.96(13)
C13-C14-C15-C16	-0.80(14)
C14-C15-C16-C17	-0.05(15)
C15-C16-C17-C12	0.75(15)
C13-C12-C17-C16	-0.60(13)
C11-C12-C17-C16	-178.13(8)

Symmetry transformations used to generate equivalent atoms:

Table 7. Hydrogen bonds for benzyl *N*-[(1*S*,7a*R*)-7-methylidenepyrrolizidin-1-yl]carbamate benzyl *N*-[(1*S*,7a*R*)-7-methylidenepyrrolizidin-1-yl]carbamate. [A and deg.].

D-H... A	d(D-H)	d(H...A)	d(D...A)	<(DHA)
N1-H1N... N4#1	0.892(13)	2.040(13)	2.9269(10)	172.7(12)
C11-H11A... O2#2	0.99	2.44	3.3741(11)	157.2

Symmetry transformations used to generate equivalent atoms: #1 -x+1, -y+1, -z+1 #2 -x+3/2, -y+1/2, -z+1

REFERENCES

1. Pan, J.; Bhardwaj, M.; Nagabhyru, P.; Grossman, R. B.; Schardl, C. L., Enzymes from fungal and plant origin required for chemical diversification of insecticidal loline alkaloids in grass-*Epichlo*ë symbiota. *PLoS One* **2014,** *9* (12), e115590.
2. Yunusov, S. Y.; Akramov, S., Investigation of the alkaloids of the seeds of *Lolium cuneatum* (Nevski). *Russ. J. Gen. Chem* **1955,** *25*, 1765-1771.
3. Dannhardt, G.; Steindl, L., Alkaloids of *Lolium temulentum*: Isolation, Identification and Pharmacological Activity1. *J Planta medica* **1985,** *51* (03), 212-214.
4. Yunusov, S. Y.; Akramov, S., Investigation of alkaloids of *Lolium cuneatum* II. *Zhurnal Obshchei Khimii* **1960,** *30*, 677-682.
5. Aasen, A.; Culvenor, C., Abnormally low vicinal coupling constants for O-CH-CH in a highly strained five-membered-ring ether; the identity of loline and festucine. *Australian Journal of Chemistry* **1969,** *22* (9), 2021-2024.
6. Bates, R.; Morehead, S., Absolute configurations of pyrrolizidine alkaloids of the loline group. *Tetrahedron letters* **1972**.
7. Faulkner, J. R., *Intermediate steps of loline alkaloid biosynthesis*. University of Kentucky: 2011.
8. Abdullaev, N.; Batirov, É. K.; Malikov, V.; Shakhidoyatov, K. M.; Kadyrov, C. S.; Yunusov, S. Y., Synthesis of some bisquaternary salts of the alkaloids loline and lolinine. *Chemistry of Natural Compounds* **1977,** *13* (3), 313-315.
9. Blankenship, J. D.; Spiering, M. J.; Wilkinson, H. H.; Fannin, F. F.; Bush, L. P.; Schardl, C. L., Production of loline alkaloids by the grass endophyte, Neotyphodium uncinatum, in defined media. *Phytochemistry* **2001,** *58* (3), 395-401.
10. Pan, J.; Bhardwaj, M.; Zhang, B.; Chang, W.-c.; Schardl, C. L.; Krebs, C.; Grossman, R. B.; Bollinger, J. M., Installation of the Ether Bridge of Lolines by the Iron- and 2-Oxoglutarate-Dependent Oxygenase, LolO: Regio- and Stereochemistry of Sequential Hydroxylation and Oxacyclization Reactions. *Biochemistry* **2018,** *57* (14), 2074-2083.
11. Riedell, W.; Kieckhefer, R.; Petroski, R.; Powell, R., Naturally-occurring and synthetic loline alkaloid derivatives: insect feeding behavior modification and toxicity. *Journal of Entomological Science* **1991,** *26* (1), 122-129.
12. Petroski, R. J.; Stanley, D. W., Natural compounds for pest and weed control. *Journal of agricultural food chemistry* **2009,** *57* (18), 8171-8179.
13. Bush, L. P.; Fannin, F. F.; Siegel, M. R.; Dahlman, D. L.; Burton, H. R., Chemistry, occurrence and biological effects of saturated pyrrolizidine alkaloids associated with endophyte-grass interactions. *Agriculture, Ecosystems & Environment* **1993,** *44* (1), 81-102.
14. Šebela, M.; Radová, A.; Angelini, R.; Tavladoraki, P.; Frébort, I.; Peč, P., FAD-containing polyamine oxidases: a timely challenge for researchers in biochemistry and physiology of plants. *Plant Science* **2001,** *160* (2), 197-207.
15. Schardl, C. L.; Grossman, R. B.; Nagabhyru, P.; Faulkner, J. R.; Mallik, U. P., Loline alkaloids: Currencies of mutualism. *Phytochemistry* **2007,** *68* (7), 980-996.
16. Pan, J.; Bhardwaj, M.; Faulkner, J. R.; Nagabhyru, P.; Charlton, N. D.; Higashi, R. M.; Miller, A.-F.; Young, C. A.; Grossman, R. B.; Schardl, C. L., Ether bridge formation in loline alkaloid biosynthesis. *Phytochemistry* **2014,** *98*, 60-68.

17. Blankenship, J. D.; Houseknecht, J. B.; Pal, S.; Bush, L. P.; Grossman, R. B.; Schardl, C. L., Biosynthetic precursors of fungal pyrrolizidines, the loline alkaloids. *ChemBioChem* **2005,** *6* (6), 1016-1022.
18. Faulkner, J. R.; Hussaini, S. R.; Blankenship, J. D.; Pal, S.; Branan, B. M.; Grossman, R. B.; Schardl, C. L., On the sequence of bond formation in loline alkaloid biosynthesis. *Chembiochem* **2006,** *7* (7), 1078-1088.
19. Spiering, M. J.; Faulkner, J. R.; Zhang, D.-X.; Machado, C.; Grossman, R. B.; Schardl, C. L., Role of the LolP cytochrome P450 monooxygenase in loline alkaloid biosynthesis. *Fungal Genetics Biology* **2008,** *45* (9), 1307-1314.
20. Martinez, S.; Hausinger, R. P., Catalytic mechanisms of Fe (II)-and 2-oxoglutarate-dependent oxygenases. *Journal of Biological Chemistry* **2015,** *290* (34), 20702-20711.
21. Müller, M.; He, J.; Hertweck, C., Dissection of the late steps in aureothin biosynthesis. *ChemBioChem* **2006,** *7* (1), 37-39.
22. Richter, M. E.; Traitcheva, N.; Knüpfer, U.; Hertweck, C., Sequential asymmetric polyketide heterocyclization catalyzed by a single cytochrome P450 monooxygenase (AurH). *Angewandte Chemie* **2008,** *120* (46), 9004-9007.
23. Borowski, T.; de Marothy, S.; Broclawik, E.; Schofield, C. J.; Siegbahn, P. E., Mechanism for cyclization reaction by clavaminic acid synthase. Insights from modeling studies. *Biochemistry* **2007,** *46* (12), 3682-3691.
24. Wang, X.; Chen, M.; Yang, C.; Liu, X.; Zhang, L.; Lan, X.; Tang, K.; Liao, Z., Enhancing the scopolamine production in transgenic plants of *Atropa belladonna* by overexpressing pmt and h6h genes. *Physiologia plantarum* **2011,** *143* (4), 309-315.
25. Baggaley, K. H.; Brown, A. G.; Schofield, C. J., Chemistry and biosynthesis of clavulanic acid and other clavams. *Natural product reports* **1997,** *14* (4), 309-333.
26. Salowe, S. P.; Marsh, E. N.; Townsend, C. A., Purification and characterization of clavaminate synthase from *Streptomyces clavuligerus*: an unusual oxidative enzyme in natural product biosynthesis. *Biochemistry* **1990,** *29* (27), 6499-6508.
27. Zocher, G.; Richter, M. E.; Mueller, U.; Hertweck, C., Structural fine-tuning of a multifunctional cytochrome P450 monooxygenase. *Journal of the American Chemical Society* **2011,** *133* (7), 2292-2302.
28. Pidot, S. J.; Herisse, M.; Sharkey, L.; Atkin, L.; Porter, J. L.; Seemann, T.; Howden, B. P.; Rizzacasa, M. A.; Stinear, T. P., Biosynthesis and Ether-Bridge Formation in Nargenicin Macrolides. *Angewandte Chemie* **2019,** *131* (12), 4036-4041.
29. Bollinger Jr, J. M.; Chang, W.-c.; Matthews, M. L.; Martinie, R. J.; Boal, A. K.; Krebs, C., Mechanisms of 2-Oxoglutarate-Dependent Oxygenases: The Hydroxylation Paradigm and Beyond. The Royal Society of Chemistry: 2015; pp 95-122.
30. Zhang, Z.; Ren, J.; Stammers, D. K.; Baldwin, J. E.; Harlos, K.; Schofield, C. J., Structural origins of the selectivity of the trifunctional oxygenase clavaminic acid synthase. *Nature Structural Biology* **2000,** *7* (2), 127-133.
31. Iwata-Reuyl, D.; Basak, A.; Townsend, C. A., β-Secondary Kinetic Isotope Effects in the Clavaminate Synthase-Catalyzed Oxidative Cyclization of Proclavaminic Acid and in Related Azetidinone Model Reactions. *Journal of the American Chemical Society* **1999,** *121* (49), 11356-11368.
32. Dunham, N. P.; Chang, W.-c.; Mitchell, A. J.; Martinie, R. J.; Zhang, B.; Bergman, J. A.; Rajakovich, L. J.; Wang, B.; Silakov, A.; Krebs, C., Two distinct mechanisms for C–C desaturation by iron (II)-and 2-(oxo) glutarate-dependent

oxygenases: Importance of α-heteroatom assistance. *Journal of the American Chemical Society* **2018,** *140* (23), 7116-7126.
33. Dunham, N. P.; Mitchell, A. J.; Del Río Pantoja, J. M.; Krebs, C.; Bollinger Jr, J. M.; Boal, A. K., α-Amine Desaturation of d-Arginine by the Iron (II)-and 2-(Oxo) glutarate-Dependent l-Arginine 3-Hydroxylase, VioC. *Biochemistry* **2018,** *57* (46), 6479-6488.
34. Doebelin, C.; He, Y.; Kamenecka, T. M., Multigram-scale synthesis of enantiopure 3, 3-difluoroproline. *Tetrahedron letters* **2016,** *57* (50), 5658-5660.
35. Goldstein, J. A.; Cheung, Y.-F.; Marletta, M. A.; Walsh, C., Fluorinated substrate analogs as stereochemical probes of enzymic reaction mechanisms. *Biochemistry* **1978,** *17* (25), 5567-5575.
36. Martin, N. I.; Woodward, J. J.; Winter, M. B.; Marletta, M. A., 4, 4-Difluorinated analogues of l-arginine and NG-hydroxy-l-arginine as mechanistic probes for nitric oxide synthase. *Bioorganic medicinal chemistry letters* **2009,** *19* (6), 1758-1762.
37. Pan, J.; Bhardwaj, M.; Faulkner, J. R.; Nagabhyru, P.; Charlton, N. D.; Higashi, R. M.; Miller, A.-F.; Grossman, R. B.; Young, C. A.; Schardl, C. L., Ether bridge formation in loline alkaloid biosynthesis. *Phytochemistry* **2014,** *98* (1), 60-68.
38. McHugh, M.; Proctor, G., Ring expansion of some heterocyclic β-ketoesters with dimethyl acetylenedicarboxylate. II: Synthesis of azepine, azocine, benzozocine, and benzazonine derivatives. *Journal of chemical research. Synopses (Print)* **1984,** (8).
39. Fulmer, G. R.; Miller, A. J.; Sherden, N. H.; Gottlieb, H. E.; Nudelman, A.; Stoltz, B. M.; Bercaw, J. E.; Goldberg, K. I., NMR chemical shifts of trace impurities: common laboratory solvents, organics, and gases in deuterated solvents relevant to the organometallic chemist. *Organometallics* **2010,** *29* (9), 2176-2179.
40. Pan, J.; Wenger, E. S.; Matthews, M. L.; Pollock, C. J.; Bhardwaj, M.; Kim, A. J.; Allen, B. D.; Grossman, R. B.; Krebs, C.; Bollinger, J. M., Jr., Evidence for Modulation of Oxygen-Rebound Rate in Control of Outcome by Iron(II)- and 2-Oxoglutarate-dependent Oxygenases. *J. Am. Chem. Soc.* **2019,** *141* (38), 15153-15165.
41. Chauhan, M. S.; Singh, S., Asymmetric reduction of ketones catalyzed by α, α-diphenyl-(L)-prolinol modified with imidazolium ionic liquid and BH3· SMe2 as a recoverable catalyst. *Journal of Molecular Catalysis A: Chemical* **2015,** *398*, 184-189.
42. Watanabe, A.; Kiyota, N.; Yamasaki, T.; Tanda, K.; Miyagoe, T.; Sakamoto, M.; Otsuka, M., Design and stereoselective synthesis of four peptide nucleic acid monomers with cyclic structures in backbone. *Journal of Heterocyclic Chemistry* **2011,** *48* (5), 1132-1139.
43. Hofman, G.-J.; Ottoy, E.; Light, M. E.; Kieffer, B.; Martins, J. C.; Kuprov, I.; Sinnaeve, D.; Linclau, B., Synthesis and Conformational Properties of 3, 4-Difluoro-l-prolines. *The Journal of organic chemistry* **2019,** *84* (6), 3100-3120.
44. Boeckman Jr, R. K.; Shao, P.; Mullins, J. J., The D ess-M artin Periodinane: 1, 1, 1-Triacetoxy-1, 1-Dihydro-1, 2-Benziodoxol-3 (1H)-One: 1, 2-Benziodoxol-3 (1H)-one, 1, 1, 1-tris (acetyloxy)-1, 1-dihydro-. *Organic Syntheses* **2003,** *77*, 141-141.
45. Bollinger, J. M.; Krebs, C., Stalking intermediates in oxygen activation by iron enzymes: Motivation and method. *J. Inorg. Biochem.* **2006,** *100* (4), 586-605.
46. Knight, D. W.; Sibley, W. A., Total synthesis of (-)-slaframine from (2R,3S)-3-hydroxyproline. *J. Chem. Soc., Perkin Trans. 1* **1997,** (15), 2179-2188.

47. Dong, S.; Indukuri, K.; Clive, D. L.; Gao, J.-M., Synthesis of models of the BC ring systems of MPC1001 and MPC1001F. *Chemical Communications* **2016,** *52* (53), 8271-8274.
48. Greshock, T. J.; Williams, R. M., Improved Biomimetic Total Synthesis of d,l-Stephacidin A. *Org. Lett.* **2007,** *9* (21), 4255-4258.
49. Keusenkothen, P. F.; Smith, M. B., Asymmetric radical cyclization with pyroglutamate: synthesis of 7-substituted pyrrolizidinones. *J. Chem. Soc., Perkin Trans. 1* **1994,** (17), 2485-2492.
50. Zhao, H.; Prosser, A. R.; Liotta, D. C.; Wilson, L. J., Discovery of novel N-aryl piperazine CXCR4 antagonists. *Bioorganic & medicinal chemistry letters* **2015,** *25* (21), 4950-4955.
51. Angelo, N. G.; Arora, P. S., Nonpeptidic foldamers from amino acids: synthesis and characterization of 1, 3-substituted triazole oligomers. *Journal of the American Chemical Society* **2005,** *127* (49), 17134-17135.
52. Reginato, G.; Mordini, A.; Messina, F.; Degl'Innocenti, A.; Poli, G., A new stereoselective synthesis of chiral γ-functionalized (E)-allylic amines. *Tetrahedron* **1996,** *52* (33), 10985-10996.
53. Wijtmans, M.; de Graaf, C.; de Kloe, G.; Istyastono, E. P.; Smit, J.; Lim, H.; Boonnak, R.; Nijmeijer, S.; Smits, R. A.; Jongejan, A., Triazole ligands reveal distinct molecular features that induce histamine H4 receptor affinity and subtly govern H4/H3 subtype selectivity. *Journal of medicinal chemistry* **2011,** *54* (6), 1693-1703.
54. Greshock, T. J.; Williams, R. M., Improved biomimetic total synthesis of D, L-stephacidin A. *Organic letters* **2007,** *9* (21), 4255-4258.
55. Souza, L. W.; Squitieri, R. A.; Dimirjian, C. A.; Hodur, B. M.; Nickerson, L. A.; Penrod, C. N.; Cordova, J.; Fettinger, J. C.; Shaw, J. T., Enantioselective Synthesis of Indolines, Benzodihydrothiophenes, and Indanes by C− H Insertion of Donor/Donor Carbenes. *Angewandte Chemie* **2018,** *130* (46), 15433-15436.

VITA

Nabin Panth

EDUCATION

Ph.D. (Synthetic Organic Chemistry)

Department of Chemistry, University of Kentucky, Lexington, KY (2016-2021)

Advisor: Dr. Robert B. Grossman

Master of Science (Organic Chemistry)

Department of Chemistry, Tribhuvan University, Kathmandu, Nepal 2015

Advisor: Dr. Niranjan Parajuli

Bachelor of Science (Chemistry)

Tri-Chandra Campus, Tribhuvan University, Kathmandu, Nepal 2010

PUBLICATIONS

- Panth, N.; Wenger, E.S.; Bollinger, J.M.; Krebs, C.; Grossman, R.B.; "*Synthesis of 6,6- and 7,7-difluoro-1-acetamidopyrrolizidines and their oxidation catalyzed by the nonheme Fe oxygenase LolO*" Biochemistry, manuscript in preparation.

TEACHING EXPERIENCE

Graduate Teaching Assistant, Department of Chemistry, University of Kentucky

Teaching Assistant, Advanced Organic Chemistry Lab, (CHE 533) Spring-2021

- Capstone course for which TA's are ***hand-picked*** from the pool by instructor to simulate a senior group member training a group of 14-18 new researchers.

Super Teaching Assistant General Chemistry Laboratory Spring 2020- Fall 2021

- ***Hand-picked*** by laboratory supervisor to lead all TA's.
- Helping supervisor to do the administrative tasks, Canvas and Lab-flow management, leading TA meetings, solving the issues related to grading and teaching.

Teaching Assistant: General Chemistry and Organic Chemistry Laboratory (Fall 2016-2019)

- Taught undergraduate laboratory techniques to 40-48 students per semester (CHE 111, 113, 231, 233)
- Basic experimental techniques like recrystallization, distillation, column chromatography, solvent extraction, and advanced lab techniques like synthesis of protected dipeptide, biodiesel from cooking oil, organic semiconductor (pentacene) and polymer, along with analytical techniques like TLC, IR, GC, and NMR spectroscopy.

Assistant Lecturer, Liverpool International College, Kathmandu, Nepal 2015-2016
Part Time Science Teacher. Sundarban School of Science, Kathmandu, Nepal 2014-2015

SYNERGYSTIC ACTIVITIES

- ***Social coordinator***, Chemistry graduate student association, July 2020-July 2021
- Volunteered as a ***judge*** in 18th Annual Kentucky Science and Engineering fair – online, Lexington, KY on March 28th, 2020.
- Volunteered as a ***judge*** in 36th Annual Kentucky American Water – Fayette County Public Schools District Science Fair, Lexington, KY on Feb 1st, 2020.
- ***Member*** of American Chemical Society and ACS 2019 - present
- ***Member*** of ACS, Division of Organic Chemistry 2019 – present
- ***Founding member*** of Nepalese Student Association, University of Kentucky, 2019. The leadership has been transferred to others which now has 40-50 members.

TALKS AND SEMINAR

- "Tandem Bond-Forming Reactions of 1- Alkynyl Ethers: [3,3]- Sigmatropic Rearrangement and [2+2] Cycloaddition" Department of Chemistry, University of Kentucky, 2018.
- "Multicomponent Hetero- [4+2] Cycloaddition/ Allylboration Reactions: From Natural product Synthesis to Drug Discovery" Department of Chemistry, University of Kentucky, 2017.
- "Synthesis of 6,6- and 7,7-difluoro-1-acetamidopyrrolizidines and their oxidation catalyzed by the nonheme Fe oxygenase LolO" GSA mini-conference, University of Kentucky, 2021.